Brush-DC Equivalent Control Based Delta Modulation for a PWM Inverter-fed Nine-Phase Induction Machine Drive

By

Lovemore Gunda

Thesis presented in partial fulfilment of the requirements for the degree of Master of Science in Electrical and Electronic Engineering at the Stellenbosch University

Supervisor: Dr Nkosinathi Gule

Department of Electrical and Electronic Engineering

December 2015

Declaration

By submitting this thesis electronically, I declare that the entirety of the work contained therein is my own, original work, that I am the authorship owner thereof (unless to the extent explicitly otherwise stated) and that I have not previously in its entirety or in part submitted it for obtaining any qualification.

Signature :

Date :

Abstract

A considerable amount of research has been done on the control of induction machines since the introduction of the power electronic inverter. The use of power electronic inverters has also opened the way for the design of multiphase induction machines. The current rating of the power electronic components used in multiphase inverters is lower than those used in three-phase inverters. On the machine side, the multiphase machines have higher power and torque density than their three-phase counterparts.

The control of these multiphase induction machines poses a challenge for the designer of the drive system. Scalar control, direct torque control and vector control methods work well in three-phase machines. However, the analysis of vector based techniques becomes complex as the number of phases increases and new methods are being proposed to reduce the complexity of implementing machine control.

The Brush-DC Equivalent (BDCE) control method was proposed to simplify the design of controllers. This method does not include complex coordinate transformations like are used in vector-based techniques. The BDCE control method is derived from the control of separately excited brush-DC machines utilising compensating windings. The induction machine controlled using the BDCE method is designed such that the phases of the machine act alternately in rime as torque-producing or field-producing phases. This is achieved by supplying the induction machine windings with specially designed trapezoidal stator current waveforms. The BDCE control method enables decoupled control of flux and torque without complex coordinate transformations. The method can be implemented for high phase-number multiphase induction machines without added complexity.

In this thesis, the BDCE control method implementing a delta modulated current controller which generates pulse width modulated signals for the power electronic inverter is presented. The delta modulation technique is proposed because it gives good inverter performance characteristics and reduces torque and current ripples. It also reduces total current harmonic distortions through the use of a fixed switching frequency. The BDCE controlled drive is simulated using Matlab/Simulink. The simulation results suggest that delta modulation gives lower current and torque ripples with attenuated low order voltage harmonics.

Practical evaluation of the drive is done using the delta modulated current controller to validate the simulation results. An alternative delta modulation scheme in which the reference current signal is integrated before being fed to the forward comparator is proposed, designed and tested. The alternative delta modulation scheme produces the required trapezoidal stator currents and allows decoupled control of the field and torque currents. The results of the practical evaluation compare

well with the simulation results and show that a delta modulated current controller can be used in the drive. Better results are expected if stator voltages are fed back to the modulator to estimate the reference signal.

Opsomming

'n Groot hoeveelheid navorsing is al gedoen oor die beheer van induksiemasjiene (IM) sedert die ontwikkeling van die drywingselektronika omskakelaar. Die gebruik van die drywingselektronika omskakelaars het die weg gebaan vir die ontwerp van veelfasige IM. Tans is die stroomkenwaarde van die drywingselektronika komponente wat in 'n veelfasige omsetter gebruik word laer as die van drie-fase omsetters. Aan die masjienkant, is beide die drywing en wringkrag digtheid van 'n van die veelfasige masjien hoër as die van hul drie-fase eweknieë.

Die beheer van dié veelfasige IM hou 'n uitdaging in vir ontwerpers van die aandryfstelsel. Alhoewel skalaar-, direkte wringkrag- en vektor-beheer metodes goed werk vir drie-fase elektriese masjiene, raak vektor-gebaseerde metodes meer kompleks soos die aantal fases van 'n masjien toeneem. Nuwe metodes word voorgestel om die kompleksiteit van masjien beheer te vereenvoudig.

Die Borsel-GS Ekwivalent (BGSE) beheer metode word voorgestel om die ontwerp van die beheerders te vereenvoudig. Die metode sluit nie komplekse koördinaat transformasies in soos met vektor-gebaseerde tegnieke nie. Die BGSE beheer metode is afgelei van die beheer van 'n afsonderlik gemagnetiseerde borsel-GS masjien met kompensasie windings. Die IM wat beheer word deur gebruik te maak van die BGSE metode word so ontwerp dat die fases van die masjien afwisselend oor tyd as wringkrag- of veld-produserende fasesoptree. Dit word gedoen deur die lM te voer met spesiaal ontwerpte trapesoïdale stator-stroom golfvorms. Die BGSE metode maak dit moontlik vir onafhanklike beheer van beide vloed en wringkrag sonder enige komplekse koördinaat transformasies. Die metode kan geïmplementeer word op hoë fase veelfasige IM sonder enige addisionele kompleksiteit.

In die tesis word die BGSE metode implementering van 'n delta modulasie stoom beheerder wat pulswydte gemodulasie seine genereer vir 'n drywing elektronika krag-omskakelaar aangebied. Die delta modulasie tegniek word voorgestel, omrede dit goeie omsetter werksverrigting karakteristieke verskaf en die wringkrag en stroom rimpel verlaag. Daarby verminder dit ook die totale harmoniese distorsies van die stroom deur gebruik te maak van 'n vaste skakelfrekwensie . Die BGSE beheer aandrywer word met. Matlab/Simulink gesimuleer. Die simulasie resultate toon dat delta modulasie 'n laer stroom en wringkrag rimpel tot gevolg het as ook verlaagte lae orde spanning harmonieke.

Die praktiese evaluering van die aandrywer word gedoen met die delta gemoduleerde beheerder om die simulasie resultate te verifieer. 'n Alternatiewe delta modulasie skema word voorgestel, ontwerp en getoets, waar die verwysing stroomsein eers geïntegreerd word voor dit aan die vorentoe vergelyker gestuur word. Die alternatiewe skema het die vereiste trapesoïdale stator strome geproduseer en het toegelaat vir die onafhanklike beheer van beide vloed en wringkrag strome. Die resultate van die praktiese evaluering vergelyk goed met die van die simulasie resultate en toon dat 'n delta gemoduleerde stroom beheerder gebruik kan word in die aandrywer. Beter resultate word

verwag indien die stator spannings teruggevoer word na die modulator om 'n beter verwysings sein af te skat.

Acknowledgements

The author is highly indebted to Dr N Gule, the project supervisor for his continuous support and guidance during the whole research period. He was a source of academic, moral and emotional support during the highly challenging research period.

Many thanks also go to:

- The Stellenbosch University Electrical and Electronic Engineering department for the departmental bursary that funded this research.
- The Electrical machines laboratory team of technicians for setting up the work benches to enable the progress of practical tests.
- Mr David Groenewald for his continued support in electronic equipment set up and the inverter board repairs.
- God Jehovah Almighty for giving power to the author to progress with the research under His guidance and protection.

"*The absence of complex analytical formulas often makes easier the concentration for the physical understanding of problems, for more lively observation and better understanding of the substance, than when the electric phenomena are viewed through the clouds of mathematical symbols*." Sir J.J. Thompson, "Elements of the Mathematical Theory of Electricity and Magnetism". 1909.

Contents

List of Figures

List of Tables

List of variables

I_s	Stator phase supply current	[A]
L_m	Motor magnetising inductance	[H]
L_r	Rotor phase inductance	[H]
L_s	Stator phase inductance	[H]
N_s	Number of statorturns per phase	[#]
R_r	Rotor phase resistance	[Ω]
R_s	Stator phase resistance	[Ω]
V_s	Stator phase voltage	[V]
E_1	Induced emf	[V]
ω_{sl}	Slip frequency	[rads^{-1}]
f	Frequency of stator phase supply voltage	[Hz]
λ	Stator phase flux linkage	[Wb]
k_w	Stator phase coil winding constant	[]

Abbreviations

ADC	Analogue to Digital Converter
AGFO	Air Gap Flux Oriented
BDCE	Brush DC Equivalent
DAC	Digital to Analogue Converter
DC	Direct Current
DMPWM	Delta Modulated Pulse Width Modulation
DSP	Digital Signal Processor
DTC	Direct Torque Control
FEA	Finite Element Analysis
FOC	Field Oriented Control
FPGA	Field Programmable Gate Array
IGBT	Insulated Gate Bipolar Transistor
IPM	Intelligent Power Module
LED	Light Emitting Diode
PC	Personal Computer
PI Controller	Proportional Integral Controller
PWM	Pulse Width Modulation
RFO	Rotor Flux Oriented
SFO	Stator Flux Oriented
SHEPWM	Specific Harmonic Elimination Pulse Width Modulation
SPWM	Sinusoidal Pulse Width Modulation
SVPWM	Space Vector Pulse Width Modulation
WPWM	Wavelet Pulse Width Modulation

Chapter 1 Introduction

The development of a mathematical model for a separately excited DC motor with independent armature and field control presented in [1] shed more light on separate control of flux and torque in DC machines. The model included mutual inductances and magnetic saturation which produced simulation results that were comparable with practical results. Flexible control of speed and torque was demonstrated and good speed regulation was achieved under varying loading conditions. The developed torque equation for a separately excited dc motor is given as:

$$T = K_m \emptyset I_a \qquad (1\text{-}1),$$

where T is the developed torque, K_m is the machine constant, $\emptyset$ is the magnetic flux and I_a is the armature current. The equation shows that there is a linear relationship between the developed torque and the armature current when the magnetic flux is kept constant.

Although the control of these DC machines is flexible and gives good performance, DC machines become costly to maintain under dusty and environmentally hostile conditions because of the brushes and commutator segments which need to be serviced regularly. DC machines also impose speed limits due to the physical contact between brushes and commutator segments and also because sparks occur between the bushes and commutator segments during commutation at high speeds. However, the simplicity of the control of dc machines made them popular in variable speed drive applications until vector controlled and direct torque controlled induction machine drives were introduced.

Three-phase induction machines are commonly used in constant speed applications because of their rugged construction, reduced frame size and smooth operation when compared to single-phase machines. The existence of standards for their construction, control, testing and commissioning makes them available off the shelf. Induction machine control techniques for variable speed applications have been developed to emulate the control of DC machines through the use of various strategies which enable the decoupled control of torque and flux. The vector control method is one of such techniques introduced in 1972 by Blaschke [2]. The study was done to investigate the possibility of manipulating stator voltage or current to control the developed torque. This led to more research into the improvement of the technique such as in [3]-[5]. The improvements include simplifying practical system implementation, designing more efficient current regulators and flux observers and also enhancing reliability through parameter adaptation. In [3], a rotor flux oriented torque control scheme was used in conjunction with stator flux vector control. The work showed the possibility of estimating the total leakage inductance instead of only identifying the stator self-inductance to improve parameter estimation. In [4], a stator flux oriented approach to vector control was used for the control of a three-phase induction machine. The research focused on implementing open loop, vector-based

constant flux control by modifying the conventional constant volt/hertz control strategy to simplify the practical implementation of the vector control technique. An air gap flux oriented vector control technique for a bearing-less induction motor was presented in [5]. The technique was based on improving performance during the high torque acceleration period of operation. It enabled the determination of optimal flux orientation for complete decoupling in radial force generation. The designed controller showed improved performance during overload conditions. A modelling technique for three-phase AC machines to mimic DC machines and reduce rotor losses was presented in [6]. The study showed that the vector control method gives decoupled control of flux and torque with minimum power losses. The details of the vector control technique are given in section A.1 of Appendix A.

Induction machines with more than three phases, referred to as multiphase or high phase order induction machines, have also been introduced mainly for specialized applications like in more-electric aircraft [7]-[9], electric ship propulsion [10]-[13], electric vehicles [14]-[16] and in renewable energy applications [17]-[18]. A literature review of the previous work related to multiphase machines with a special focus on induction machines is presented in this chapter. The motivation to this study and the objectives thereof are stated at the end of this chapter. The work presented in this thesis focuses on a nine-phase cage rotor induction machine drive controlled using a non-vector based technique which enables decoupled control of flux and torque.

1.1 Literature Review: Multiphase Induction Machines and Drives

The research in multiphase induction machine drives can be traced back to late twentieth century around the 1960s. Due to advances in power electronic technology, the research has shown a considerable increase due to the benefits realized from the use of such systems. In this section, a review of the work done in multiphase induction machines is presented. The sub sections are presented according to the number of phases used in the machines. A general review of the multiphase technology is presented at the end.

1.1.1 Motivation to Using Multiphase Systems

Apsley et al [19] made experimental comparisons of three-phase, four-phase, six-phase and twelve-phase winding configurations applied to a standard cage rotor induction machine. Rajambal and Renukadevi [20] presented simulation results for induction machines with odd number of phases from three to eleven. Both studies presented in [19] and [20] showed that as the number of phases was increased, the torque ripples were reduced significantly. It was observed in [19] that the torque pulsations decreased in magnitude and increased in frequency as the number of phases increased. The mean phase current, the stator losses and the rotor losses also decreased as the number of phases increased. It was also noted in [19] that unbalanced currents increased the torque fluctuations and this

called for proper modelling of the machine to produce balanced currents. In general, it can be said that the performance of induction machines improves considerably as the number of phases increases. The studies done using various phase numbers on the induction machines are presented in the following sections

1.1.2 Five-Phase Induction Machines

The first multiphase cage rotor induction machine on record was developed and analysed in [21]. Preliminary experiments were done on a five-phase induction machine supplied from a ten-pulse inverter. It was shown that the five-phase induction machine torque fluctuations were a third of the fluctuations produced by an equivalent three-phase machine. However, the use of an inverter introduced harmonics in the supply line thereby increasing motor losses due to the poor form factor of the currents. It was proposed that the harmonics could be eliminated by changing the voltage waveform to a near-rectangular waveform.

A research dedicated to the direct torque and flux control of a five-phase induction motor using fuzzy logic was presented in [22]. Direct torque and flux control with fuzzy logic was compared to conventional direct torque and flux control. The results showed that the use of fuzzy logic produced less torque ripples, less stator flux variations and improved dynamic performance than the conventional method. The study is evidence of the growing interest in improving the utilization of multiphase systems in induction machine applications through the implementation of more intelligent control.

Guzman et al [23] presented the development of a fault tolerant scheme for a speed controlled five-phase induction motor using a predictive current control technique. The five-phase induction machine was tested under one open-phase fault. The results showed that the five-phase machine had inherent fault tolerance and gave low current ripples as well as good speed and torque response under faulty conditions. The performance was close to normal operation giving smooth transition from the pre-fault to the post-fault condition.

Shreier et al [24] investigated the performance of a five-phase cage rotor induction machine with various stator winding layouts. A five-phase voltage source inverter was used to supply the five-phase machine. The different connections that were used and tested are shown in Figure 1-1. Considering the connections shown in the figure, it was observed that the drive produced less torque fluctuations and less ripples when the second delta connection, δ_2 was used. The first delta connection, δ_1 gave the worst performance while the star connection, λ gave relatively good performance but with slightly higher current distortions. The study showed that the performance of a multiphase machine is also affected by the type of winding layout and inverter connection used.

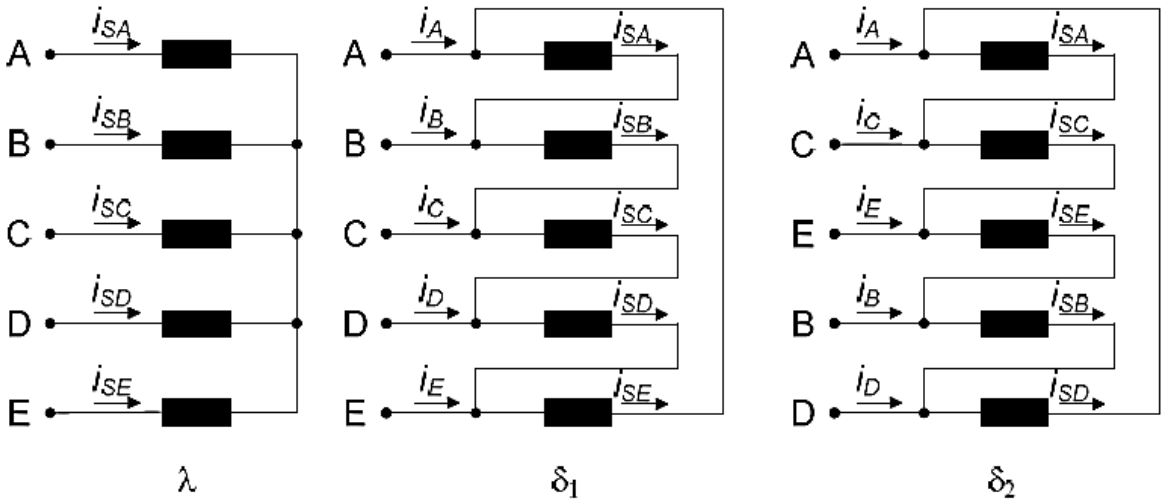

Figure 1-1. Three ways of connecting five-phase stator windings to a converter [24].

1.1.3 Six-Phase Induction Machines

Patkar and Jones [25] investigated the performance of an asymmetrical six-phase induction machine with a single- and with a two-neutral point configuration. The single-neutral point configuration is shown in Figure 1-2. The configuration showed good fault tolerance but with high phase current total harmonic distortions. The two-neutral point configuration of Figure 1-3 showed high dc bus voltage utilization, required a simpler PWM control strategy and produced less current total harmonic distortions than the single-neutral point configuration. However, the two-neutral point configuration showed poor fault tolerance.

The studies presented in [24] and [25] showed that the design of the stator winding layout is an important factor in the implementation of multiphase systems. A design which gives balanced currents in the stator circuit is the best for PWM inverter-fed drives. The design should consider ease of control, current harmonics, dc bus voltage utilization and performance under faulty conditions.

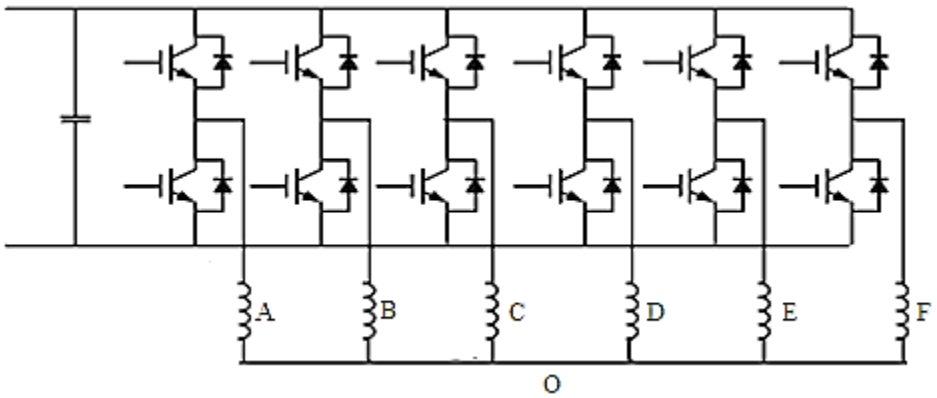

Figure 1-2. Six-phase induction machine with a single-neutral point stator connection configuration.

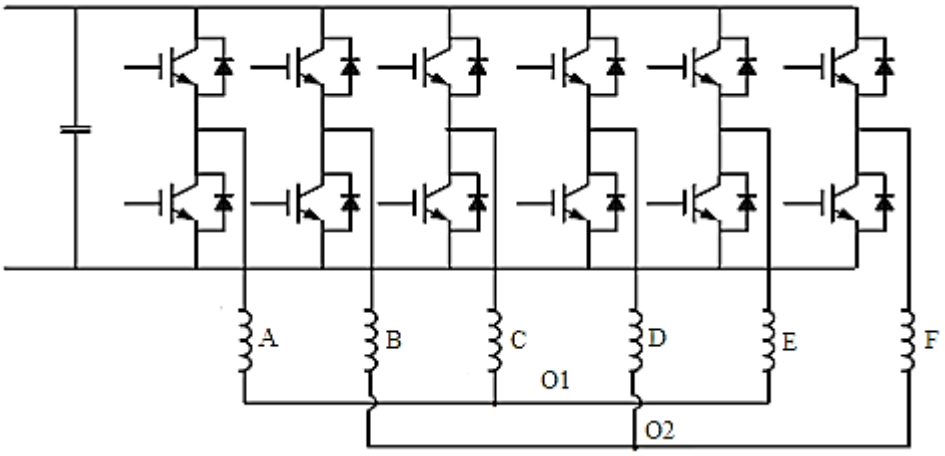

Figure 1-3. Six-phase induction machine with a two-neutral point stator connection configuration.

A six-phase squirrel cage induction motor with two, three-phase windings was designed and tested using a six-step voltage source inverter in [26]. The stator of a three-phase squirrel cage induction machine was rewound into two, three-phase windings to produce a six-phase machine. The study was carried out to compare the performance of a six-phase machine to that of an identical three-phase machine. It was observed that the harmonics of order $6k \pm 1; (k = 1; 3; 5 ...)$ could be eliminated in the six-phase machine. The torque produced was free of the sixth harmonic torque ripple which is dominant in three-phase systems. The study showed that multiphase induction machines can be used in high power density electric motor drives.

Lyra and Lipo [27] did investigations to improve the torque density of a six-phase induction machine by injecting third order zero sequence current components into the stator current. A dual three-phase connection where the three-phase groups were spatially shifted by 30 degrees was used. A six-leg current regulated pulse width modulation (PWM) inverter was used to supply the machine. The inverter was controlled by a PI controller to implement the indirect flux control based on a digital signal processor (DSP). It was observed that the torque could be increased through third harmonic current injection as a result of the increase in the fundamental component of current and flux. This resulted in a reduction of the torque pulsations and the harmonic content of the currents. The study showed that the use of near-flat topped current waveforms reduced torque pulsations and improved the harmonic content of the inverter output.

Nagaraj et al [28] developed a model of a modified dual-stator, six-phase induction machine to determine the starting torque performance of the machine. Two models of three-phase inverter were developed to supply power to the stator. The six-phase induction machine was compared to an identical three-phase induction machine. The six-phase machine produced higher starting torque than the three-phase machine. In [29], a direct torque control technique was simulated for a double-stator, six-phase induction machine using Matlab. Adaptive control was used to achieve stability and

disturbance rejection. The results showed that the performance of the six-phase induction machine could be improved through the design of an efficient control technique.

In [20] it was shown that as the number of phases was increased, the number of dimensions and variables required for system analysis also increased. For a five-phase system, a four dimensional analysis was done and a six dimensional analysis would be required for a seven-phase system. A study by Ai et al [30] showed that the system design could be simplified by using a non-vector based control technique which gives decoupled control of flux and torque. The control method was evaluated for a six-phase wound rotor induction machine with near square air-gap flux density. The stator windings of the machine acted alternately in time as torque or flux-producing phases when supplied with specially designed trapezoidal stator current waveforms. Decoupled control of flux and torque was achieved without the use of complex transformations involved in vector-based techniques. The results showed a linear relationship between developed torque and torque current thus enabling direct torque control.

1.1.4 Seven-Phase Induction Machines

Iqbal et al [31] presented the indirect rotor flux oriented control of a seven-phase induction motor drive. The model developed in the study was based on the assumption that both the stator and the rotor had seven phases. This simplified the modelling of the machine and a three-phase based model was used. Simulations were done for the seven-phase machine using a hysteresis current controller to generate the inverter PWM switching signals. Full decoupling of rotor flux and torque was demonstrated. It was observed that the dynamics of the seven-phase induction machine were identical to those of a three-phase induction machine if the rotor and the stator have the same number of phases.

In [32], stator flux oriented vector control was implemented on a seven-phase cage rotor induction machine. The model of the system employed multiple space vector analysis combined with conventional carrier-based pulse width modulation. The modulation technique was implemented in a digital signal processor. A seven-phase voltage source inverter was used and it gave full utilization of the dc bus voltage. The control also achieved decoupled control of stator flux and torque.

1.1.5 Nine-Phase Induction Machines

The control technique proposed in [30] was extended for the control of a nine-phase cage rotor induction machine in [33]. The stator phases of the machine acted alternately in time as field- or torque-producing phases when supplied with specially designed trapezoidal stator current waveforms. The construction of the stator current waveform was presented in [34] to show that there is an optimal ratio of field to torque phases for maximum torque to be developed in a machine controlled through this method. The method was termed the “Brush-DC Equivalent” (BDCE) control method due to its

similarities to the control of brush-dc machines with compensating windings. The results showed that the BDCE control method worked satisfactorily in the sub-base and the field weakening speed regions of the drive. It was noted that the method could be implemented on machines with large phase numbers due to its simplicity. This method is presented in more detail in section 2.3.

A study by Sowmiya et al [35] presented the simulation of a nine-phase induction motor controlled using the indirect flux oriented control strategy. The study was done to investigate the implementation of the drive in motion control at low speeds. A nine-phase inverter with nine legs was controlled using a hysteresis current controller. A PI speed controller was used to generate speed control pulses. The simulation results showed that decoupled control of flux and torque could be achieved at low speeds in motion control.

1.1.6 Eleven-Phase Induction Machines

A research presented in [36] focused on steady state performance evaluation of an eleven-phase induction machine. A comparison was made between the performances of the machine when supplied with a square-wave current and when supplied with a sinusoidal current with third harmonic injection. It was observed that the use of a square wave supply caused large distortions in the currents with high peaks. Third harmonic injection reduced the distortions but was less efficient compared to the supply of a square wave for a wide power output range. The use of a square wave supply also reduced the inverter switching losses.

A finite element analysis simulation model of an experimental eleven-phase induction machine was presented in [37]. The finite element analysis model was developed to simulate the performance of the eleven-phase machine under fault conditions. A current source inverter and a voltage source inverter were compared to determine which type of inverter gave better performance. It was shown that an open circuit fault caused larger torque and current ripples when a current source inverter was used. The starting torque was observed to be higher when the voltage source inverter was used.

1.1.7 Fifteen-Phase Induction Machines

In [38], a fifteen-phase, 20 MW, voltage source inverter-fed induction machine was modelled to determine its performance under fault conditions. The machine was modelled for implementation in electric ship propulsion systems. The phasor diagram of the stator winding layout of the machine is shown in Figure 1-4. It consisted of five phase groups and each group had three phases. The phases in each group were spaced by an angle α_s of magnitude 120 degrees Adjacent phase groups were separated by an angle β_s of magnitude 12 degrees. A single neutral point was used in the inverter connection configuration. The single-phase open circuit fault condition was investigated. The results showed that there was a slight increase in stator currents due to an open circuit stator fault. There was a slight decrease in speed accompanied by an increase in developed torque with large ripples due to

the open circuit fault. This was attributed to the use of one neutral point in the stator windings. The connection caused circulating currents to flow in the circuit in case of a stator winding fault.

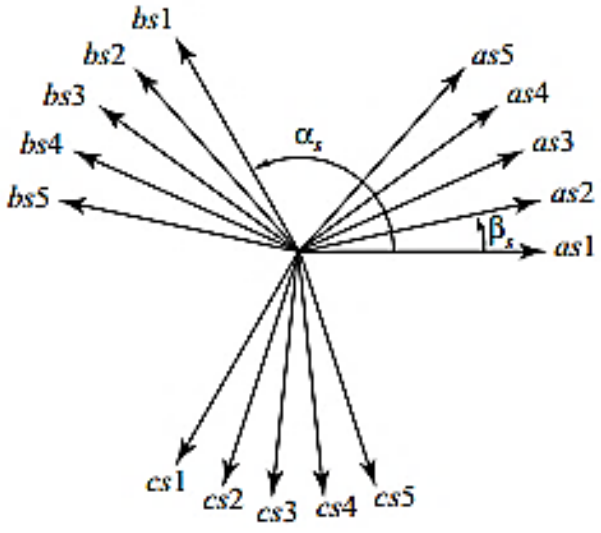

Figure 1-4. Phasor representation of the fifteen-phase induction machine stator winding connection [38].

Weichao et al [39] presented the prototyping of a fifteen-phase induction machine using the dSPACE real-time prototyping system and Matlab simulations. Matlab auto-coder was used to generate code for an FPGA used to produce PWM signals for the inverter. Hardware emulators were used to investigate the performance of a fifteen-phase induction machine supplied through a fifteen-phase voltage source inverter. The inverter used the full H-bridge configuration and hence required sixty control signals. Testing of the design was simplified by the use of hardware emulators instead of electronic hardware. FPGA based PWM generators were used with sinusoidal pulse width modulation. The test results from Matlab simulations were comparable to those obtained using emulators and the fifteen-phase machine. The results were comparable under normal operation of the system. Third harmonic injection was also tested and produced less total harmonic distortions than the use of sinusoidal currents. The work presented a simpler and flexible technique for evaluating machines with large phase numbers without being limited by electronic circuit complexity and size.

1.1.8 General Multiphase Technology Reviews

The general theoretical analysis of multiphase induction machines (high phase order machines) was presented by Klingshirn [40]. The different stator winding layouts that can be used in multiphase machines were illustrated and analysed. The analysis showed that some flux harmonics did not induce rotor currents in multiphase machines. This reduced the torque pulsations and rotor I^2R losses to values below those produced by three-phase machines. Six-phase, nine-phase and eleven-phase induction machines were considered to be more attractive because they could be modelled using three-phase based models. It was also noted that with rectangular voltage supplies, the stator copper

losses increased but the rotor I^2R losses were reduced. Smaller torque pulsations were observed when using non-sinusoidal supplies compared to the use of sinusoidal voltage sources.

Other studies focussing on the review of developments in multiphase systems are presented in [41] - [45]. In [42], the analysis was based on split-phase, dual-phase and single-star point machines. It was noted that the split-phase winding layout enabled equal sharing of power between inverters thereby lowering the current rating per phase. The dual-stator arrangement enabled direct separate control of flux and torque and the multiphase arrangement with one neutral point enabled the supply of multiple machines from one multiphase inverter.

The work presented in [43] was a review of multiphase systems focussing on the technology state of the art. The review was based on work done by various researchers and it was noted that the design of multiphase systems required a system approach rather than independent component design. A drive consists of the power supply, the power electronic circuitry, the induction machine and the control system. The design of these components has to be done considering how they interact with each other to produce an efficient drive. In references [44] and [45], it was shown that the multiphase systems in general have better performance than their three-phase counterparts in terms of torque and current ripples. The current harmonics are pushed to higher frequencies that can be easily filtered off by machine inductances.

The advantages of using multiphase induction machines over their three-phase counterparts which were observed in the literature above can be summarized as:

i. The required current rating of the power electronic switching devices used in the inverters and converters is reduced as the number of phases increases for the same machine power rating [42].
ii. The torque harmonics and ripples are reduced in magnitude and increased in frequency when the multiphase machines are used thereby enabling easy filtering [19]-[21], [44]-[45].
iii. Stator and rotor copper losses are reduced leading to higher efficiency [19], [40].
iv. Power per root mean square (rms) current ratio is increased [42].
v. Smaller rotor current harmonics are produced leading to more stable and reliable operation [39].
vi. Multiphase machines have inherent fault tolerance [23].
vii. Multiphase machines have higher power and torque density for the same machine size [26]-[27].
viii. There is less interaction between the machine and the dc link when voltage source inverters are used [37].
ix. The motors produce less noise and vibrations when running under normal conditions [27].

1.2 Motivation to the Study

The brush-dc equivalent control method applied to a nine-phase cage rotor induction machine drive was implemented and presented in [46]. The efficiency of the nine-phase drive system was comparable to that of an equivalent three-phase drive. In the study, it was noted that there were losses in the inverter indicated by a considerable rise in inverter temperature during operation [46]. This happened at low speeds and it was recommended that the power electronic converter design and the method of operating the inverter switches must be investigated to improve the efficiency of the drive.

A current controlled PWM inverter was used in the control system presented in [30] and [33] through the implementation of a hysteresis current controller. The hysteresis controller was used because of its fast response and simplicity of implementation. It utilised a variable switching frequency which makes it difficult to filter the current harmonics. Hysteresis control operation is also highly dependent on the width of the hysteresis band and the slope of the reference signal. The method exhibits instabilities under varying loading conditions. The protection of the inverter and design of filters is difficult to implement due to the variable frequency.

Delta modulation was therefore considered as an alternative modulation technique to be implemented in the current controller. The work presented in [47]-[53] showed that the delta modulated controller had inherent constant v/f characteristics when used with PWM inverters supplying induction machines. The work also showed that delta modulation enabled smooth transition between PWM mode of operation and single pulse mode. Low order harmonics were attenuated thereby producing less torque ripples in the machine under varying loading conditions. The switching frequency could be fixed through the use of a constant sampling frequency in the sample and hold block.

It is against this background that a delta modulated current controller is proposed to replace the hysteresis controller in the BDCE controlled drive. Delta modulation has several performance characteristics mentioned above which make it attractive for use with a PWM inverter. The aim of this study is to model, design and implement a delta modulated current controller on the nine-phase induction machine drive presented in [33]. This is done in order to investigate the feasibility of using the delta modulated current controller instead of the hysteresis controller in the drive. The current control algorithm is to be implemented in software thereby removing the need for electronic circuit implementation of the delta modulator circuit.

1.3 Objectives of the study

The above aim is achieved by addressing the following objectives:

- Modelling of the BDCE controlled nine-phase induction machine drive.

- Development of a Matlab/Simulink simulation model of the BDCE controlled nine-phase induction machine drive.
- Simulation of the drive using a delta modulated current controller and also using the hysteresis current controller and comparing the results.
- Practical implementation of the software-based delta modulated current controller.
- Evaluation of the use of the delta modulated current controller and comparison to the hysteresis controller in producing PWM signals for the voltage source inverter driven nine-phase induction machine drive.

1.4 Dissertation Layout

The dissertation is centred on the goal of implementing the delta modulated current controller to generate PWM switching signals for driving the nine-phase inverter under BDCE control.

The remainder of this dissertation is organized as follows:

Chapter 2: The BDCE control method is presented in this chapter. The production of the rotating flux and the construction of stator current waveforms are also explained.

Chapter 3: The delta modulation technique is presented in this chapter. Focus is put on the use of delta modulated current control in PWM inverters used in machine control. The development of the numerical integration algorithm is presented for the integrator used in the delta modulator.

Chapter 4: The BDCE controlled induction machine drive is modelled for use with the delta modulated controller and also for use with the hysteresis controller. The electrical model and the mechanical model are presented and several characteristic equations are derived. Matlab/Simulink simulation of the BDCE controlled drive is presented. Simulation results are presented in this chapter by comparing the delta modulated controller to the hysteresis controller.

Chapter 5: Experimental evaluation of the nine-phase BDCE controlled drive is presented in this chapter. The experimental results obtained from the use of the delta modulated controller and by the use of the hysteresis controller are presented and discussed.

Chapter 6**:** Conclusions drawn from the study and recommendation are presented in this chapter together with the limitations which affected the implementation of the control technique.

Chapter 2 Brush-DC Equivalent Control

The Brush-DC Equivalent control method is an alternative to vector-based control techniques used in decoupled control of flux and torque in induction machines. The method presents a simpler way of achieving the decoupled control without including complex vector transformations. Because of its simplicity, the BDCE control method can be used to control induction machines with a large number of phases. In this chapter, the BDCE control method applied to a theoretical twelve-phase induction machine and to a practical nine-phase cage rotor induction machine is presented. The design of the stator winding and the trapezoidal stator current waveforms is considered. The stator winding layout and the trapezoidal current waveforms are used to describe how the BDCE controlled machine operates.

2.1 Development of the Stator Current Waveforms

The number of stator phases for a BDCE controlled induction machine is always a multiple of, but excluding, three. The stator phases should act alternately in time as field- or torque-producing phases when the machine is controlled using the BDCE control method. The analysis presented in [34] showed that at least three field phases and at least three torque phases are required for an induction machine to be controlled using the BDCE control method. This implies that the BDCE controlled machine should have at least six stator phases.

The trapezoidal stator current waveforms used in the BDCE controller are constructed such that the torque phase at an instant acts as a torque-producing phase and the field phase acts as a field-producing phase not the other way round. This is verified by considering the stator induced voltage on a phase when the machine is running. From the analysis done in [30], it was noted that when the phases are acting in the correct way, the maximum stator voltage per phase is induced when a phase is acting as a torque-producing phase. Similarly, the induced voltage is minimal when a phase is acting as a field-producing phase.

There are two possible ways in which the waveform can be constructed, that is, with the field current leading the torque current, or with the torque current leading the field current. The two possibilities for an M_p-phase machine with m_f field phases and m_t torque phases are illustrated in Figure 2-1. The tests done in [30] showed that the maximum voltage was induced during the torque producing phase when torque current was leading the field current. This was confirmed by the torque measurements under locked rotor conditions. Higher torque was developed when the torque current was leading the field current than when the field current was leading the torque current. For proper control, the torque current leads the field current as shown in Figure 2-1(a) since this is the current waveform which satisfies the conditions required for proper control.

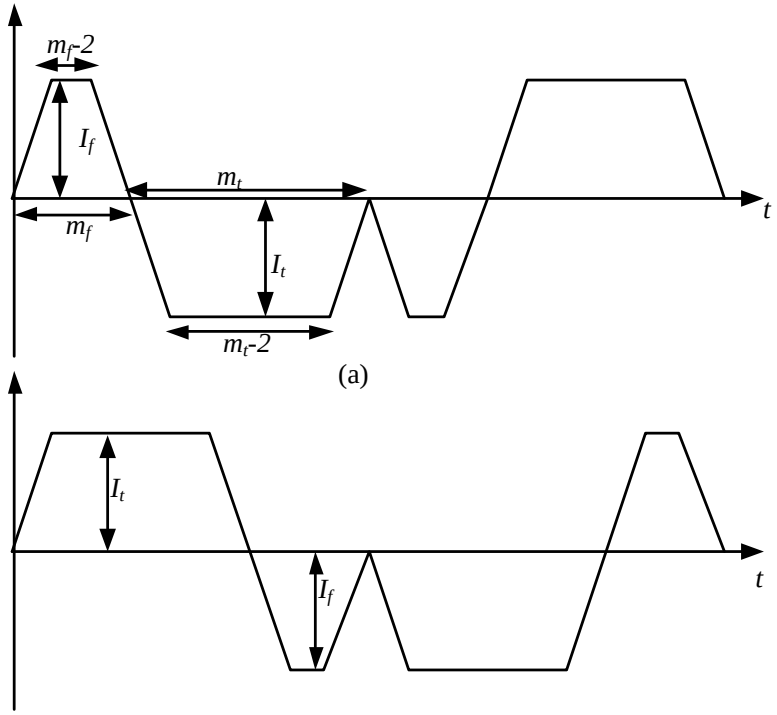

Figure 2-1. Trapezoidal stator current waveform with torque current leading field current (a) and field current leading torque current (b).

The stator winding layout of the machine is also designed to fulfill the requirements for BDCE control. For an M_p-phase induction machine, the phases are divided into three groups of $Mp\ /\ 3$ phases each, where M_p is the total number of phases and is a multiple of three. An appropriate ratio of the number of field phases (m_f) to the number of torque phases (m_t) is determined as described in [34]. By analysing the developed power, the developed torque and the rotor copper losses of the machine, it was realised that there is an optimal ratio of m_f/m_t for a BDCE controlled machine to produce maximum torque with minimum losses. It was noted that the number of torque phases should be as large as possible. However, an increase in m_t increased the level of saturation. The analysis of the stator copper losses showed that the minimum losses occur when I_t and I_f are approximately equal in magnitude. This implies that the values of I_f and I_t should be selected such that I_t and I_f are approximately equal such that there is limited stator and rotor yoke saturation [34].

The trapezoidal stator current is constructed considering the number of phases M_p, the number of field-producing phases, m_f, the number of torque producing phases, m_t and the polarity of the torque current as shown in Figure 2-1. Once the first single-phase current has been constructed, the other stator current waveforms are constructed by phase shifting the first waveform by φ radians. An expression for the phase angle φ is given in [34] as:

$$\varphi = \frac{2\pi}{3}(\mathrm{z}-1) + \frac{\pi}{M_p}(i-1) \qquad (2\text{-}1),$$

where, z is the group index (1, 2 or 3) and i is the phase index. A twelve-phase machine with three field phases and nine torque phases is considered as an example. The number of field and torque phases is chosen to satisfy the condition in [34] that the ratio $m_{f/}m_t$ can be between 0.25 and 0.50 and that fewer field phases can be used as the machine gets bigger. For a twelve-phase machine, each group has four phases and the phases are spaced by $\pi/12$ radians (15 electrical degrees). Figure 2-2 shows the twelve-phase stator current waveforms with the torque current leading the field current.

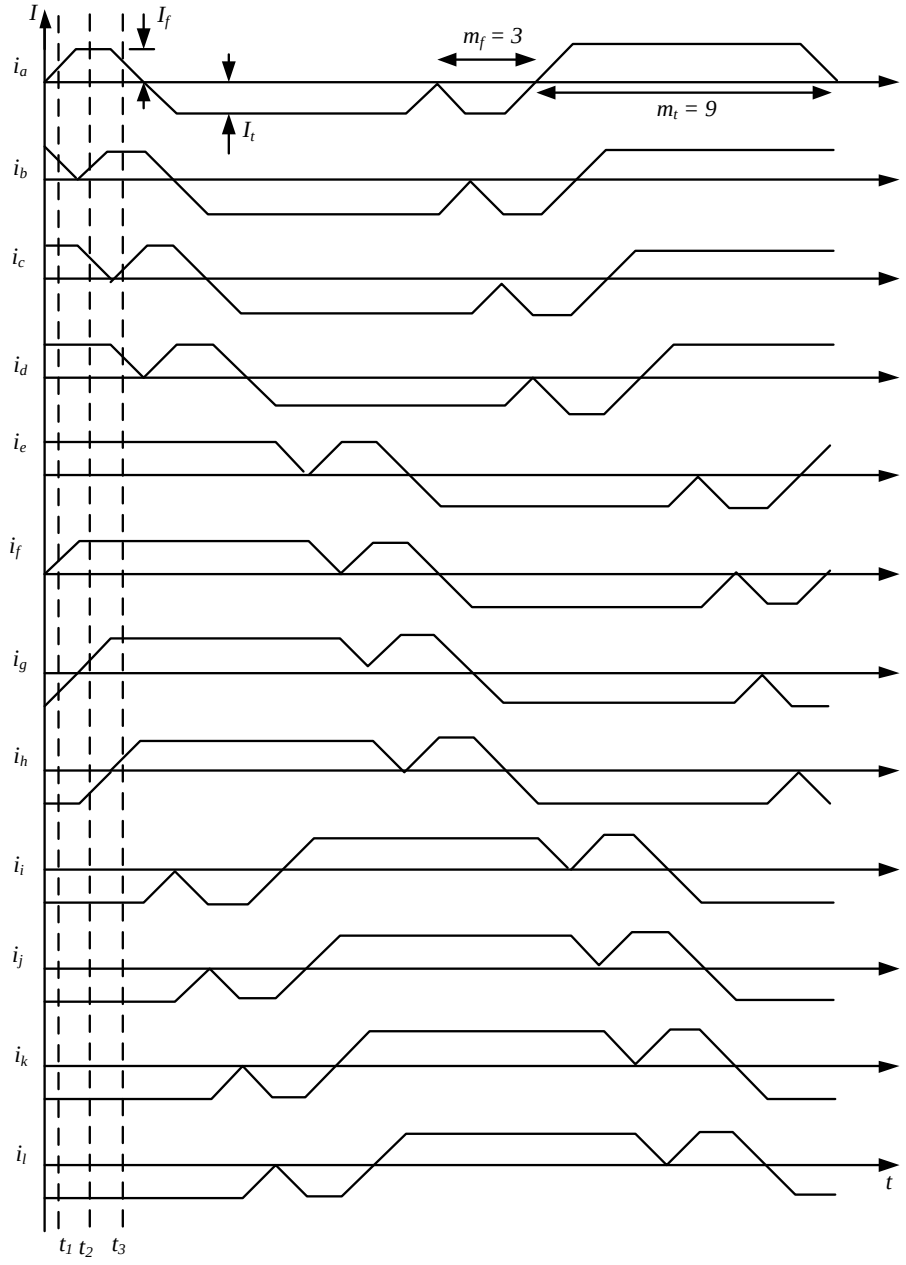

Figure 2-2. Twelve-phase stator current waveforms used in BDCE control of a twelve phase induction machine

2.2 Determination of the Stator Winding Layout

The stator winding layout is determined by selecting a time instant in the multiphase induction machine stator current waveforms and determining the torque phases and the field phases. In this example, time t_1 in Figure 2-2 is chosen. For proper operation, the field-producing phases should be next to each other and the torque-producing phases should be next to each other at each time instant. Phases "A, G and H" are acting as the field phases at time t_1. Figure 2-3 shows the phasor diagram for the twelve stator phases determined by examining the phases at time t_1.

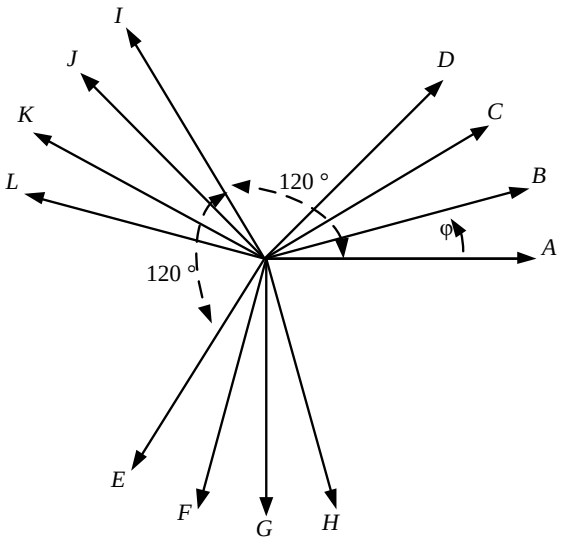

Figure 2-3. Phasor representation of the twelve-phase induction machine stator winding connection.

The angle φ is the phase angle between any phase and the reference phase, phase "A". For the phases A, G and H to act as field-producing phases at the same time, it implies that the phases should be wound next to each other. Considering times, t_1, t_2 and t_3, it can be seen that the winding layout suggested in Figure 2-3 gives the required operation. The stator is therefore wound following the layout in Figure 2-3.

The expression for the number of slots that can be used in a multiphase induction machine with a single layer concentrated winding layout under BDCE control is given in [46] as:

$$M_s = 2pM_p \tag{2-2}$$

where p is the number of pole pairs and M_p is the number of stator phases. This implies that a four-pole, twelve-phase induction machine is designed with 48 stator slots for a single layer concentrated winding layout. From Figure 2-2 and Figure 2-3, the stator winding layout for the twelve-phase machine can be deduced. Figure 2-4 shows a quarter of the twelve-phase, four pole induction machine stator winding layout designed for BDCE control by considering the time instant t_1 in Figure 2-2.

The crosses in the figure show current flowing into the page and the dots show current flowing out of the page. The small circles show that the magnitude of the current is of the half the maximum value of the current at that instant. The direction of the current and the polarity of the winding connection to the supply are of importance in determining the direction of the magnetic field in the air gap when stator currents are supplied to the machine. The direction of current in the coils changes as the motor rotates and therefore the directions shown in Figure 2-4 are at time t_1 of Figure 2-2. The stator is wound such that when supplied with an appropriate trapezoidal stator current waveform, a rotating magnetic field is produced in the air gap. The stator phases act alternately in time as field-producing or torque-producing phases.

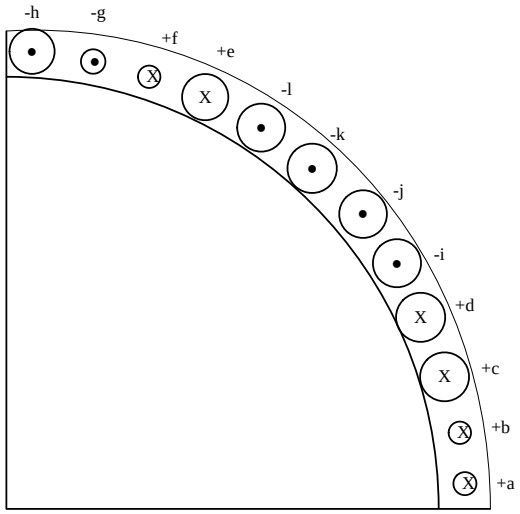

Figure 2-4. Stator winding for a twelve-phase induction machine with three field phases and nine torque phases.

2.3 Brush-DC Equivalent Control Principle of Operation

The stator winding layout and the stator current waveforms are designed such that when appropriate trapezoidal current waveforms are applied to the stator, a moving magnetic field is produced in the air gap. When the stator currents of Figure 2-2 are applied to a twelve-phase cage rotor induction machine with the stator winding layout of Figure 2-4, a moving air gap magnetic field is produced. At each time instant, this field is produced by three field phases. It can be observed by considering the three different time instants that each phase acts alternately in time as a torque- or as a field-producing phase. The field around the air gap for half the induction machine stator at the three time instants is shown in Figure 2-5 with $I_t = 0$. The figure shows that the flux is moving with time as phases act alternately in time as field- or torque-producing phases.

The moving magnetic field produced by the field phases will induce phase voltages in the rotor windings. With the rotor windings shorted, rotor currents will flow and these flowing currents produce a magneto-motive force (mmf), F_r. As the machine rotates, the overall mmf in the air gap, F is distorted by an angle α shown in Figure 2-6. The magnitude of the air gap flux density is reduced

because of this distortion. By supplying an appropriate amount of I_t on the stator torque-producing phases, an mmf, F_t is produced that cancels the distortion and the reduction in air gap flux density caused by F_r. In this way, the air gap flux density magnitude is kept constant. Therefore, it is necessary for F_t to be equal to F_r in BDCE control. This is the balanced mmf condition; ($F_t = F_r$) whereby the mmf produced by the torque producing stator phases is exactly equal and opposite of that produced by the rotor currents [34]. Figure 2-7 shows the mmf phasor diagram under balanced mmf conditions.

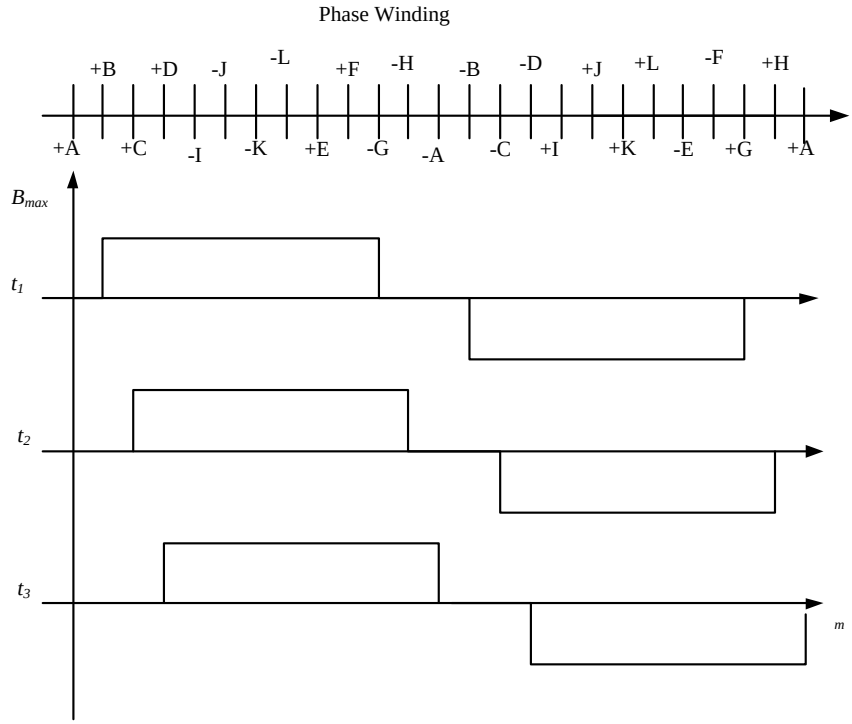

Figure 2-5. Moving magnetic field for half of the twelve-phase machine stator windings at times t_1, t_2 and t_3 with $I_t = 0$.

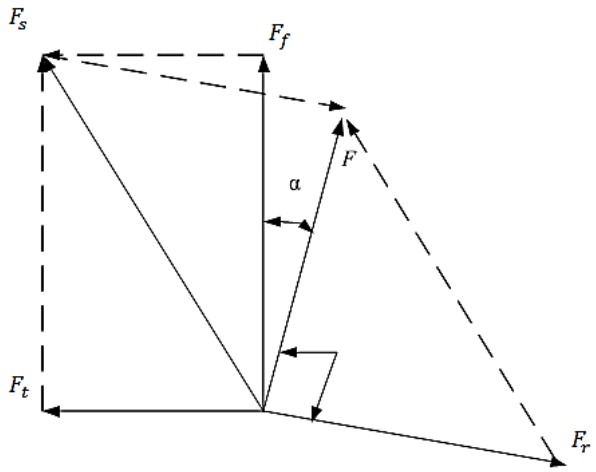

Figure 2-6. MMF phasor diagram for a BDCE controlled induction machine with flux distortion due to rotor mmf.

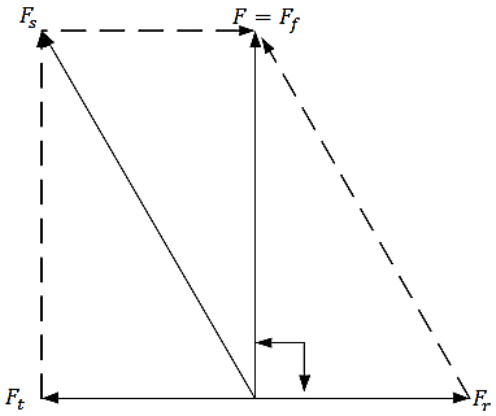

Figure 2-7. MMF phasor diagram for a BDCE controlled induction machine at balanced mmf condition.

As the machine rotates at a slip speed of ω_{sl} rad/s, a quasi-square wave voltage is induced in the rotor phases due to the rotating air gap magnetic flux. This flat-topped voltage has a value given in [46] as:

$$E_r = 2N_r B l \omega_{sl} r_g \tag{2-3}$$

where N_r is the number of turns (bars) per rotor phase, B is the air gap magnetic flux density, l is the stack length and r_g is the air gap radius. Since the rotor bars are shorted, rotor currents flow in the bars and the value of the induced current per rotor phase is given by:

$$I_r = \frac{E_r}{R_r} \tag{2-4}$$

where R_r is the rotor phase resistance. Considering equations (2-3) and (2-4), the rotor phase current is given by:

$$I_r = \frac{2N_r B l \omega_{sl} r_g}{R_r} \tag{2-5}$$

The rotor mmf produced in the nine-phase machine is given in [46]:

$$F_r = m_{ra} N_r I_r \quad , \tag{2-6}$$

where m_{ra} is the number of active conductors carrying the current which produce the mmf , N_r is the number of rotor turns (bars) per phase.

At any time instant, the effective value of the the field mmf is given by:

$$F_f = (m_f - 1) N_s I_f \tag{2-7}$$

where m_f is the number of field phases, N_s is the number of stator turns per phase and I_f is the magnitude of the field current. Similarly, the torque mmf is given by:

$$F_t = (m_t - 1) N_s I_t \tag{2-8}$$

where m_t is the number of torque phases and I_t is the magnitude of the torque current.

Under balanced mmf conditions, the rotor mmf is equal to the torque mmf. This implies that:

$$m_{ra}N_rI_r = (m_t - 1)N_sI_t \tag{2-9}$$

From (2-9), the value of the rotor current under balance mmf conditions is given by:

$$I_r = \frac{(m_t-1)N_sI_t}{m_{ra}N_r}. \tag{2-10}$$

The magnitude of the torque current I_t required to establish the balanced mmf conditions is found by equating the torque mmf to the rotor mmf and solving for I_t.

$$m_{ra}N_r\frac{2N_rBl\omega_{sl}r_g}{R_b} = (m_t - 1)N_sI_t \tag{2-11}$$

therefore:

$$I_t = \frac{2m_{ra}{N_r}^2r_gBl}{(m_t-1)R_rN_s}.\omega_{sl} \tag{2-12}$$

It can be observed from equation (2-12) that there is a relationship between the magnitude of the torque current and the slip speed. Assuming that the rotor resistance does not change significantly as the machine runs, and that there is a constant air gap flux density in the machine, then there is a constant relating the torque current to the slip speed. The work presented in [46] showed that there is a control gain, k, representing the relationship between I_t and the slip speed ω_{sl}which arises from the balanced mmf condition and is essential for proper BDCE control of multiphase induction machines.

$$k = \frac{\omega_{sl}}{I_t} \tag{2-13}$$

where k is the control gain and ω_{sl} is the slip speed. Considering equations (2-12) and (2-13) it can be observed that:

$$k = \frac{(m_t-1)R_rN_s}{2m_{ra}{N_r}^2r_gBl} \tag{2-14}$$

The other variable in equation (2-14) depend on the physical motor design parameters but the flux density B and the rotor phase resistance can change while the machine is in operation. A change in the value of the constant k directly affects the magnetic flux density and hence the balance mmf condition.This has been demonstrated in [46] where it was shown experimentally that the developed torque is sensitive to changes in the control gain. The control gain should be kept constant in order to maintain the balanced mmf conditions.

2.4 The BDCE Controller

The BDCE control method is completed by executing the control algorithm in software. The complete schematic diagram of the control system utilizing a hysteresis current controller on a nine-phase induction machine drive is shown in Figure 2-8.

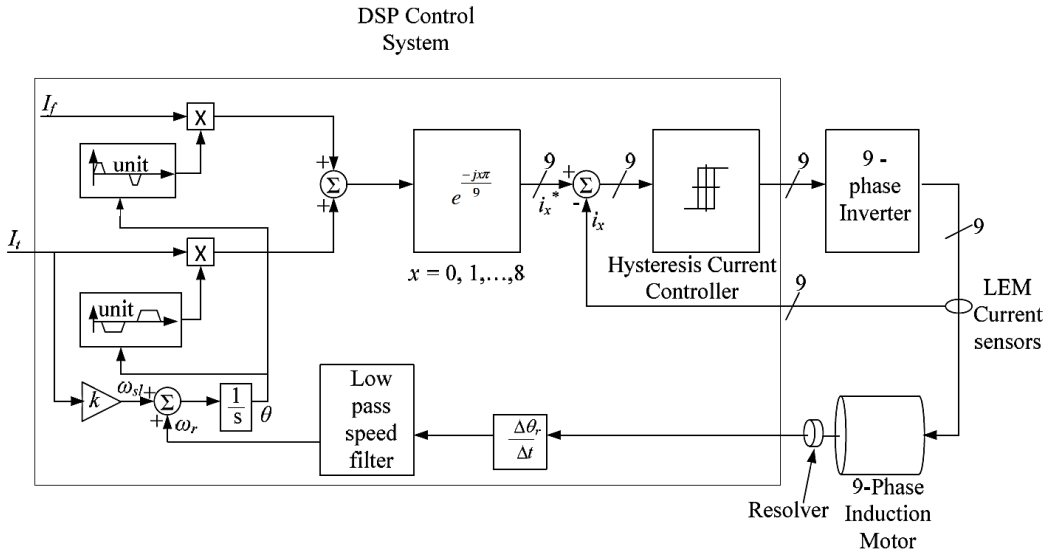

Figure 2-8. Schematic diagram of the BDCE controller utilizing a hysteresis current controller on a nine-phase induction machine drive.

The inputs to the control system are the magnitudes of the torque current I_t and the field current I_f as determined by the required flux and torque respectively. The field current is fixed according to the required air gap flux density in the machine. The torque current is adjusted according to the torque requirement. In software, look up tables are used to produce the reference currents used in the current controller. The value of the current in the unit field current look up table is multiplied by the reference value of I_f to determine the field current. The torque current is determined by multiplying the value of the current in the unit torque look up table by the reference torque current I_t. A reference stator current waveform is generated by combining the field current and the torque current at each time instant as shown in Figure 2-9.

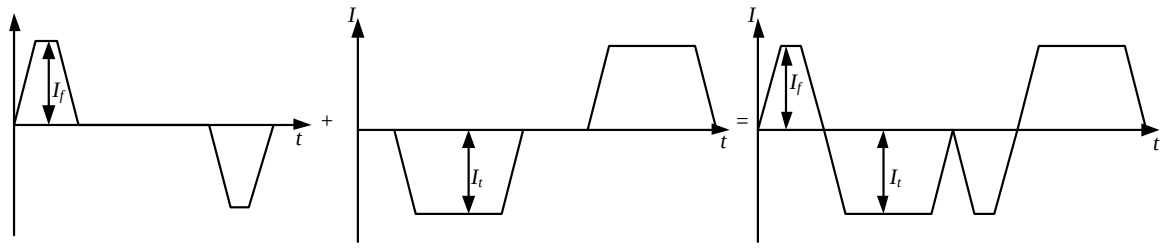

(a) Field current component

(b) Torque current component

(c) Full current waveform

Figure 2-9. Generation of the reference stator current from look up tables.

Since the phases are shifted by a defined phase angle, a phase shifter is used to produce the nine stator current waveforms. The reference waveforms are fed to the current controller where they are compared with measured current values. The comparison produces a difference which is compared to the hysteresis band value to produce inverter switching signals. A nine-phase inverter is used to

supply power to the nine-phase induction machine. As the motor rotates, a resolver attached to the shaft is used to measure the angular position of the rotor. This angle, θ is calculated in software and is used to determine the actual rotor speed, ω_r by calculating the rate of change of the angle with time.

$$\omega_r = \frac{d\theta}{dt} \tag{2-15}$$

The calculated rotor speed is added to the slip speed, ω_{sl} to determine the synchronous speed, ω_s.

$$\omega_s = \omega_r + \omega_{sl} \tag{2-16}$$

The calculation of the slip speed is done by multiplying the torque current magnitude, I_t and the control gain, k so that the slip speed and the torque current ratio is always constant to maintain the balanced mmf condition.

$$\omega_{sl} = k * I_t \tag{2-17}$$

The synchronous speed is used to calculate the synchronous position angle θ_s for use in the look up tables.

$$\theta_s = \int \omega_s dt \tag{2-18}$$

Current transducers are used to measure the phase currents. The value of the current is manipulated through current measuring cards for use in the DSP controller. Analogue to digital converters (ADCs) are used to convert the measured analogue signals to digital values that can be used in software. The ADC modules are connected to a Field Programmable Gate Array (FPGA) module which pre-processes the data before it can be used in the DSP. The DSP handles the computations while the FPGA handles communication with peripheral devices.

2.5 BDCE Control of the Nine-Phase Cage Rotor Induction Machine

The stator phases of the nine-phase induction machine are divided into three groups of three phases each. The phase groups are spaced by $2\pi / 3$ radians (120 electrical degrees).while the phases within each group are spaced by $\pi / 9$ radians (20 electrical degrees). Table 2-1 shows the phase grouping used in the BDCE control method for the nine-phase induction machine drive.

Table 2-1. Nine phase BDCE controlled induction machine phase grouping.

Phase Group Number	1			2			3		
Phase Label	A	B	C	D	E	F	G	H	I
Electrical Angle (^{0})	0	20	40	120	140	160	240	260	280

Phase "A" is the reference phase at the 0 degree position. The other phase angles are produced by phase shifting phase "A" by the phase angle φ calculated using equation (2-1), Figure 2-10 shows the nine-phase stator current waveforms used in the control of a nine-phase machine with three field phases and six torque phases. I_f is the magnitude of the field current and I_t is the magnitude of the torque current.

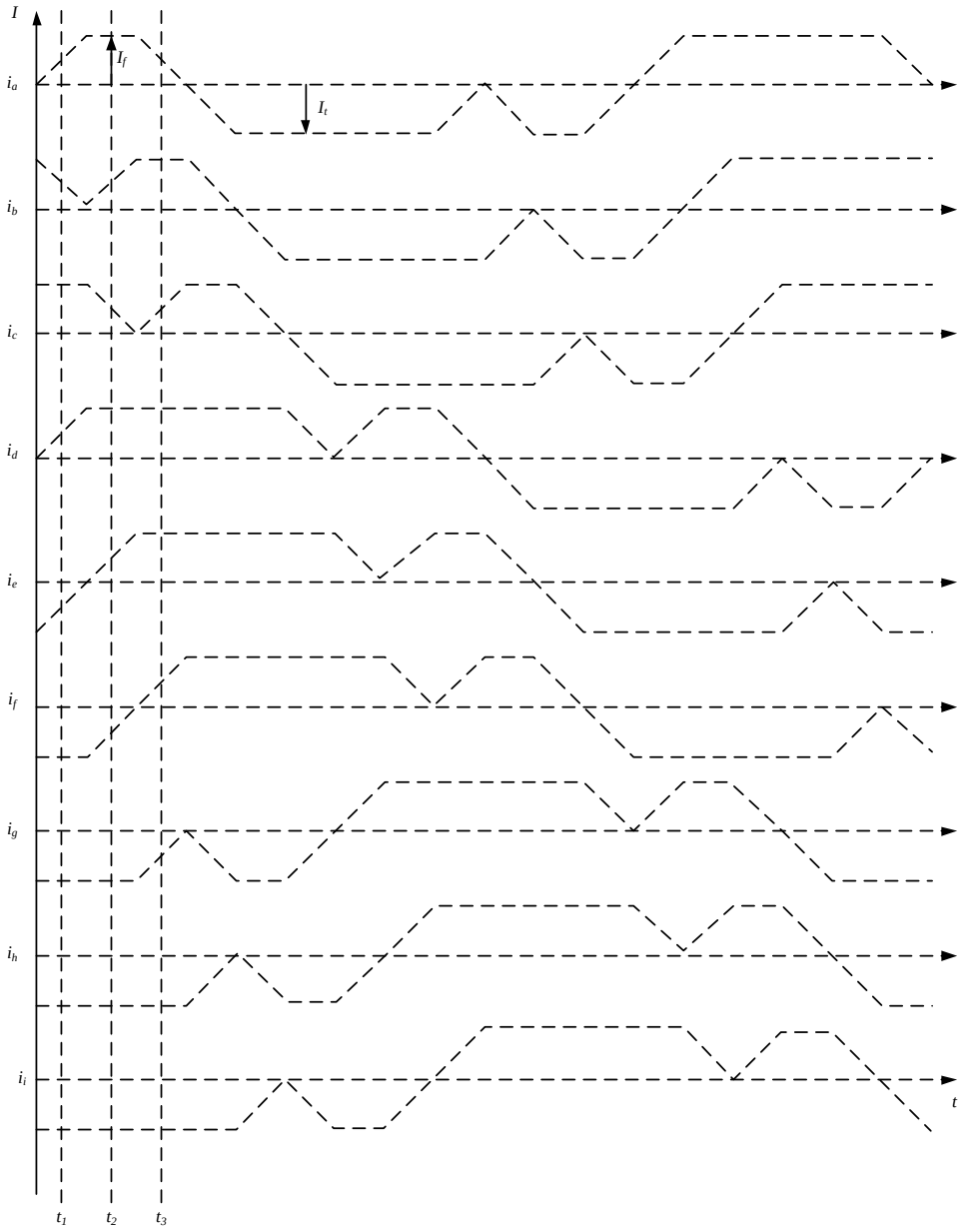

Figure 2-10. Nine-phase trapezoidal stator current waveforms for a BDCE controlled nine-phase induction machine.

Considering the time instants t_1, t_2 and t_3, it can be observed that the phases act alternately in time as either torque- or flux-producing phases as shown in Table 2-2. These observations are used to design the stator phase winding layout. Figure 2-11 shows the stator winding layout for the nine-phase

induction machine controlled using the BDCE method. The phases acting as field phases are wound next to each other and the machine operates as required.

Table 2-2. Magnitude and polarity of nine-phase stator currents

	Current Value		
Time →	t_1	t_2	t_3
Phase Label ↓			
A	$I_f/2$	I_f	$-I_t$
B	$I_t/2$	I_f	$-I_t/2$
C	I_t	$I_f/2$	$I_f/2$
D	$I_t/2$	I_t	$I_t/2$
E	$-I_f/2$	I_t	I_t
F	$-I_f$	$I_t/2$	I_t
G	$-I_t$	-I_t/2	$-I_f$
H	$-I_t$	-I_t	$-I_f/2$
I	I_t	-I_t	$-I_t/2$

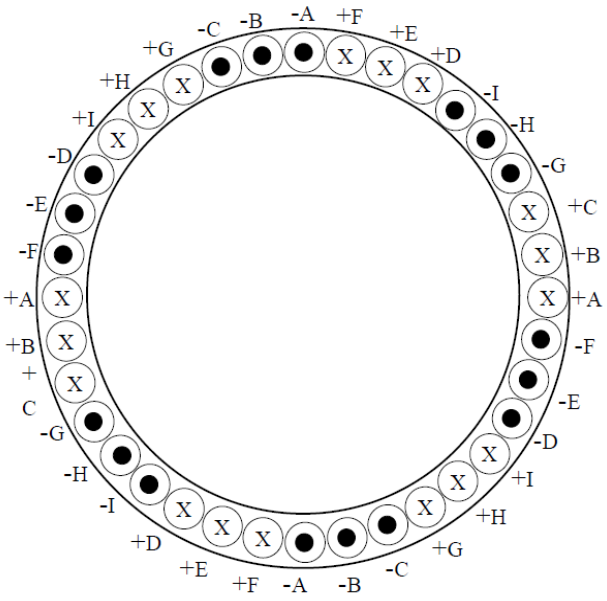

Figure 2-11. Stator winding layout for a BDCE controlled four-pole, nine-phase cage rotor induction motor utilizing three field phases and six torque phases [46].

If the stator current waveforms of Figure 2-10 are supplied to the nine-phase cage rotor induction machine with the stator winding layout shown in Figure 2-11, a rotating magnetic field is produced in the air gap. Figure 2-12 shows the change in the magnetic flux density with time. It is this rotating magnetic field which is responsible for inducing voltages in the rotor bars. The interaction between

the air gap magnetic field and the current in the rotor bars results in torque being developed in the rotor.

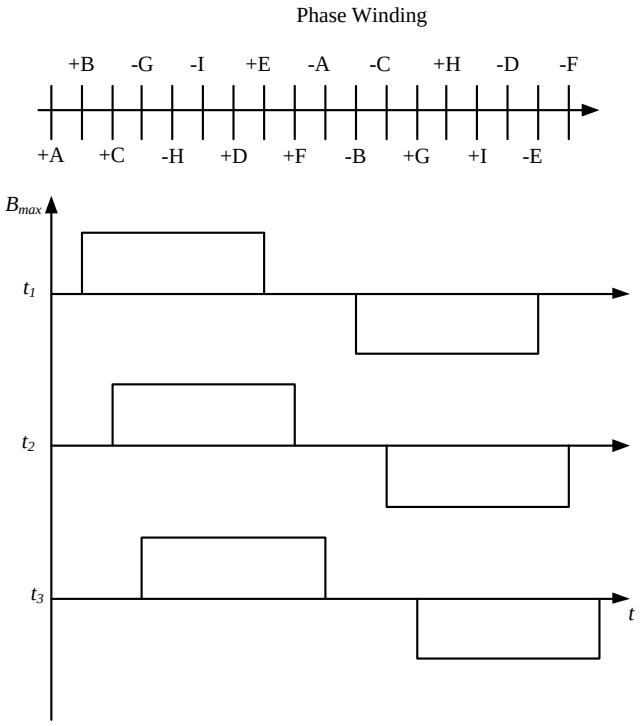

Figure 2-12. Change in magnetic flux density around the air gap of half of the nine-phase induction machine with time.

The nine-phase cage rotor machine presented in this thesis has three field phases and six torque phases. It is a rewound three-phase induction machine with thirty six stator slots and a twenty eight slot cage rotor. The design parameters of the nine-phase induction machine are shown in Table 2-3.

Table 2-3: Parameters of the nine-phase cage rotor induction motor

Rated Power, P_n	11kW
Air-gap length, g	0.5mm
Stack length, l	127mm
Rotor radius	84.5mm
Number of field phases, m_f	3
Number of torque phases, m_t	6
Number of rotor bars, M_r	28
Number of stator slots, M_s	36
Number of series turns per stator phase, N_s	170
Torque current, I_t	5.5A
Field current, I_f	5.83A
Operating speed	1466 rpm
Flux density	0.7T

2.6 Summary

The BDCE control method has been described in this chapter. It has been shown that the trapezoidal stator currents produce a rotating field in the air gap when applied to the stator windings in the correct sequence. It has been shown that the minimum number of phases required in an induction machine for BDCE control is six. The importance of the control gain in ensuring balanced mmf conditions has been explained. The BDCE control method is less complicated than the vector based control methods because there are no complex transformations used to determine the flux and torque currents. The BDCE control technique presented in this thesis uses a delta modulated current controller. The current controller is used to generate the PWM signals for the nine-phase inverter which supplies power to the nine-phase induction motor. The delta modulation technique is discussed in chapter 3 and a model for simulation and practical implementation is developed.

Chapter 3 The Delta Modulated Current Controller

The current controller used in the BDCE control method generates the PWM switching signals for controlling the operation of the inverter. The delta modulated current controller is used in this study and hence the background information about the delta modulation techniques is presented in this chapter. A presentation of the previous work done on the implementation of the delta modulated current controllers in PWM inverter applications is given. The development of the delta modulated current controller is presented to produce a model that can be used for both simulations and practical implementation. The delta modulation algorithm is also developed for digital implementation.

3.1 Introduction

Delta modulation is a variation of pulse code modulation used in communication systems. It is an analogue to digital conversion method which presents a simple way of encoding and decoding voice and video messages over different communication links. The modulation technique can also be used in inverter applications to produce the PWM signals required to control the power electronic inverters supplying power to electrical machines [54],[55]. The delta modulator uses an integrator as a low pass filter which produces an estimate of the modulating signal in the same way that a delta modulation receiver operates in communication systems. The estimated signal is used as the carrier signal in the delta modulator.

Figure 3-1 shows the waveforms produced through the use of rectangular wave delta modulation. The modulating signal, V_R is the waveform of the signal to be transmitted. The estimated signal, V_F is the carrier waveform which is compared to the modulating signal to determine the PWM output, V_0. A two level quantizer is used to decode the value of the difference between V_R and V_F and produce a pulse of magnitude ±E. A sample and hold block is used to hold the quantizer output at a constant value until the next sampling instant.

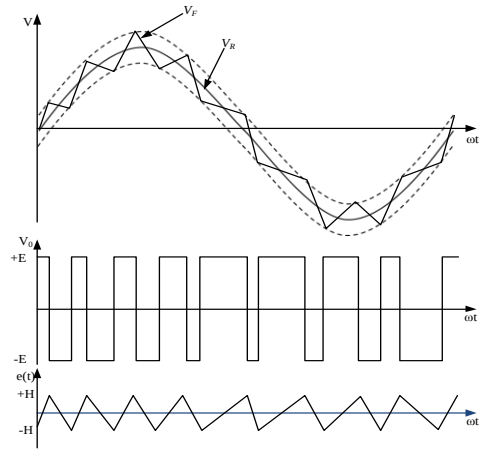

Figure 3-1. Delta modulation signals for rectangular wave delta modulation: (a) carrier, V_F and reference signal,V_R (b) quantizer PWM output, (c) error signal [47].

The simplicity of delta modulation made it attractive for use in current controlled PWM inverters [50],[54]-[57]. It was observed that delta modulation has inherent constant v/f control without requiring additional circuitry. The other benefits of using delta modulation in PWM inverters are that it allows smooth transition from the PWM mode to the constant pulse mode and has inherent lower order harmonic attenuation because of the filter in the feedback loop. The delta modulator was first proposed in [47], presented in [50] for software implementation and analysed in [56]-[57] forming the basis for its use in variable speed drives. The other alternative current controllers popularly used in PWM inverters are the PI controller and the hysteresis controller presented in detail in Appendix B.

3.2 Literature Review on Implementation of Delta Modulation in PWM Voltage Source Inverters

Ziogas [47] introduced the use of delta modulation for static PWM inverters. The delta modulation technique was implemented using op-amp circuits on a single-phase induction motor. The constant Volt per Hertz (v/f) control characteristic of delta modulation was demonstrated in the measured results. The work introduced the use of delta modulation only for a single-phase system and theoretical analysis of the control system was not presented. Although delta modulation has these advantages, its major drawback is that it enters the idle state when the reference signal has a constant value for the greater portion of the waveform. This causes granular noise and hence the output waveform will be a poor representation of the reference signal [52], [53].

The delta modulator was implemented on electronic circuitry which is prone to failure. A research was done by Strivastava et al [50] to implement the technique in software. Software implementation is easier than electronic circuit implementation because the electronic component limitations are eliminated.

Due to the introduction of digital signal processors (DSPs) and related micro-computers, the delta modulation algorithm can be executed in software thereby removing the need for electronic circuit hardware which can cause unpredictable system failures [47], [57]. In [47], the switching sequences corresponding to specified set of parameters were stored in a look-up table. The parameters used are the reference signal, the sampling frequency and filter coefficients. The look-up table was used to determine the switching states of the inverter depending on the values of the variables in the look-up table. The method proved to be more effective than natural sampling and regular sampling since the estimated carrier signal closely followed the reference signal. The method enabled operation optimization by varying the delta modulator parameters in software but had high system memory demand for storing the look-up tables and also for computing the input values to the look up tables.

In most delta modulation applications, the input reference signal to the delta modulator is a sinusoidal waveform [49]-[51],[56],[57]. The use of sinusoidal modulating signals causes limited

input voltage transfer and the voltage transfer of a sinusoidal modulating signal is at most 87% [47], [58]. This can be improved by over-modulation but with loss of performance because over-modulation introduces distortions in the output waveform. It also causes large sub-harmonic currents and reduces the fundamental voltage gain.

It has been shown in [58] and [59] that a flat topped modulating signal has better voltage transfer characteristics and less total harmonic distortion than conventional sinusoidal signals. Third harmonic injection was used to generate a flat topped signal from a sinusoidal signal as presented in [27]. The use of a trapezoidal modulating signal was proposed in [58] and it had the advantages of improving voltage transfer, harmonic reduction and elimination of some harmonics by proper selection of a triangular factor;

The delta modulation technique has variations which are; linear-delta modulation [47], [53], sigma-delta modulation [57], rectangular wave delta modulation [60] and adaptive delta modulation. [61], [62]. The techniques are differentiated by the position of the filter, the use of a hysteresis comparator and the determination of the parameters of the delta modulator.

3.3 Linear Delta Modulation

The delta modulator converts an analogue input reference signal, V_R to a binary output, V_o which is a series of positive and negative pulses representing the analogue input. The number of positive and negative pulses depends on the slope of the input signal. If the slope is positive, there will be more positive pulses and if the slope is negative, there will be more negative pulses. Linear delta modulation is the technique in which a forward comparator is used to compare the carrier signal to the reference signal to generate the error signal. Figure 3-2 shows the conventional linear delta modulation block with a sample and hold block which dictates the maximum switching frequency.

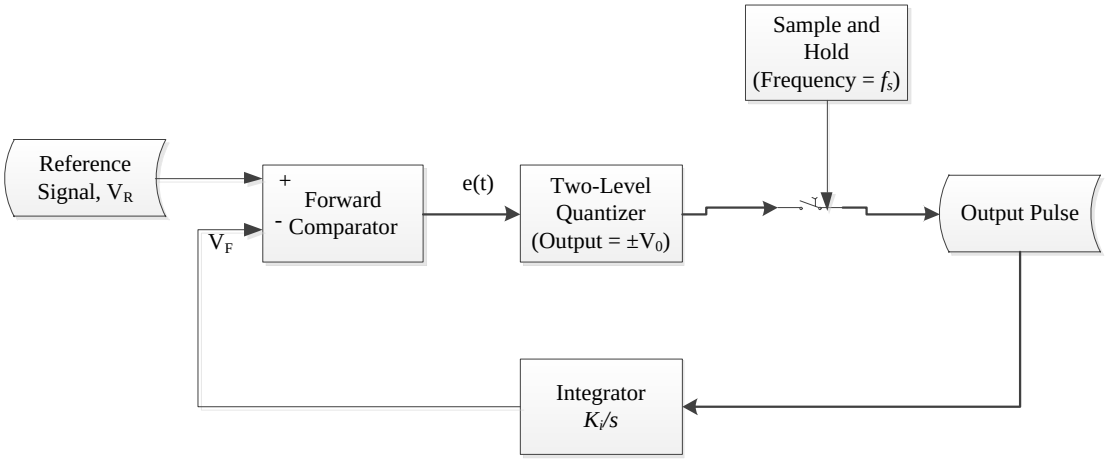

Figure 3-2. Block diagram of the conventional linear delta modulator.

When there is no input to the modulator, an idle condition occurs. This is the condition whereby the quantizer output alternates between the negative value and the negative value at regular intervals. If an input is fed to the modulator, the error value *e(t)* changes according to the slope of the input. The error is the difference between the modulating signal and the carrier.

$$e(t) = V_R - V_F \tag{3-1}$$

The error *e(t)* is quantized to $\pm V_0$ according to its sign using the signum function. The two level quantizer implements the signum function. Mathematically, the signum function is represented by the expression:

$$sgn\big(e(t)\big) = \begin{cases} +V_0; & e(t) \geq 0; \\ -V_0; & e(t) < 0. \end{cases} \tag{3-2}$$

Figure 3-3 shows the two-level quantizer which implements the signum function. The output of the two-level quantizer has the same sign as the error value.

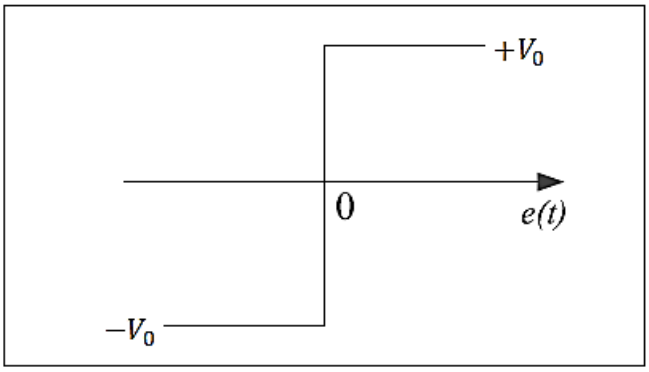

Figure 3-3. The two-level signal quantizer implementing the signum function.

A sample and hold block is used to sample the quantizer output at a constant frequency, f_s. It holds the output at a constant value until the next sampling instant. When a positive pulse is produced, it is integrated thereby causing the value of the carrier, V_F to increase by a value proportional to $K_i * V_0$. The new value of V_F is subtracted from V_R to produce a new error signal. If the value of *e(t)* remains positive, the quantizer output remains positive and the process continues until the error value becomes negative. When it becomes negative, a negative pulse is produced in the quantizer. The output is integrated and the value of V_F is reduced. In this way, the modulator always tries to minimize the error value and make the carrier track the reference signal more accurately. When the slope of the reference signal is zero, the idle condition occurs and the quantizer output alternates between the positive value and the negative value at regular intervals.

An expression of the carrier signal can be deduced as shown in [50] and is expressed as:

$$V_F = \sum_{x=0}^{n} V_0 * sgn\big(V_R(xT) - V_F(xT)\big).\delta(t - xT) \tag{3-3}$$

where $V_R(xT)$ is the value of the reference signal at the x^{th} clock instant. $V_F(xT)$ is the value of the carrier signal at the x^{th} clock instant and T is the sampling period of the sample and hold block.

The carrier signal can only track the reference accurately if an overload condition is considered in the design of the modulator. The condition is that the slope of the reference signal must never be greater than that of the carrier signal. The slope overload condition therefore depends on the slope of the reference signal, the magnitude of the quantizer output, the frequency of the reference signal and the sampling frequency of the sample and hold block. In [50], a sinusoidal reference signal was considered and it was deduced that the maximum amplitude of the reference signal that satisfies the overload condition but without overloading the modulator is given by:

$$V_{Rmax} = \frac{V_{0*}f_s}{2\pi f_R} \qquad (3\text{-}4).$$

where f_R is the frequency of the reference signal.

When the overload condition depends on the frequency of the reference signal, it implies that the maximum value of the reference signal is limited by the frequency of the signal. This is the reason why delta modulation becomes unreliable at high frequencies. An alternative linear delta modulation technique can be used in which the overload condition is independent of the frequency of the reference signal. The alternative linear delta modulator uses an integrator at the input. Figure 3-4 shows the block diagram of the alternative delta modulator.

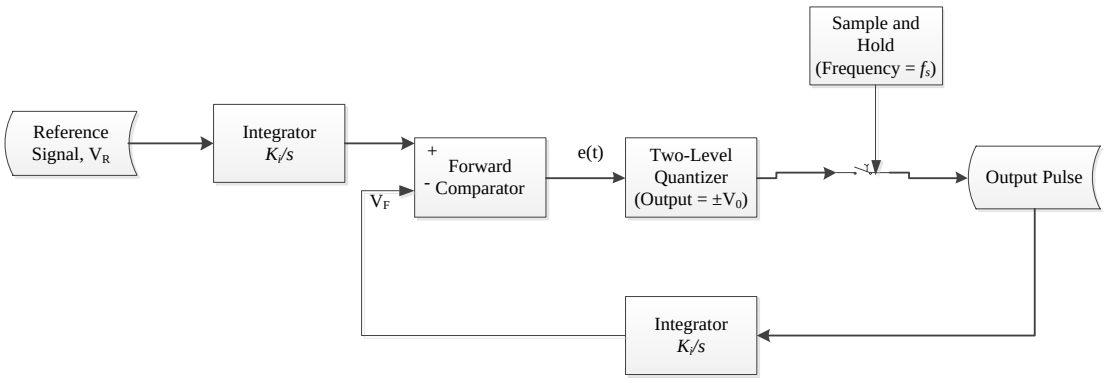

Figure 3-4. Alternative linear delta modulator using integrator at the input.

The input to the forward comparator is the integral of the reference signal. Considering a sinusoidal reference signal, the input to the comparator is given by:

$$V_{Ri} = K_i * \mathrm{V} \int Sin\ \omega_r t\ dt = -\frac{K_i V Cos\omega_r t}{\omega_r} \qquad (3\text{-}5)$$

where V is the magnitude of the reference signal and ω_r is its angular frequency. The slope of V_{Ri} is equal to $K_i V Cos\omega_r t$ and its maximum value is independent of the frequency of the input signal. The condition for the overload condition is determined by relative magnitude of the reference signal with respect to the magnitude of the quantizer output. The necessary condition for the overload condition is that the slope of the reference signal should be less than the slope of the carrier signal, that is:

$$V * K_i \leq V_0 * K_i \quad \text{(3-6).}$$

This implies that the integrator gain is no longer a design constraint and hence only the magnitudes of the reference signal and the quantizer output need to be monitored. If the integrator gain and the reference signal values are restricted, then the carrier will always track the reference accurately as long as the reference signal magnitude is less than the quantizer output value.

3.4 Sigma-Delta Modulation

The alternative linear delta modulator can be modified to produce the sigma-delta modulator. The two integrators in the alternative linear delta modulator are replaced by a single integrator in the feed forward loop. A unit feedback loop is used in this type of modulator. Figure 3-5 shows the sigma-delta modulator block diagram.

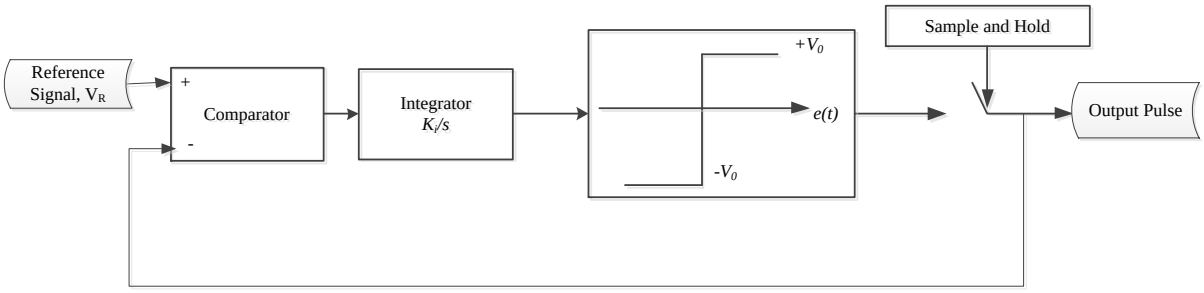

Figure 3-5. Block diagram of the sigma-delta modulator

Since the integrator is in the feed forward loop, the integrated error signal is quantized. This technique is useful where the reference signal energy spectrum is approximately flat. The integrator shapes the flat spectrum such that it has attenuations at high frequencies. This produces output pulses with lower harmonic content than linear delta modulation.

Considering a sinusoidal reference signal, it can be shown that the overload condition is independent of the frequency of the reference signal. In essence, sigma delta modulation is a variation of the alternative linear delta modulation technique.

3.5 Rectangular Wave Delta Modulation

The delta modulation techniques discussed above use a hard limiter without a hysteresis band to quantize the error signal. The switching frequency is determined by the sample and hold sampling frequency. Rectangular wave delta modulation differs from the above in that it uses a hysteresis comparator to quantize the error signal and may not use a sample and hold block. It is similar to a hysteresis controller except that an estimated value of the reference signal is compared to the reference signal while the hysteresis controller uses measured output values.

Figure 3-6 shows the rectangular wave delta modulator. The mathematical analysis of the performance of the delta modulation technique in this section is done using the rectangular wave delta modulator.

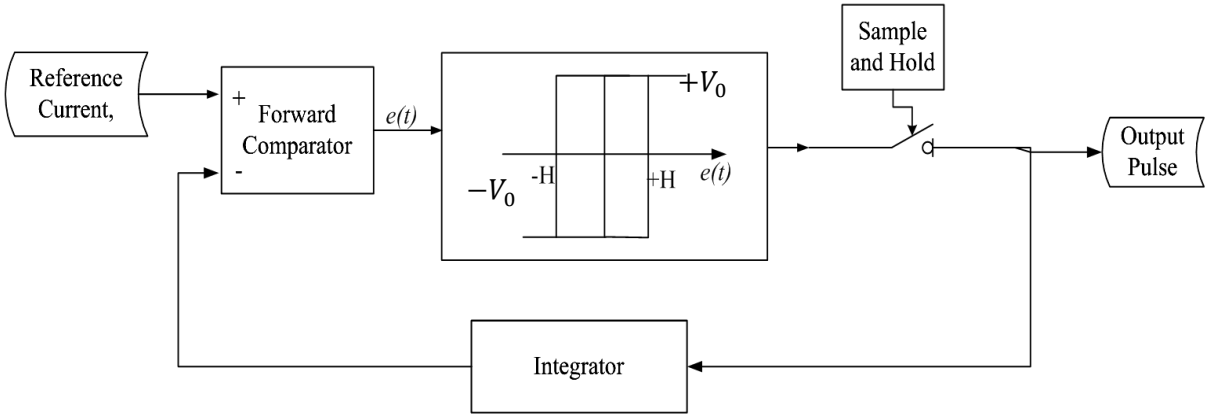

Figure 3-6. Block diagram of the rectangular wave delta modulator.

In literature [47],[49] - [51],[53],[57], the delta modulation technique is described for sinusoidal reference waveforms and hence the theoretical analysis is based on the use of a sinusoidal modulating signal. The performance of the delta modulator is determined by the following:

- Maximum slope of the reference signal, S_r.
- The two-level quantizer output magnitude, V_0.
- The magnitude of the delta window width (hysteresis band) , H.
- The sampling frequency of the sample and hold block, f_s and
- The integrator gain K_i.

Considering a reference modulating signal given by:

$$V_r = V\ Sin\ \omega_r t\ , \tag{3-7}$$

where, V is the amplitude of the reference signal and ω_r is the signal angular frequency, then the switching frequency and the duty cycle can be calculated as presented in [52]. The minimum window width and the carrier signal slope determine the maximum switching frequency. The values of these two parameters are selected such that the resulting switching frequency allows the switching devices to properly switch on and off before the next transition period. As a result, fast switching devices are more convenient for high switching frequencies.

The switching frequency of the delta modulator when a delta window (hysteresis band) is used without a sample and hold is given in [60] as:

$$f_s = \frac{{S_c}^2 - {S_r}^2}{4 * H * S_c}\ , \tag{3-8}$$

where, S_c is the slope of the carrier signal.

$$S_c = K_i * V_0 \tag{3-9}$$

The duty cycle of the PWM output is given by:

$$D = \frac{1}{2}\left(1 + \frac{S_r}{S_c}\right), \tag{3-10}$$

From equation (3-7), the slope of the reference signal is given by:

$$S_r = V * \omega_r * Cos\ \omega_r t, \tag{3-11}$$

When the reference signal is a constant value, then:

$$dV_r/_{dt} = 0 \tag{3-12}$$

$$\Rightarrow S_r = V * \omega_r * Cos\ \omega_r t = 0 \tag{3-13}.$$

The switching frequency is solely dependent on H and V_0. At this instant, f_s is maximum while the duty cycle $D = 0.5$. At the maximum frequency, there is no net power transfer between the source and the load due to the 50% duty cycle.

For the carrier V_F to track the reference V_R with minimum error,

$$\left|dV_R/_{dt}\right|_{max} \leq \left|dV_F/_{dt}\right|_{max} \tag{3-14}$$

This implies that

$$|V * \omega_r * Cos\ \omega_r t|_{max} \leq |K_i * V_0|_{max} \tag{3-15}.$$

If the magnitude of the reference signal changes unexpectedly while the filter (integrator) coefficient or gain and the quantizer output are fixed, the operation of the delta modulator is altered. Linear delta modulation runs into slope overload when the reference signal frequency becomes very high unless if the integrator gain or the quantizer output is adjusted accordingly. In this case, the maximum frequency is bound by the integrator gain and the quantizer output, assuming that the input signal magnitude is restricted.

For practical implementation in PWM inverters, it was observed in [63] that good performance is achieved if the switching voltage across the load is fed back and filtered to produce the carrier than when the quantizer output is used to reconstruct the modulating signal. This is because the switching voltage automatically includes the load dynamics which would need to be modelled if the quantizer output was used. The technique also has inherent error detection because the input to the filter is an indication of the changes occurring in the load.

The variations in the reference signal can cause unexpected performance when the variables considered in the analysis of the rectangular modulation are fixed. In order to enable predictable

performance when the reference signal or the load changes, adaptive delta modulation can be used. Adaptive delta modulation techniques can be complex to design but give good performance.

3.6 Adaptive Delta Modulation

When the properties of the carrier signal cannot be modelled using simple sinusoidal expressions and when there are random changes in the modulating signal, an adaptive technique is required to optimize system performance. The adaptive techniques are designed to adjust one or all of the delta modulator parameters in response to the changes in the modulating signal.

The quantizer output can be adjusted if the modulating signal has a variable frequency and if there are random changes in the slope of the reference signal. The delta window or the modulator time constant can also be adjusted for the same reason or if the magnitude of the modulating signal changes at random [49]. A detailed approach to adaptive delta modulated is presented in [61] where a variable frequency delta modulator is designed for a single-phase inverter. The design gives good harmonic performance as it eliminates the lower order harmonics.

In [62], the fixed window delta modulator and the variable window delta modulator are compared. It was observed that an adjustable window delta modulator gives stable switching frequency and this improves the performance of the inverter. Adaptive delta modulation makes use of predictive algorithms to adjust the desired parameter and this introduces complexities in the design of the system. The prediction and estimation of parameters should be accurate since any errors in the estimations negatively affect the performance of the whole system. The technique is demanding in system memory because a number of algorithms are run in parallel to achieve adaptive control.

3.7 Design of the Software based Delta Modulated Current Controller

In this study, the design of the delta modulated current controller is made simple by implementing the delta modulator in software rather than in hardware where the device limitations restrict the design optimization. Software control of the delta modulated PWM inverter allows parameter tuning without redesigning the overall control circuit. Different control parameters can be tested by changing their values in software and this makes the design simpler, faster and cheaper. The delta modulator is implemented in software and bilinear Z-transformations are used in the development of the digital integration algorithm.

3.7.1 Derivation of the Numerical Integration Algorithm

The integrator is used to estimate the reference signal in the delta modulator. The integration function can be deduced by considering a simple RC integrator. A first order integrator developed using an operational amplifier is shown in Figure 3-7. The circuit is the first step towards the development of the software based numerical integrator and the software based delta modulated current controller.

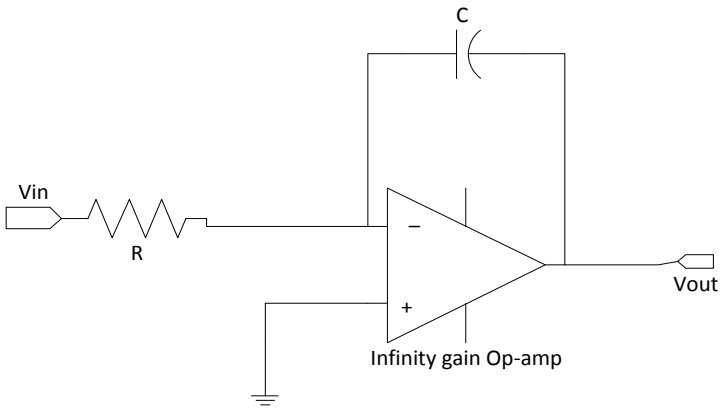

Figure 3-7. First order RC integrator circuit.

Assuming infinity op-amp gain, the transfer function of the integrator is given by:

$$\frac{Vout(s)}{Vin(s)} = -\frac{1}{RCS} \tag{3-16}$$

The integrator is implemented in software and therefore a discrete form of the integrator transfer function is used. Using conversion tables, to convert the transfer function from the Laplace transform to the Z transform, it is noted that:

$$s = \frac{2(1-z^{-1})}{(1+z^{-1})} \tag{3-17}$$

The transfer function of the integrator in the Z-transformation is therefore given by:

$$\frac{Vout(z)}{Vin(z)} = \frac{T(1+z^{-1})}{2RC(1-z^{-1})} \tag{3-18},$$

where *T* is the sampling period of the integrator and RC is the integrator time constant.

Rearranging (3-18), an expression for the integrator can be written as:

$$V_{out}(z) = \frac{T}{2RC}(V_{in}(z) + V_{in}(z-1)) + V_{out}(z-1) \tag{3-19}.$$

If $\frac{T}{2RC}$ is represented by a constant g_0 then (3-19) can be written as:

$$V_{out}(z) = g_0(V_{in}(z) + V_{in}(z-1)) + V_{out}(z-1) \tag{3-20}.$$

For digital implementation, the integrator is developed using unit delays and the complete delta modulation block is shown in Figure 3-8.

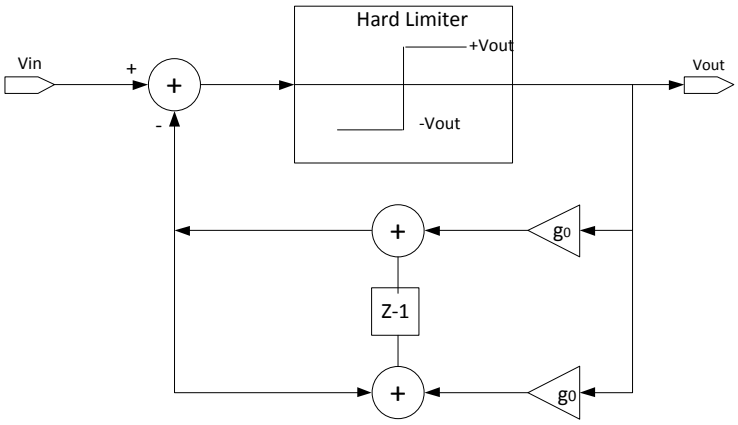

Figure 3-8. Delta modulator implementation using Z-transformation blocks.

The integrator time constant is determined by the maximum magnitude of the reference signal V_{max}, the maximum value of the op-amp output V_s, and the designed integrator "break frequency" at which the integrator output saturates. From [47], the time constant is given by:

$$RC = \frac{4V_s}{\pi * V_{in} * \Omega_{rb}} \qquad (3\text{-}21),$$

where Ω_{rb} is the break frequency. The designed break frequency for the input signal in this study is 55 Hz, hence $\Omega_{rb} = 2 * \pi * 55$. The maximum value of the reference signals is 11.66 and the designed maximum value of the op-amp comparator output is 12 for the delta modulator under consideration. Substitution of these values into the time constant equation (3-21) gives a time constant of 0.00381 seconds. Using a sampling frequency of 10 kHz, then the constant g_0 becomes 0.01312. This constant is used in the practical implementation of the delta modulator in the DSP controller program.

3.7.2 Design Considerations for the Delta Modulator

The performance of the delta modulator is dependent on the magnitude of the reference signal, the frequency of the reference signal, the integrator coefficient (gain) and the sampling frequency as discussed earlier on. The level of the reference signal should be in the medium input range for normal operation. A high input value overloads the decoder and a low input value causes the idle condition. The input signal frequency should also be in the medium range with the signal to noise ratio high enough to avoid overloading at low frequencies.

The sampling frequency is chosen such that it is high enough to allow accurate tracking of the reference signal and improve the signal to noise ratio. It should however be low enough to reduce the switching losses. The minimum value of the sampling frequency is determined by the Nyquist frequency criterion which states that the sampling frequency should be at least twice the highest frequency in the input signal. Sampling at higher than twenty times the Nyquist frequency rate is desirable to move the lower order harmonics to higher frequencies which are easier to filter.

The output of the quantizer is chosen such that the slope of the carrier signal is always greater than that of the reference signal considering that it is the value which is integrated to generate the carrier. However, for normal operation, the value can be between 50% and 150% of the maximum input signal amplitude [50]. The integrator gain depends on the variations of the sampling frequency. Simulations can be used to iterate the values of the gain for optimal performance.

3.7.3 Delta Modulated Current Controlled PWM Inverter Design Considerations

The PWM inverter control requirements are also considered when designing the current controller. The changes of the error signal in the delta modulator determine the switching sequence and the switching frequency of the inverter switches. The sampling technique for the delta modulator determines the amount of control than can be achieved on the sampling frequency.

Natural sampling is used in rectangular wave delta modulation. The switching instant occurs when the carrier signal falls out of the hysteresis band. This sampling technique causes the switching frequency to be highly dependent on the value of the hysteresis band as well as the slope of the reference signal. This technique is undesirable where a constant switching frequency is required. Adaptive delta modulation is required to achieve a constant switching frequency while using rectangular wave delta modulation.

Another sampling technique is the regular sampling technique whereby the reference signal and the carrier signal are sampled at regular intervals. The switching state is determined by the values of the signals at the sampling instant. The technique requires that the computation time of the processor must be less than the sampling period. If the computation time is longer than the sampling period, the delta modulator produces wrong results.

The switching frequency is also determined by the turn-on and turn-off times of the power electronic switches used in the inverter. For high frequency applications, fast switching devices are required. The sampling frequency of the modulator is therefore chosen such that the devices can be switched on and off completely before the next sampling instant. The sampling frequency must also allow the design of a dead band between switching instants to avoid the shoot through problem in the inverter legs.

The overall design of the delta modulated PWM inverter is shown in Figure 3-8. The various processes involved in the software implementation of the delta modulated current controller are shown in the figure.

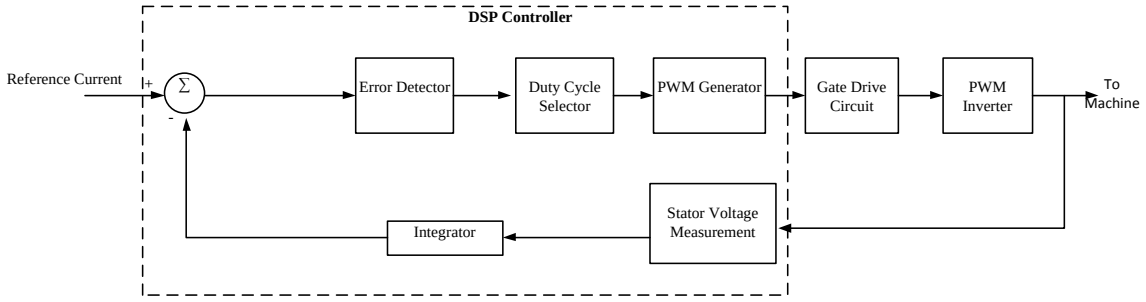

Figure 3-9. Block diagram of the delta modulated current controller implemented on a BDCE controlled induction machine drive.

3.8 Summary

In this chapter, the different delta modulation techniques have been discussed. The method of deriving the numerical integrator algorithm to be implemented in software has been presented. The factors considered in the design of the delta modulator for use with the PWM inverter have been highlighted. It has been shown that the switching frequency is determined by the modulator design parameters and the type of switching devices used in the inverter. The delta modulation model developed in this chapter is used in the Simulink simulation model and for practical software implementation.

Chapter 4 Nine-Phase Induction Machine Drive Modelling and Simulation using Matlab/Simulink

The nine-phase cage rotor induction machine drive presented in Chapter 2 is modelled for simulation using Matlab/Simulink. Mathematical models of the components of the drive are required to build a simulation model. The relationships between the mathematical expressions are used to produce a complete simulation model. Stator voltage and current equations are derived and methods of calculating machine inductances are presented. The mechanical induction machine model is developed for calculating the rotor speed. Developed models of the simulation blocks are simulated and combined to produce the complete simulation block of the drive.

In this chapter, the nine-phase drive is simulated and the results are presented. The simulations are done to determine the ideal performance of the drive. They also help in fine tuning the drive parameters for better performance.

The main building blocks of the nine-phase induction machine drive simulation model are:

- The PI speed controller: It uses the difference between the command speed and the measured rotor speed to determine the magnitude of the torque current.
- The synchronous speed and the synchronous position calculation block: These are used to calculate the synchronous rotor position which is used in producing the reference current waveforms.
- The nine-phase reference current generation block: Uses look up tables to produce the reference current waveforms.
- The current controller and the inverter block: These are the components of the drive which determine the quality of the stator current waveform. The current controller produces the PWM signals which control the inverter. The inverter produces the pulse width modulated voltage pulses which push the current through the machine stator phases.
- The nine-phase induction machine stator model: This is the electrical equivalent circuit of the machine stator. It includes the stator resistance and inductance which filters the PWM voltage pulses to produce the desired stator current waveform.
- The mechanical motion system block: Is used to calculate the rotor speed using the command torque and the developed electromagnetic torque.

Figure 4-1 shows the full simulation block of the nine-phase BDCE controlled drive. The building blocks developed from the induction machine model equations are combined and simulated in the process of building the complete drive model.

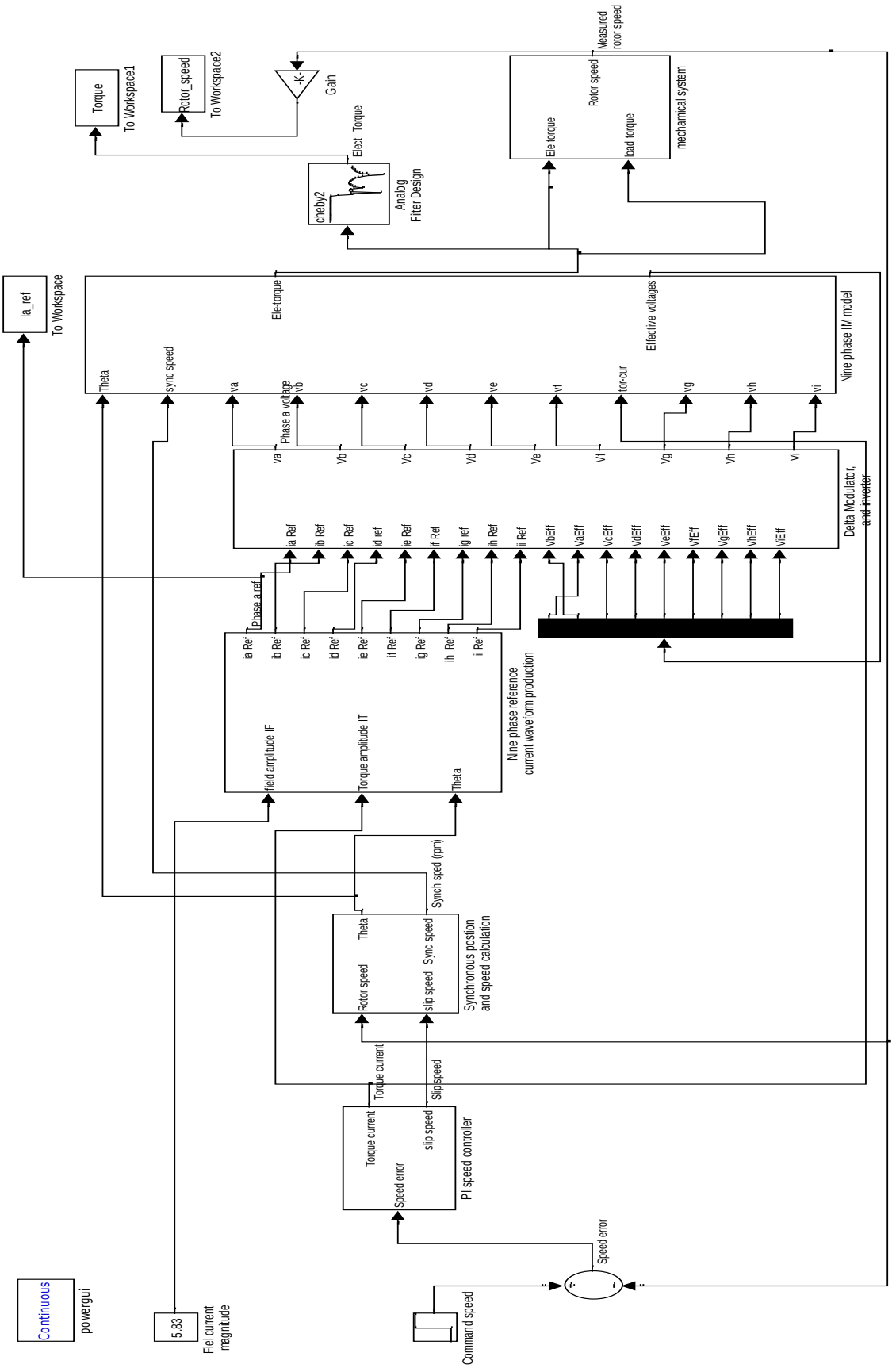

Figure 4-1. Full nine-phase induction machine drive simulation block used in Simulink.

4.1 The PI Speed Controller

The inputs to the simulation model are the field current magnitude, which determines the magnetic flux density, and the command speed at which the motor should run during the simulation. The rotor speed should be fixed at the command speed value and the machine should respond quickly to the changes in the speed. This is achieved through the use of a PI controller which ensures that the rotor speed follows the command speed with zero steady state error. The calculated rotor speed is subtracted from the reference speed to determine the speed error.

$$e_s(t) = \omega_{ref} - \omega_r \tag{4-1}$$

where $e_s(t)$ is the speed error, ω_{ref} is the command speed and ω_r is the rotor speed. The PI speed controller uses the speed error value to produce an output which determines the torque current. The PI controller is represented by the equation:

$$output(t) = K_p * e_s(t) + K_i \int e_s(t)dt \tag{4-2}$$

where K_p is proportional constant and K_i is the integral constant.

The determination of the PI controller parameters is simplified by the use of the SISO tool found in Matlab which uses the mechanical motion system transfer function of the induction machine as the plant variable in determining the PI controller parameters.

To develop the plant model, the torque constant of the machine is calculated and included in the transfer function. In BDCE control theory, the developed electromagnetic torque is given by:

$$T_e = k_T I_T, \tag{4-3}$$

where k_T is the torque constant and I_T is the torque current. There is linear relationship between torque and torque current. The rated speed is 1466 rpm and the rated power is 11kW. The rated torque is therefore 71.65Nm approximated to 72Nm at a rated torque current of 5.5A and a flux of 0.7T. The torque constant is found to be 13.03 Nm/A.

The general mechanical motion system transfer function is given by:

$$G(s) = \frac{k_T}{Js+\beta_{eq}} \tag{4-4}$$

where J is the moment of inertia and β is the frictional constant. For the 11kW, nine-phase cage rotor induction motor under consideration, J=0.0724 kgm^2, β_{eq}=0.01 Nm/$rad.s^{-1}$and k_T =13.03. The transfer function when the torque limit imposed in the PI controller block is ignored is given by:

$$G_{(s)} = \frac{13.03}{0.0724s+0.01}. \tag{4-5}$$

The transfer function in (4-5) is loaded to Matlab and used in the SISO tool as the continuous plant transfer function. A SISO tool design interface is used to design the controller with a 10 seconds rise time and a 15 seconds settling time.

Figure 4-2 shows the block diagram of the control system used in tuning the PI controller using the SISO tool and Figure 4-3 shows the root locus plot and the step response of the PI controller system. The output of the PI controller is the torque current which is used to calculate the rotor slip speed.

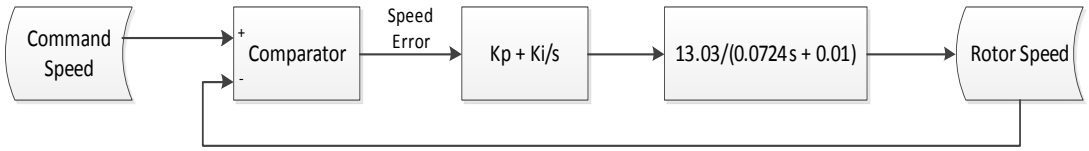

Figure 4-2. PI speed controller tuning block using the SISO tool of Matlab.

The root locus method is used to tune the PI controller parameters. The position of the poles and zeros of the system are adjusted while monitoring the response of the system to step inputs or ramp inputs. When the desired response curve has been produced, the controller transfer function from the SISO tool is used as the transfer function for the PI controller. The root locus plot of the system is shown to the left in Figure 4-3.

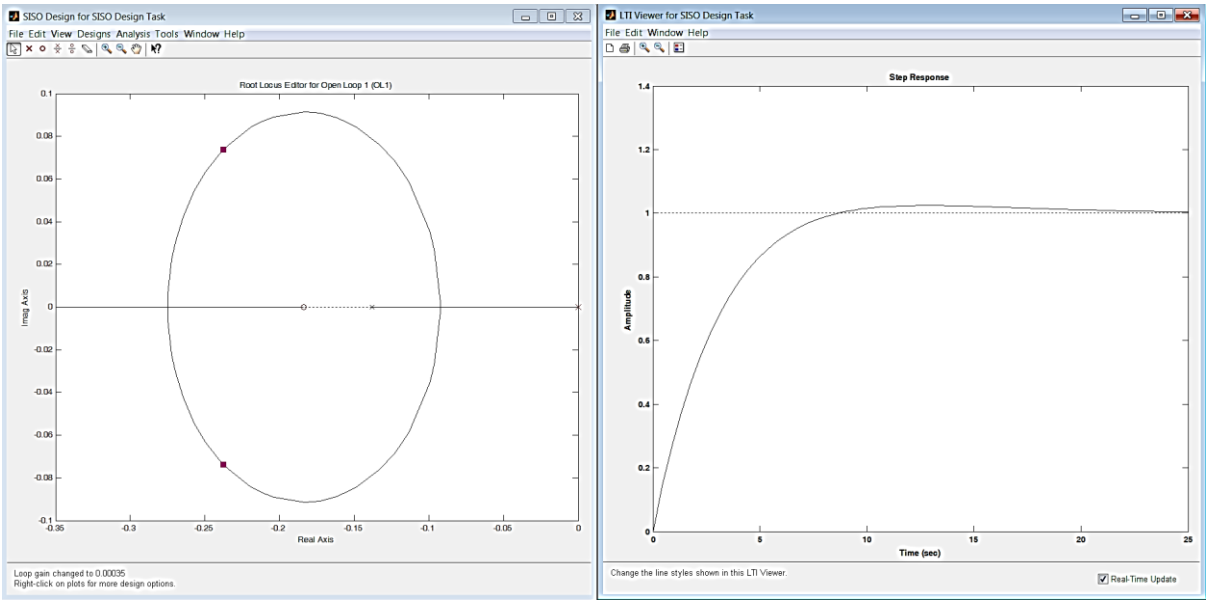

Figure 4-3. Step speed response of the nine-phase drive: root locus [left] and magnitude step response [right] using the PI controller.

The corresponding step response is shown in the plot on the right and this is used to set the rise time and the settling time. The transfer function obtained from the SISO tool is:

$$D(s) = 0.00035007 * \frac{(1+5.4s)}{s} \quad = 0.00189 + \frac{0.00035}{s}, \qquad (4\text{-}6)$$

It can be deduced from the equation that the proportional constant, $K_p = 0.00189$ and the integrator constant, $K_i = 0.00035$. The output of the PI controller is the magnitude of the torque current. The torque developed by the machine is a function of the magnitude of the current reference produced by the PI controller. Therefore the response of the torque to changes in speed is also determined by the response of the current.

Figure 4-4 shows the PI controller block used in the simulations. The outputs of the block are the slip speed in rad/s and the torque current in Amperes. Larger values of the PI controller gain parameters are used in the simulation model to speed up the simulations since the PI controller is not a critical component under investigation in the simulations.

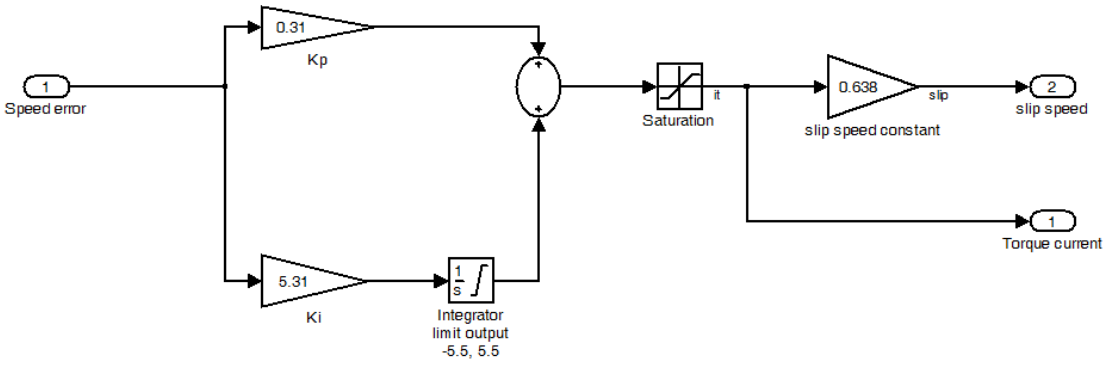

Figure 4-4. PI controller simulation block and outputs.

The output of the PI controller is the torque current magnitude and is limited to 5.5A for the nine-phase induction machine drive. The torque current is used to calculate the slip speed using the relationship:

$$\omega_{sl} = k * I_t \qquad (4\text{-}7),$$

where $k = 0.638$ is the control gain of the drive. With a rated torque current of 5.5A, the rated slip speed is 34 rpm and the rated speed of the motor is 1466 rpm. The performance of the PI controller is tested by giving a step speed command to the system and observing the response of the rotor speed, the torque current and the developed torque. A rectangular command speed signal of magnitude 1500 rpm is given to the system. The field current is fixed at 5.83A which is the rated value for the drive to maintain the required flux density of 0.7T in the machine. The stator current is supplied at the rated frequency of 50Hz. The PI controller rise time is designed to be 0.25s and the settling time to be 0.15s to reduce the simulation time. Figure 4-5 shows the simulated response of the drive to a step speed command with the use of the PI controller.

The results in Figure 4-5 show the response of the torque and the torque current when a step speed command is given to the machine. It can be observed from the figure that the torque current magnitude increases when there is a difference between the command speed and the rotor speed to develop the torque to accelerate or decelerate the machine to the reference speed. An overshoot is observed in the rotor speed before the speed settles at the command speed showing the effect of the machine inertia which is included in the speed calculation block. The level of dumping designed in the PI controller determines the magnitude and number of oscillations that the value of the speed goes through before it settles at the reference value.

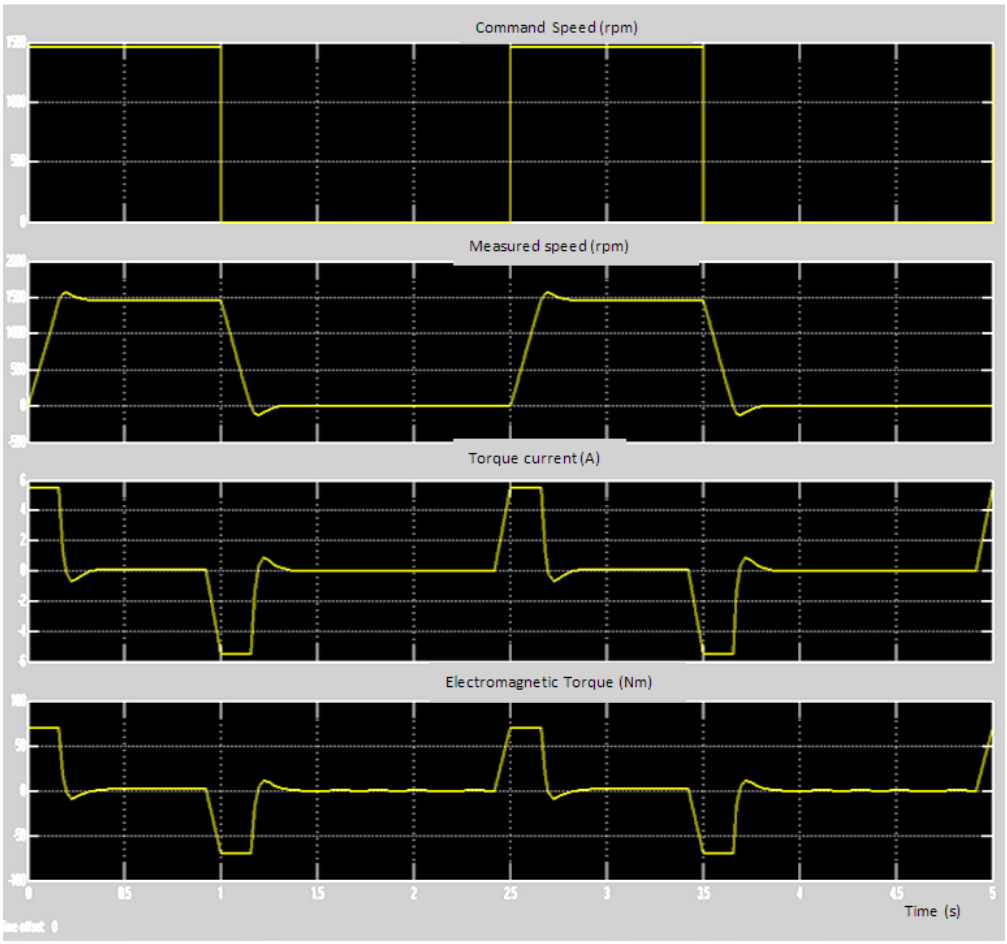

Figure 4-5. Response of the machine to a step speed command using the PI speed controller. [from top to bottom: Command speed, rotor speed, torque current and developed torque.]

4.2 Synchronous Speed and Position Calculation

The synchronous speed of the induction machine is given by the sum of the rotor speed and the slip speed. It has been observed above that the value of the slip speed depends on the value of the torque current. This implies that an increase in rotor speed leads to a reduction in the torque current so that the synchronous speed remains constant during the simulation. The expression of the synchronous speed is given by:

$$\omega_s = \omega_{sl} + \omega_r \tag{4-8}$$

where ω_s is the synchronous speed, ω_{sl} is the slip speed and ω_r is the rotor speed. The synchronous position is calculated by integrating the synchronous speed to determine the angular position of the rotor at any instant. Figure 4-6 shows the speed calculation block and its outputs.

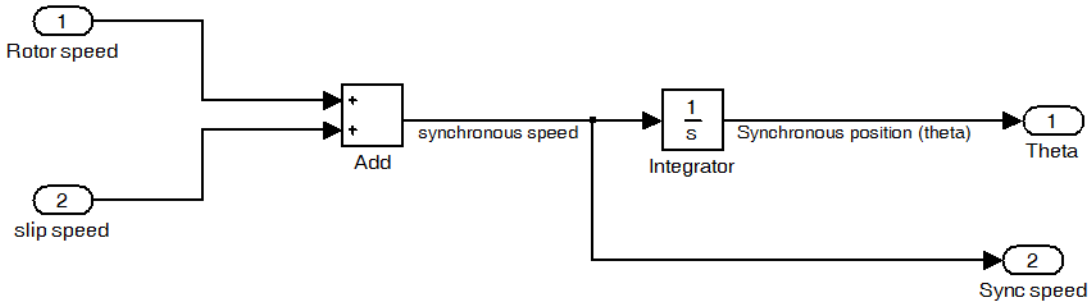

Figure 4-6. Synchronous speed and position calculation block.

The synchronous position is given as the angle:

$$\theta(t) = \int \omega_s(t)dt \qquad (4\text{-}9)$$

The synchronous speed of the four pole induction machine supplied from a 50Hz supply is 1500 rpm. It is used in the stator circuit block to calculate the induced emf in the stator. The synchronous position ($\theta(t)$) is used in the lookup tables to determine the magnitude of the reference stator current in the reference current generator. It is also used in the current decoupling sub-system which separates the field component of the stator current from the torque component for flux and torque calculation respectively.

4.3 Reference Current Generation

The synchronous position, the torque current magnitude and the field current magnitude are used to determine the reference current for each phase. The calculated phase shift from phase "A" is used to determine the magnitude and position of the reference current for each of the nine phases. A saw-tooth function is used to look up the current values. It is given by:

$$f(u) = 0.01 \times \big(1 + sawtooth(u)\big) \qquad (4\text{-}10),$$

where (u) is the value of the angle at the time instant. The saw-tooth function generates a saw-tooth waveform of period 2π and has a value of -1 at multiples of 2π. Multipliers are used to scale the saw-tooth function according to the requirements of the control program. In this model, the saw-tooth function is scaled such that its magnitude is between 0 and 0.02 to fix the period of the current waveform at 50Hz. The reference current generation block for phase "A" is shown in Figure 4-7. The same block configuration is used for all the nine phases but the output waveforms are phase shifted as described earlier on.

The nine-phase stator currents are shown in Figure 4-8. The phase shift between the phases in each group can be easily observed from the waveforms. The phase shift between the different phase groups can also be observed.

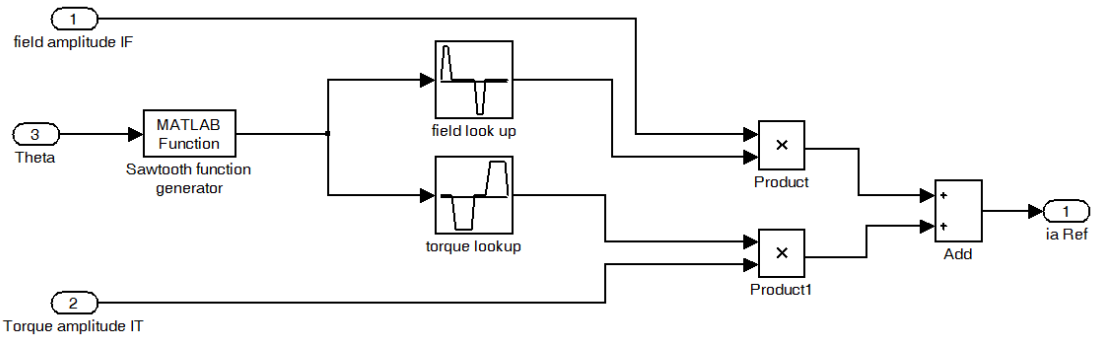

Figure 4-7. Reference current generator simulation block for phase A.

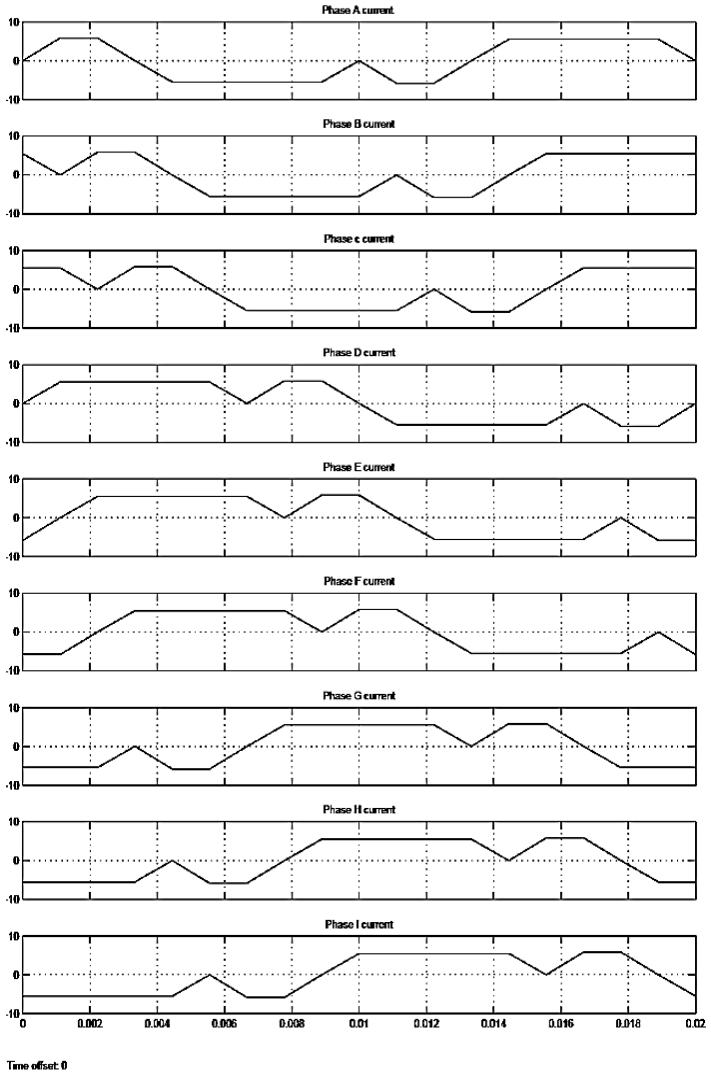

Figure 4-8. Nine-phase reference stator currents generated at 50Hz with $I_f = 5.83A$ and $I_t = 5.5A$. [at the top: phase "A" down to phase "I" at the bottom]

4.1 PWM Inverter and Delta Modulator Model

Due to the separate control of current per phase, the full H-bridge inverter configuration is used in the inverter. Figure 4-9 shows the PWM inverter model using an ideal voltage source and IGBT modules.

The rated voltage of the nine-phase induction machine is 400V and therefore a 400V DC source is used in the dc link. The parallel capacitor is used to simulate the dc link capacitor used in voltage source inverters. It is used to smoothen the dc voltage from the rectifier and reduces the voltage ripples in the dc link. IGBT modules are used to simulate the fast switching IGBTs used in the Intelligent Power Modules (IPM).

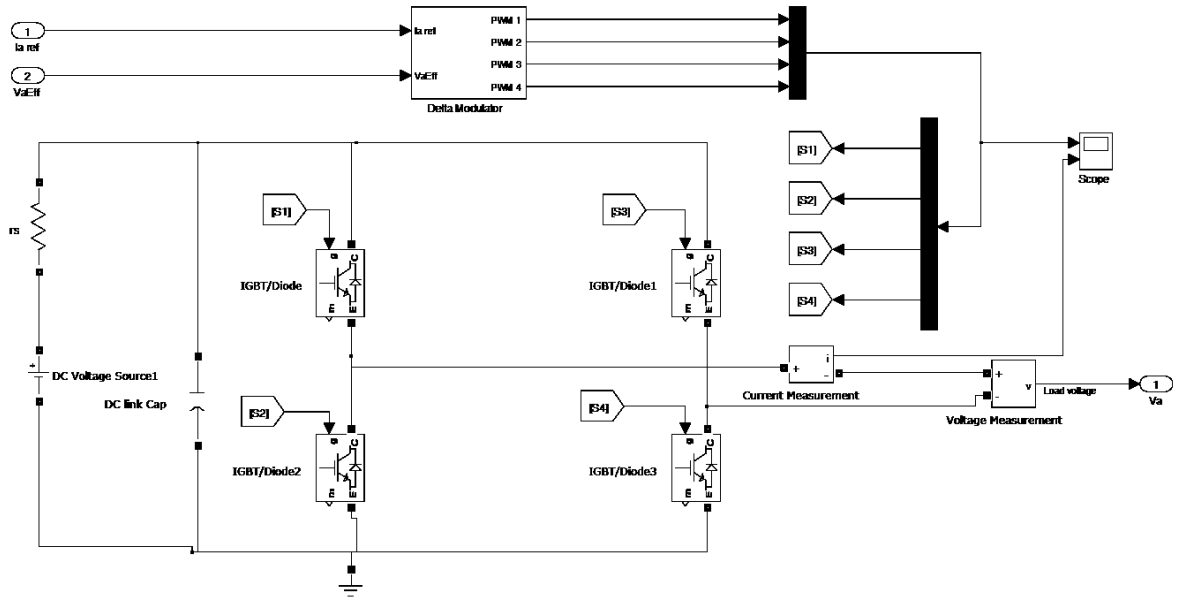

Figure 4-9. PWM Inverter model controlled by PWM signals from the delta modulated current controller.

The delta modulated current controller is used to generate the PWM switching signals for the inverter. The full delta modulated current controller model is shown in Figure 4-10. The reference current is used in the current controller as the modulating (or reference) signal. The delta modulated current controller uses the measured stator voltage as the input to the integrator. Stator voltage pulses are integrated to reconstruct the reference current waveform.

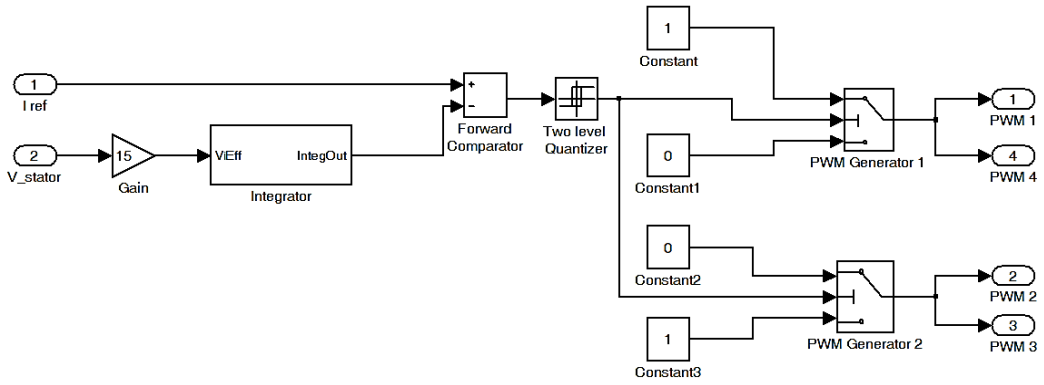

Figure 4-10. Rectangular wave delta modulated controller and PWM signal generators.

Rectangular wave delta modulation illustrated in Figure 3-6 is used in the current controller because the use of a zero-hysteresis comparator causes convergence errors in the simulations. A hysteresis band of 0.2A is used in the two-level quantizer to enable comparison with the hysteresis controller

which uses the same value of the hysteresis band from previous studies [30],[46]. In practical implementation, the hysteresis band is not used and the switching frequency is determined by the sampling frequency used in the DSP controller

The output of the quantizer is either positive or negative according to the difference between the reference signal and the carrier signal. A positive output implies that the inverter should produce a positive voltage across the machine phase. The PWM generator block is designed such that, switches [S1] and [S4] in Figure 4-9 are switched on while [S2 and S4l are off to produce a positive voltage across the phase. A negative pulse switches on [S2] and [S3] and switches off [S1] and [S4] to produce a negative voltage across the phase.

The integrator used in the modulator is implemented using the Z-transformations presented earlier on in section 3.7.1. The integrator block is shown in Figure 4-11. Unit delays are used to hold the previous values of the variables and the gain *K* is used to represent the integrator time constant τ_i and the sampling frequency f_s. The gain *K* is given by:

$$K = \tau_i * f_s \tag{4-11}$$

From section 3.7.1, the time constant of the integrator is 0.00381. A sampling frequency of 10 kHz is chosen for use in the integrator so that the carrier can accurately track the reference signal.

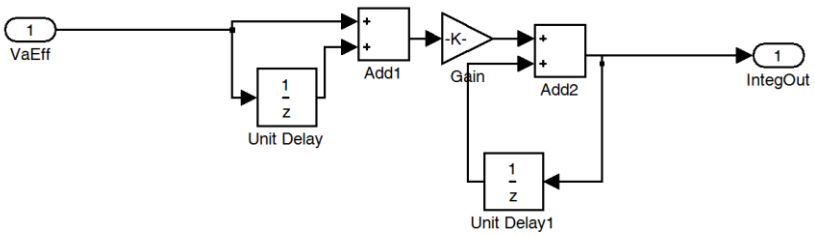

Figure 4-11. Simulation block of the integrator using the Z-transformation transfer function.

4.2 Per-Phase Stator Electrical Circuit Model

Each stator phase of a BDCE controlled induction machine is supplied from a separate full H-bridge inverter. This enables the use of the per phase equivalent circuit in modelling the stator electrical circuit. The effect of other machine phases is taken into consideration by the inclusion of mutual inductances in the model.

The following general assumptions about the induction motor are made in order to develop the induction machine model:

- Air gap magnetic field has a sinusoidal distribution.
- The iron has infinity permeability.
- There is no saturation.

- The machine has a uniform air-gap.

When the steady state performance of the machine is to be analysed, a single phase steady state induction machine electrical model can be used in the analysis. Figure 4-12 shows the single phase steady state model of an induction machine. The model takes into consideration the rotor current which flows when the machine runs at slip speed as well as the magnetizing current that produces the flux in the machine.

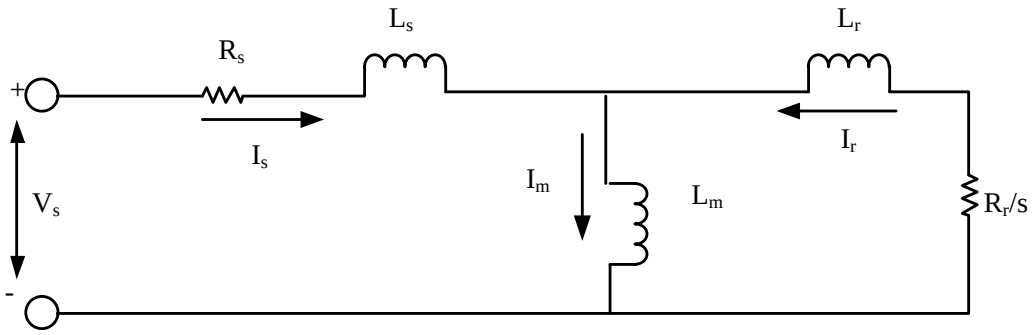

Figure 4-12. Single-phase induction machine steady electrical model.

The analysis of the effect of rotor currents on the stator phase flux was done in [30] and showed that the stator circuit can be simplified by ignoring the effect of the rotor current under balanced mmf conditions. The stator electrical circuit can therefore be simplified to the one shown in Figure 4-13.

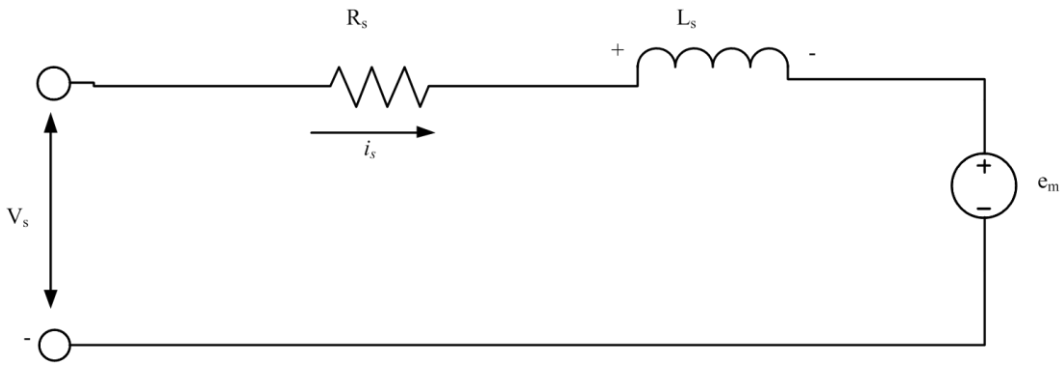

Figure 4-13. Simplified BDCE controlled induction motor per phase equivalent circuit

The stator voltage equation derived from the simplified stator circuit is given by:

$$V_s = V_{Rs} + V_{Ls} + e_m = I_s R_s + L_s \frac{di_s}{dt} + k_e \omega_s, \qquad (4\text{-}12)$$

where V_{rs} is the stator resistance voltage drop, V_{Ls} is the stator reactance drop, e_m is the mutually induced voltage, k_e is the mutual induced voltage constant and ω_s is the synchronous speed.

The stator current is found by solving for I_s in (4-12);

$$`L_s \frac{di_s}{dt} = V_s - R_s I_s - k_e \omega_s, \qquad 4\text{-}13)$$

$$\Rightarrow i_s = \int \frac{(V_s - R_s I_s - k_e \omega_s)}{L_s} dt, \tag{4-14}$$

In the induction machine, the stator mutually induced voltage e_m is a function of the machine winding self-inductance and the mutual inductance due to the other phases. The inductance values can be calculated using different approaches presented in detail in Appendix C.

4.2.1 Self-Inductance Calculation Using Flux Linkages

Inductance can be viewed as a measure of the flux linkage to a coil due to a unit current flowing in the coil. Inductance can therefore be expressed in terms of flux linkage as:

$$L = \lambda / i \tag{4-15}$$

where L is the inductance, λ is flux linkage and i is the current flowing to produce the flux. To determine the inductance, the rate of change of flux linkage with current is used.

$$L = \frac{\delta \lambda}{\delta i} \tag{4-16}$$

If the change in flux linkage due to a small change in current is known, the forward difference equation is used to calculate inductance. The self-inductance of phase "A" using the forward difference equation is given by:

$$L_a = \frac{\lambda_a (i_a + \Delta_i) - \lambda_a (i_a)}{\Delta_i}, \tag{4-17}$$

where, λ_a is the instantaneous flux linkage, i_a is the instantaneous phase current and Δ_i is a small change in the current which causes a small change in flux linkage without affecting the balanced mmf condition in the BDCE controlled machine. The flux linkage values were determined using JMAG finite element analysis software simulations. The details of the simulations are fully presented in Appendix D.

4.2.2 Mutual induced voltage calculation

The equivalent circuit of the induction machine in Figure 4-12 shows that the induced voltage across the stator is significant in the steady state model. In equation (4-12), mutually induced voltage is presented as a function of a constant k_e and the synchronous speed ω_s. In developing the model, the constant is calculated using the equation:

$$k_e = \sum_{j=a}^{j=i} \frac{L_{mji}}{\omega_s} \frac{di}{d\theta} . \frac{d\theta}{dt} = \omega_s / e_{mj} \quad ; [j \neq i], \tag{4-18}$$

where k_e is the induced voltage constant. The rate of change of current can be determined using finite element analysis simulations. The induced voltage is measured under synchronous speed simulation conditions. Since the synchronous speed is known, the induced voltage can then be calculated using the constant k_e. The simulation results are shown in Figure 4-14. They show that the induced voltage

across the phase is higher when the phase is acting as a torque producing phase thereby confirming that the polarity of the torque current is correct.

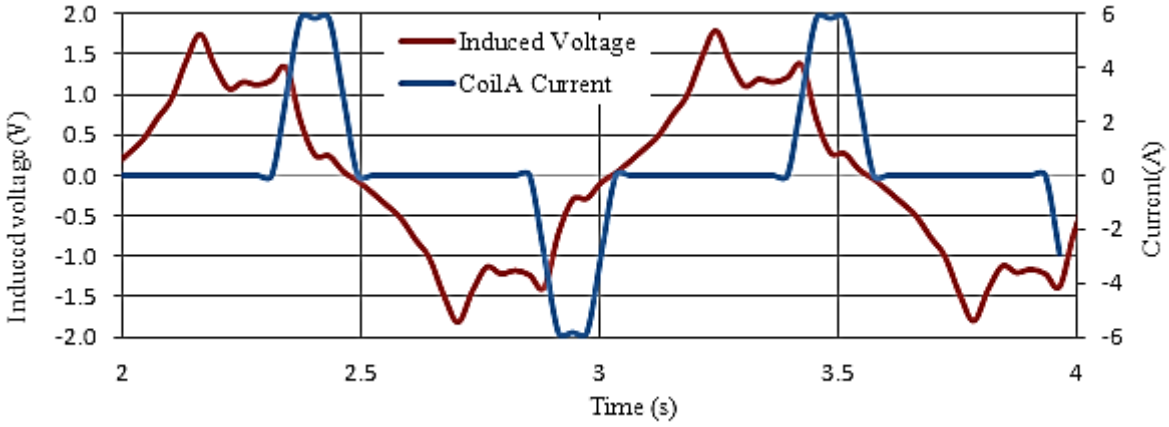

Figure 4-14. Stator phase induced voltage and stator current against time.

4.2.3 The Stator Circuit Simulation Model.

The stator electrical circuit is designed from the stator current equation (4-13). The equation takes into consideration the machine stator inductance, the stator resistance as well as the mutually induced voltage. Figure 4-15 shows the stator electrical circuit model derived from the stator current equation in equation (4-14).

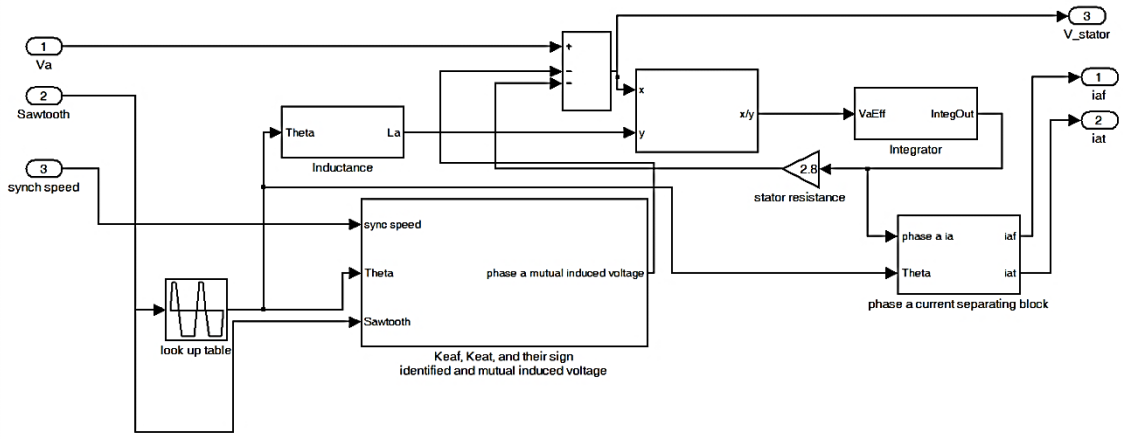

Figure 4-15. Stator phase electrical circuit simulation model.

The stator resistance of 2.8Ω is used assuming that the phase coils are connected in series. In the practical machine, the coils are connected in parallel and hence the reference currents are double the values used in simulations. The stator phase current waveform is generated by low pass filtering the stator voltage as shown by the integrator used in the simulation block. The machine inductance performs the filtering in the real induction machine.

4.3 The Stator Current Decoupling Model and Torque Calculation

The stator current is decoupled into the field and the torque components using a stator current separation block shown in Figure 4-16. The field component is denoted I_{af} and the torque component is denoted I_{at} for phase "A". The decoupled control of the flux and torque is implemented by separating the torque component of the stator current from the field component. A current decoupling look up table is used for this purpose and the graphical representation of the look up table is shown in Figure 4-17 to determine whether a phase is acting as torque or field producing phase. The negative values are used to select a torque producing phase and the positive values are used to select the field producing phase.

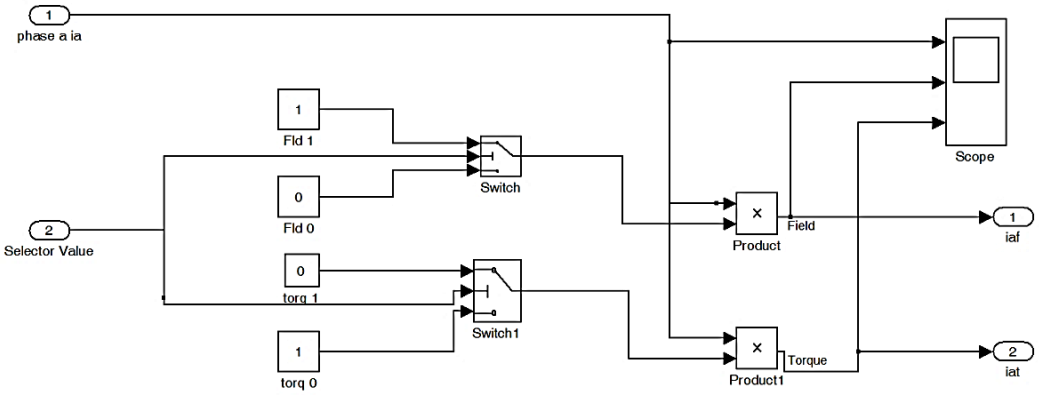

Figure 4-16. Stator current decoupling block

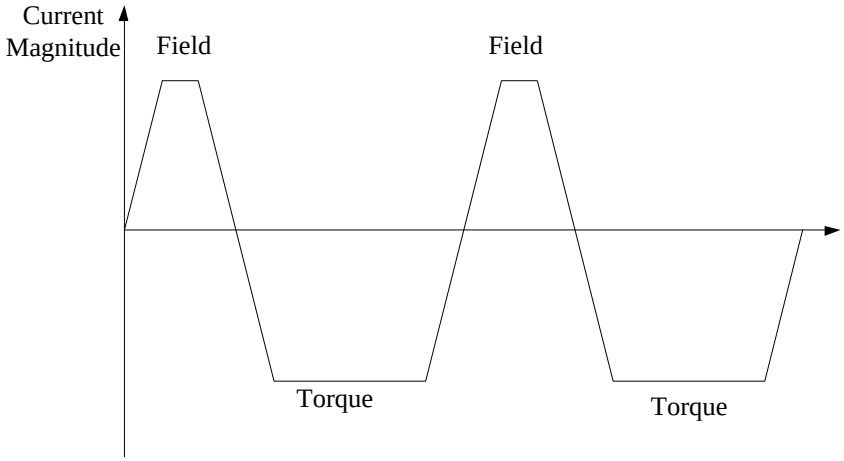

Figure 4-17. Waveform representing the look up table used to decouple stator current into the field and the torque current components.

The decoupled stator wave components are used to determine the torque and the flux separately. The field current components are added together at each time instant to determine the resultant field current. By denoting the field current for a phase as I_{fx}, then the resultant field current is given by:

$$I_f = \sum_{x=1}^{n} |I_{fx}| \qquad (4\text{-}19)$$

where *n* is the number of stator phases. The resultant torque current is determined in the same way by summing up the magnitudes of the torque currents. The flux is determined by the value of the flux corresponding to the resultant field current using the graph in Figure 4-18.

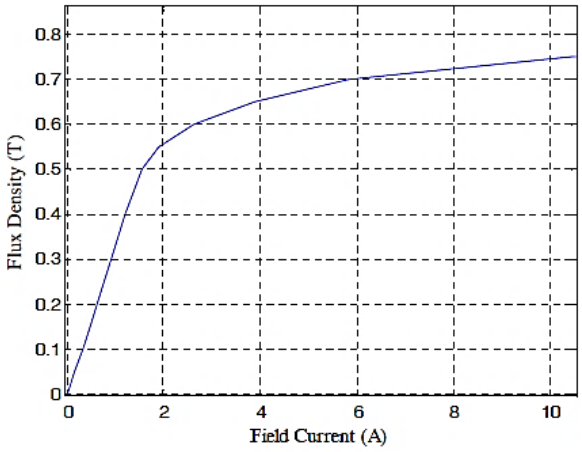

Figure 4-18. Relationship between air gap flux density and field current for the nine-phase induction machine [46].

The electromagnetic torque equation for the BDCE controlled machine is derived from the torque equation of the separately excited dc machine. The development of the torque equation for a separately excited dc machine is presented in Appendix E. The derived torque equation for the dc machine is given by:

$$T = M_{rg} r_g l B I_a \tag{4-20}$$

where M_{rg} is the number of active armature conductors, r_g is the rotor radius, B is the air gap magnetic flux density and I_a.is the armature current. For a BDCE controlled cage rotor induction machine, the armature current is analogous to the rotor current.

A BDCE controlled motor operates on the principle that the magnitude of the stator torque current is proportional to the magnitude of the rotor current under balanced mmf conditions. The torque equation for the BDCE controlled motor can therefore be presented in terms of the stator torque current. From the analysis presented in [46], the torque is calculated by considering the number of torque phases. The torque equation for BDCE controlled machine was derived and given as:

$$T_e = 2(m_t - 1) N_s l r_g B I_{tsum} \tag{4-21},$$

where m_t is the number of torque phases, N_s is the number of stator windings per pole per phase, l is the stack length, r_g is the air gap radius, B is the magnetic flux density and I_{tsum} is the sum of the torque currents contributed by each phase. By denoting the torque current for a phase as I_{tx}, then the resultant torque current is given by:

$$I_{tsum} = \sum_{x=1}^{n} |I_{tx}| \tag{4-22}$$

The equation is used in calculating the developed torque in Simulink by substituting for the machine parameters in the equation. The developed torque equation used in the simulation was determined by substituting the variables in equation (4-21), by the corresponding values in Table 2-3 to get torque equation as:

$$T_e = 3.65 * B * I_{tsum} \quad (4\text{-}23).$$

4.4 Mechanical Motion System Model of the Induction Machine

The interaction between the rotor current and the air gap magnetic field causes electromagnetic torque, T_e to be developed in the rotor. The total torque developed in the shaft, T_L is less than the electromagnetic torque due to frictional losses and the torque developed against the load inertia. The mechanical motion system equation of the motor gives the relationship between the load torque, T_L the electromagnetic torque,T_e, the rotor speed,ω_r, the moment of inertia,J and the frictional constant of the motor, β_{eq}. The mechanical motion equation is given by:

$$T_e = T_L + J\frac{d\omega_r}{dt} + \beta_{eq}\omega_r, \quad (4\text{-}24)$$

Rewriting equation (4-24) using the Laplace transforms gives:

$$T_e(s) = T_L(s) + Js\omega_r(s) + \beta_{eq}\omega_r(s), \quad (4\text{-}25)$$

The motor mechanical motion system transfer function is therefore given by:

$$\frac{\omega_r(s)}{T_e - T_L} = \frac{1}{Js+\beta_{eq}}, \quad (4\text{-}26)$$

The rotor speed is used to calculate the synchronous speed and the synchronous position in the simulation model. The rotor speed is given by:

$$\omega_r(s) = (T_e - T_L)\frac{1}{Js+\beta_{eq}} \quad (4\text{-}27)$$

The rotor speed calculation shows that changes in load torque cause changes in the rotor speed. In order to keep the speed at the set value, the electromagnetic torque has to change in such a way that the rotor speed remains constant. This is achieved through the use of the PI speed controller.

It can be observed that by substituting for the values of the moment of inertia J=0.0724 kgm^2 and the frictional coefficient β_{eq}=0.01 Nm/$rad.s^{-1}$ in equation (4-27), the rotor speed can be calculated using the value of the developed torque and the load torque. The transfer function expression for the rotor speed is therefore given by:

$$\omega_r(s) = (T_e - T_L) * \frac{1}{0.0724s+0.01} \quad (4\text{-}28)$$

where T_L is the load torque. Figure 4-19 shows the Simulink model of the mechanical system. The rotor speed is fed back to the PI controller to be used for speed control.

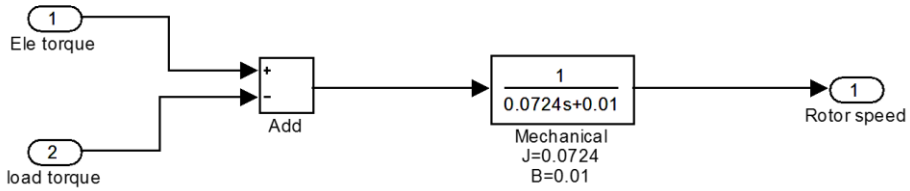

Figure 4-19. Induction motor mechanical system simulation model.

4.5 Simulation of the Nine-Phase Induction Machine Drive

The developed sub-systems are linked through their input and output variables to produce the complete simulation model of the drive. The focus of the simulations is to determine the performance of the drive using the delta modulated current controller and also using the hysteresis current controller in the control system. The current controller is an important component in the BDCE control strategy because it determines the response of the system and how accurately the stator current tracks the reference current. The hysteresis controller was used in the previous study presented in [46] in the BDCE control method and the delta modulated controller is proposed in this study. The two controllers are simulated and the results are compared to determine if the delta modulated controller can be used in place of the hysteresis controller.

The stator current waveforms produced by each controller give an indication of its effect on the performance of the drive. The effectiveness of the BDCE control method is based on the shape of the stator current waveform. The controller which produces a stator current waveform that is closer to the reference waveform in both magnitude and phase is expected to give better drive performance.

Both the hysteresis controller and the delta modulated controller are simulated while using a current hysteresis band of 0.2A to enable comparison with results obtained in the previous studies. Figure 4-20 shows the hysteresis controller block used. The output of the relay is the pulse width modulated 400V pulse required to drive the motor. A single-phase block of the controller is shown and the same block configuration is used for the other eight phases with different reference currents which are phase shifted as shown in Figure 4-8. The controllers are simulated to show the performance of the drive with varying torque current magnitude, varying speed and loading conditions. The PI speed controller settling time is reduced to 0.2s for purposes of simulation to reduce simulation time.

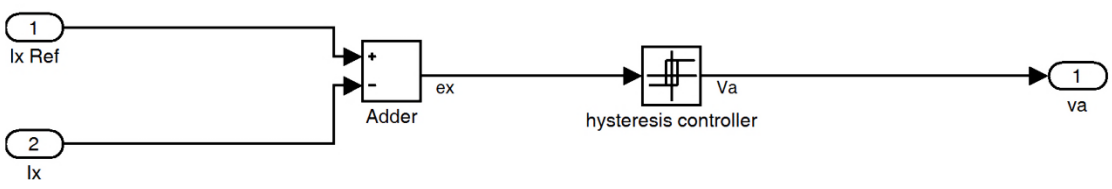

Figure 4-20. Per phase simulation model of the hysteresis controller.

When the difference in magnitude between i_x and $i_{x\,Ref}$ (the error signal) is less than 0.2, the inverter remains in its current state but when the magnitude of the error becomes greater than 0.2, the inverter switches toggle states. If the difference is positive, the inverter switching state is such that v_a becomes +400V and if negative, the inverter switching state is such that v_a is equal to -400V.

The delta modulator used for simulations is shown in Figure 4-10. In the delta modulated current controller, the stator voltage is fed back to the integrator to estimate the reference current waveform and the estimated signal is used as the carrier signal. The carrier signal is compared to the reference current and the error value so produced is used in the two-level quantizer (hard limiter) to generate the PWM signals which drive the inverter as described in Chapter 3.

4.5.1 The locked rotor condition simulation

The stator currents are supplied at a frequency of 12.5Hz for an induction machine with a rated frequency of 50 Hz as given in the IEEE test standard manual [64]. The test is done at rated field current of 5.83A and different torque current magnitudes under locked rotor conditions. The locked rotor condition is simulated by connecting the load torque to the electromagnetic torque according to the relationship given by:

$$\omega_r(s) = (T_e - T_L)\frac{1}{Js+\beta_{eq}} \tag{4-29}$$

which implies that if $T_e = T_L$ then $\omega_r(s) = 0$. The locked rotor test is conventionally done to determine the winding resistance and the leakage reactance. It is also performed to determine the locked rotor torque and the locked rotor current [64]. The equivalent circuit in the locked rotor test has very low input impedance [65] and hence a lower frequency and a lower voltage is used in the test since rated current can flow at the low voltage. However, the test is simulated in this study to determine the maximum electromagnetic torque that the machine can develop at different magnitudes of the torque current. This test is done to verify if there is indeed a linear relationship between torque and torque current.

4.5.1.1 Stator current waveforms

The locked rotor test is simulated using the hysteresis current controller and then using the delta modulated current controller. Figure 4-21 shows the stator current waveform produced when the hysteresis controller is used to generate the PWM signals. Figure 4-22 shows the magnified stator current waveform produced using the same current controller. The magnified waveform shows a varying switching frequency caused by the hysteresis control mechanism and this can be observed at the point where the slope of the reference signal turns to zero. However, the hysteresis controller gives stator current waveforms which closely track the reference currents. The effect of the hysteresis band can be observed in the waveform of Figure 4-21.

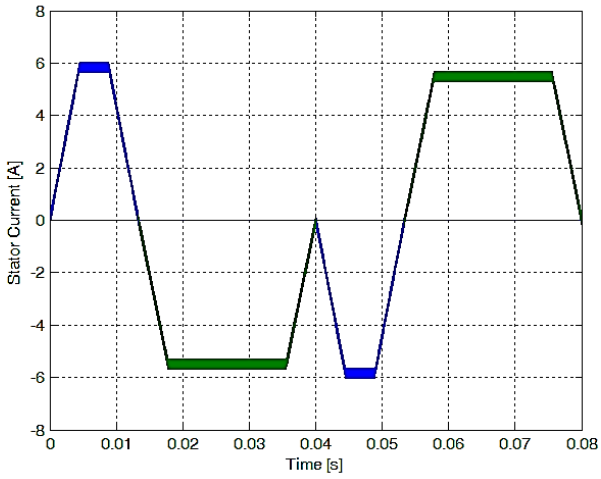

Figure 4-21. Stator current waveform produced using the hysteresis controller in the system [I_f = 5.83A, I_t = 5.5A]

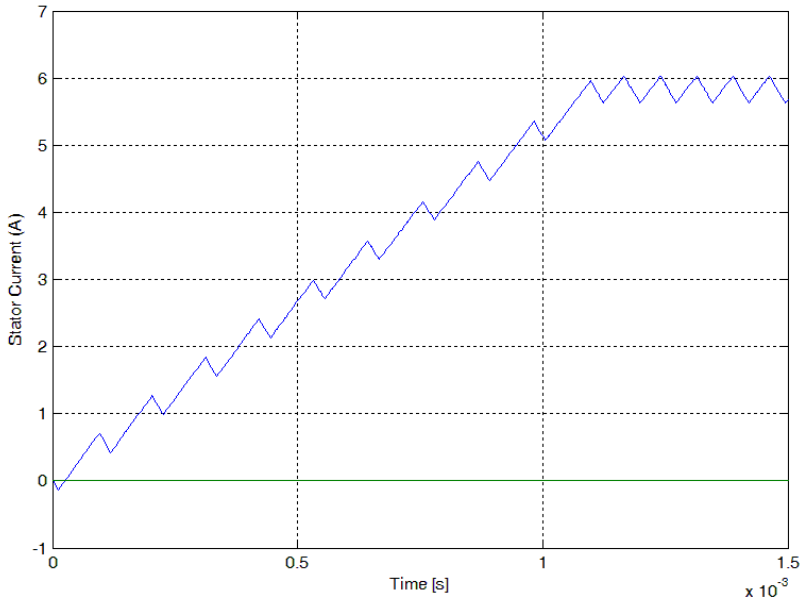

Figure 4-22. Magnified stator current switching waveform produced by the hysteresis controller

Figure 4-23 show the stator current waveform produced using the delta modulated current controller. Figure 4-24 shows the stator current waveform further magnified to show that at the point where the slope goes to zero, there is still a constant switching frequency of 10 kHz as determined by sampling frequency of the sample and hold block. The delta modulated current controller gives a higher switching frequency than the hysteresis controller using the same hysteresis band and quantizer output. This is because the quantizer output is integrated and hence the carrier signal has a higher rising rate than the stator current waveforms used in the hysteresis controller. The current waveforms produced by the two controllers are quite comparable under locked rotor conditions in general but the delta modulator gives smooth switching operation as shown due to the high switching frequency.

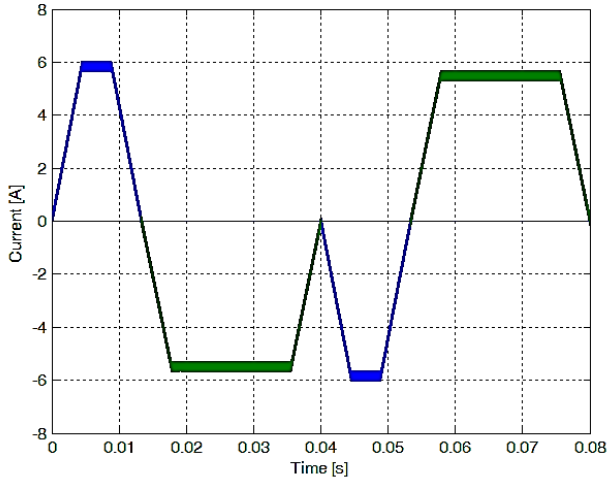

Figure 4-23. Stator current waveform produced by simulating conventional delta modulated current controller using stator voltage output as feedback [I_f = 5.83A, I_t = 5.5A].

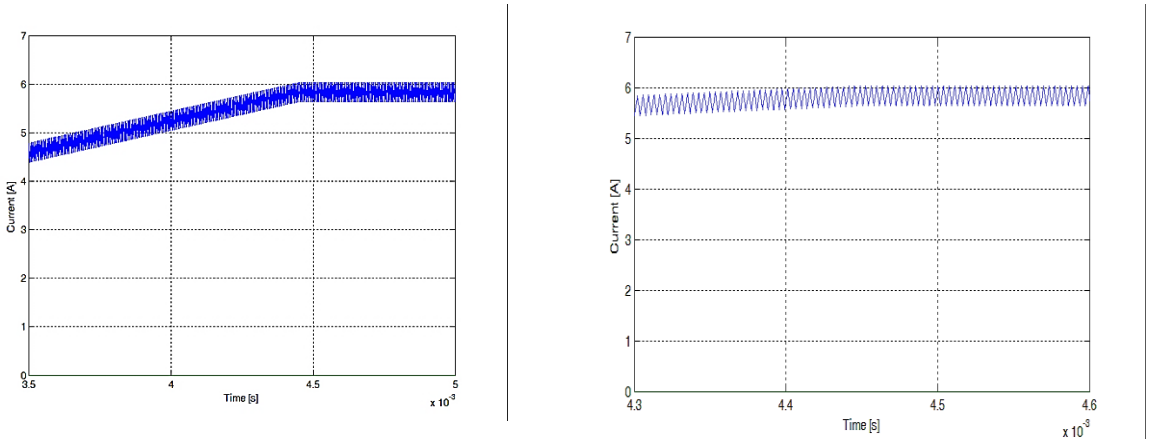

Figure 4-24. Magnified stator current waveforms produced by using the delta modulated controller. [Right: Magnified section of the waveform]

4.5.1.2 Developed torque under locked rotor conditions

After observing the stator current waveforms, the torque developed using the current controllers is also investigated. The waveforms of the torque developed using the hysteresis controller and using the delta modulated controller are shown in Figure 4-25 and Figure 4-26 respectively. The results show that the torque stabilizes faster when delta modulation is used and takes longer when the hysteresis controller is used. This can be explained by the fact the delta modulated controller produces a higher switching frequency such that the current error is reduced at a faster rate. Since the developed torque is directly proportional to the torque current, then less torque fluctuations are expected.

The results also show that the motor can develop a maximum stable torque of 72Nm under the simulation conditions of rated torque current and rated filed current. The torque settles at the load

torque value with a smoother steady state torque waveform when the delta modulated current controller is used than when the hysteresis controller is used.

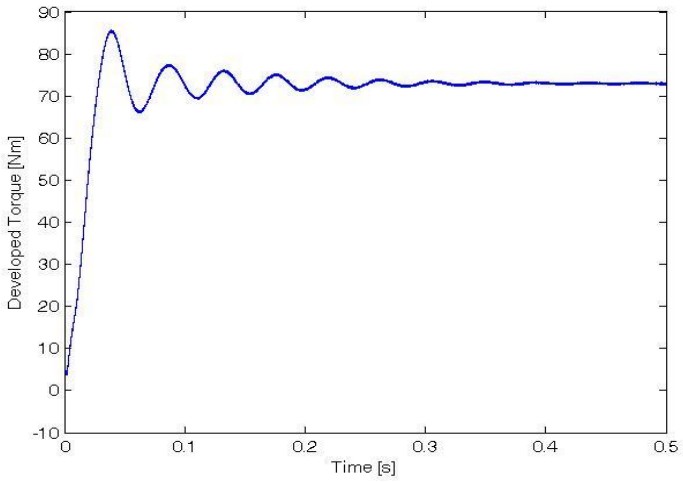

Figure 4-25. Developed torque under locked rotor conditions using the hysteresis current controller.

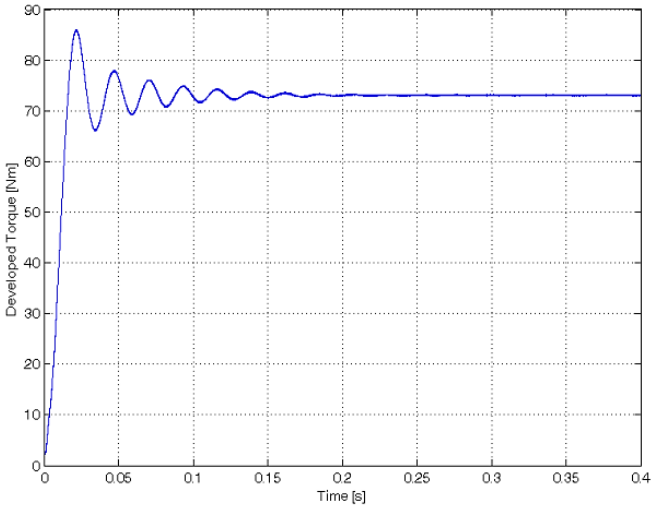

Figure 4-26. Developed torque under locked rotor conditions using the delta modulated controller

The calculated torque ripple at steady state from simulations is 0.55% when the hysteresis current controller is used and is 0.53 % for the delta modulated controller. The calculation is done using the relationship:

$$Torque\ ripple = \left(\frac{Maximum\ Torque - Minimum\ Torque}{Average\ Torque}\right) * 100\% \qquad (4\text{-}30).$$

4.5.1.3 Stator voltage power spectral density

The power spectral density of a signal describes how the signal power or energy is distributed across frequencies. The power spectral density of the third and the fifth harmonics of the stator voltages are observed to validate the theory that delta modulation has inherent harmonic attenuation

characteristics. In order to get a fair comparison, the delta modulated current controller is implemented using the rectangular wave delta modulator which uses a hysteresis band as the one used in the hysteresis current controller. Figure 4-27 shows the power spectral density of the third and the fifth harmonics of the stator voltage produced using the hysteresis controller. The power spectral densities of the harmonics are higher in magnitude compared to those produced by the use of the delta modulated current controller shown in Figure 4-28. When the hysteresis controller is used, the third harmonic has a power spectral density of 0.16 while that of the voltage produced by the delta modulated current controller has a value of 0.103. The power spectral densities of the fifth harmonic have a smaller difference, thereby confirming the previous statement. The results show that the delta modulator attenuates the lower order harmonics better than the hysteresis controller in general. The attenuation is achieved by the use of the integrator which has filtering characteristics.

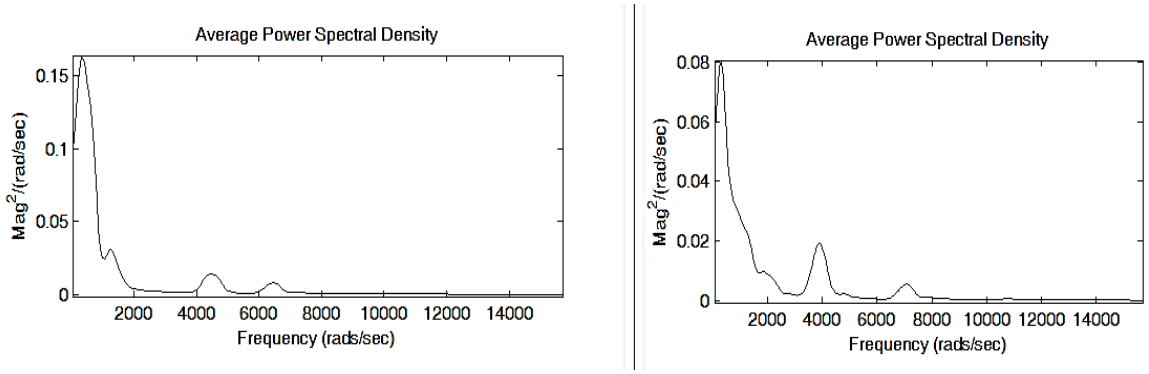

Figure 4-27. Power spectral density of the third (left) and the fifth (right) harmonics of the stator voltage using the hysteresis controller

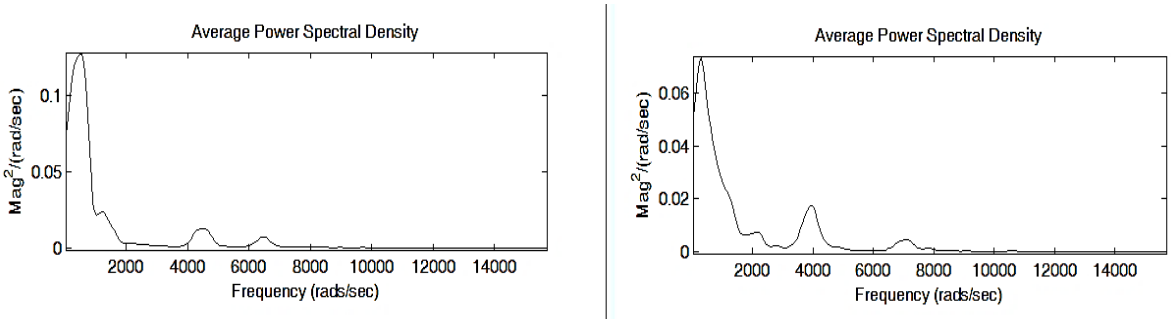

Figure 4-28. Power spectral density of the third (left) and the fifth (right) harmonic of the stator voltage using the delta modulated controller.

4.5.2 Relationship between developed torque and torque current

The relationship between developed torque and torque current is investigated by supplying the stator with a constantly increasing torque current and observing the corresponding change in developed torque while fixing the field current at the rated value of 5.83A. The current is increased to twice the rated current to observe if the linear relationship goes beyond rated conditions. Figure 4-29 shows the change in developed torque with torque current when using a hysteresis controller. The effect of the hysteresis band is observed in the diagram showing how the current ripples directly cause the torque

ripples. Figure.4-30 is a plot of the change in developed torque with torque current when using the delta modulated current controller. The plot shows that there is less hysteresis effects on the torque when the delta modulated controller is used with a very small hysteresis band. A zero value hysteresis band could not be used due to convergence issues in the solver used by the Matlab processor. There is evident of reduced torque fluctuations. There is a linear relationship between developed torque and torque current as expected of the BDCE controlled drive. This linear relationship exists as long as the gain constant *k* is maintained for balanced mmf conditions as discussed in section 2.3.

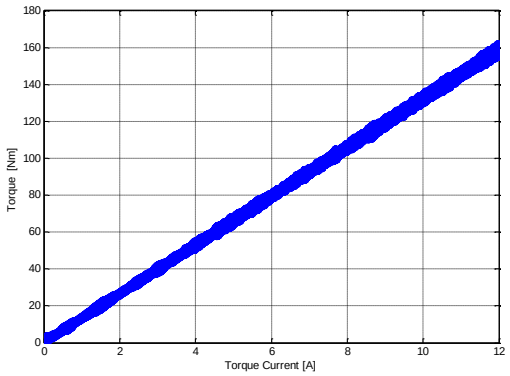

Figure 4-29. Electromagnetic torque against torque current using hysteresis controller.

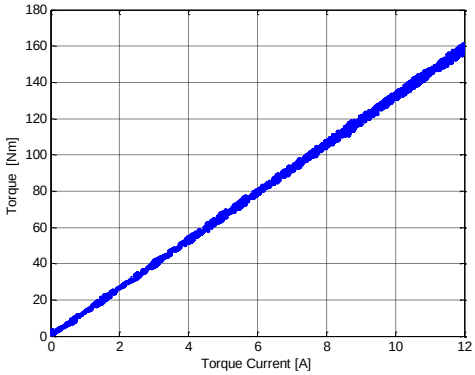

Figure.4-30. Electromagnetic torque against torque current using the delta modulated controller.

4.5.3 Torque response to step speed command

The response of the drive to a step change in the command speed is tested under light loading conditions to enable fast response. The command speed is set at synchronous speed since the machine is expected to develop very low torque. A value of 5Nm is used by assuming a 90% to 95% efficiency which can be used to assume that the torque lost due to frictional losses and the machine inertia can be close to 5Nm.

The command speed is varied with a step change and the developed torque is observed. The results of the test using the hysteresis controller are shown in Figure 4-31. The rotor speed ramps up to the command speed with a delay of 0.2 seconds which corresponds to the PI controller rise time and also decreases with a delay of 0.15 seconds since it cannot stop instantly due to the machine inertia. The figure also shows that the developed torque rises to a high value close to rated torque during the acceleration phase and falls to the command torque value when the rotor speed reaches the command speed value. The torque developed during the acceleration phase is the acceleration torque of the machine. The field component of the current remains constant to produce the required flux density while the torque component varies with torque and speed. The frequency of the stator current shows some dependence on the rotor speed as determined by the controller. Figure 4-32 shows the response of the system when using a delta modulated current controller in the system.

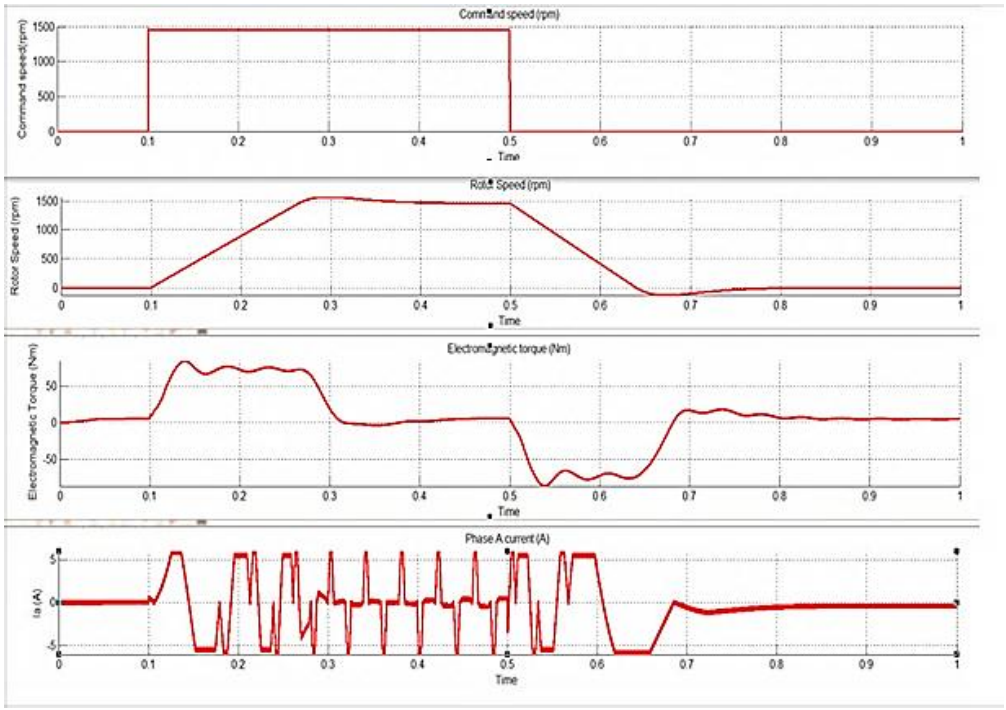

Figure 4-31. Response of system to step command speed under light load of 5Nm using hysteresis controller. Command speed (top), Rotor speed (second from top), Developed torque (third trace) and stator current (bottom trace).

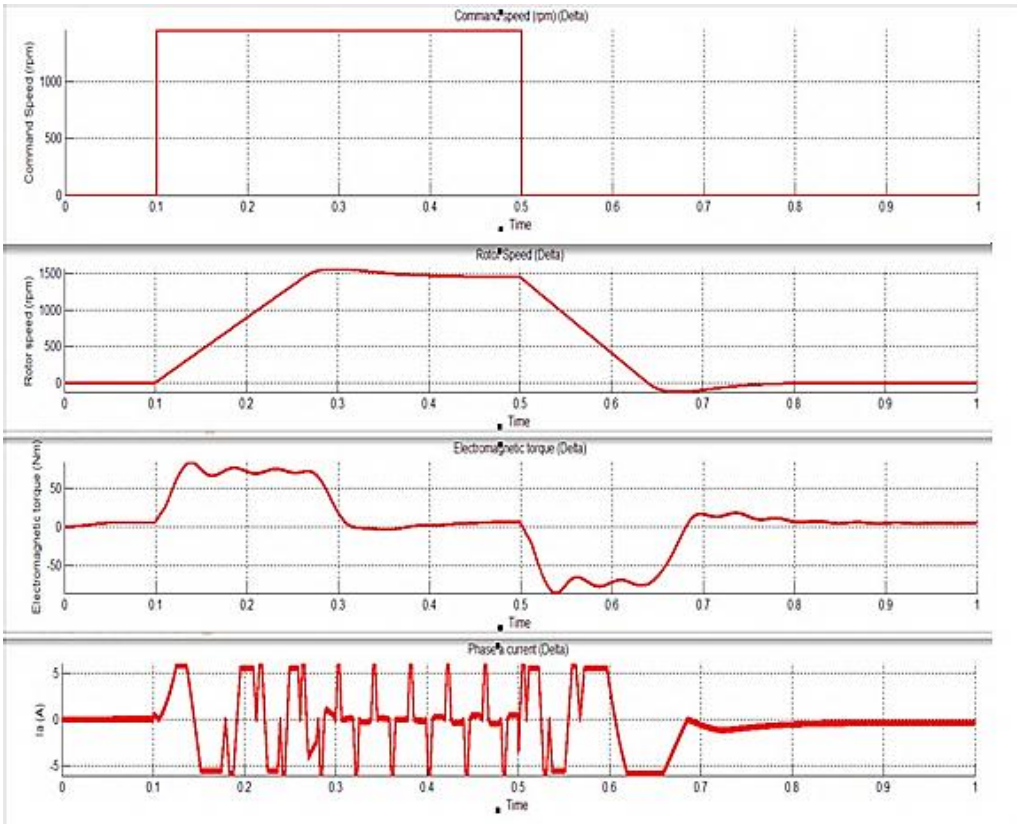

Figure 4-32. Response of system to step command speed under light load of 5Nm using delta modulated controller. Command speed (top), Rotor speed (second from top), Developed torque (third trace) and stator current (bottom trace).

The changes in the stator current waveform as the speed and the torque changes are observed clearly in these traces. The rotor speed does not rise instantaneously to the command speed because the machine has inertia. When the command speed is higher than the rotor speed, a torque is produced to accelerate the machine to the command speed. When the command speed is lower than the rotor speed, the motor develops negative torque to decelerate to the command speed. The magnitude of the torque current changes with developed torque and this shows the control action of the PI speed controller. The stator current waveform frequency shows that it depends on the speed of the motor.

4.6 Summary

The nine-phase induction machine drive has been modelled and the equations required for the development of a simulation model have been derived. The steady state equivalent circuit of the induction motor has been used for modelling the stator electrical circuit. Simulink has been used to simulate the nine-phase drive and the results show the overall performance of the machine drive. Its static, transient and dynamic responses have been simulated. The simulation results are used as a reference in the experimental evaluation of the drive.

Chapter 5 Experimental Evaluation of BDCE Controlled Drive

In this chapter, the experimental evaluation of the delta modulated current controller applied to a BDCE controlled nine-phase induction machine drive is presented. The evaluation is done to validate the performance of the drive that was shown by simulation results using the delta modulated current controller and also using the hysteresis controller for comparison. The simulations presented in Chapter 4 give a lead to the expected experimental evaluation process and results. The experimental evaluation presented in this chapter is done by performing the following tests:

i. Testing the DSP based controller board.
ii. Testing the connection between the resolver and the DSP controller board.
iii. Testing the current measuring cards for use with the hysteresis controller.
iv. Testing the PWM outputs to the inverter.
v. Testing the inverter operation.
vi. Testing the nine–phase drive with and without the PI speed controller to verify system functionality.
vii. Testing the drive using the delta modulated current controller and also using the hysteresis controller.

5.1 The Induction Machine Drive Test Bench

The schematic diagram of the test bench is shown in Figure 5-1 and is made up of the following components:

i. Nine-phase voltage source PWM inverter supplied from a 400V DC power supply
ii. TMS320VC33 DSP controller board with an Altera Cyclone EP1C6Q240C8 FPGA to communicate with the peripheral devices through Analogue to Digital Converter (ADC) and Digital to Analogue Converter (DAC) modules.
iii. PC where the control program is developed and compiled before being downloaded to the DSP.
iv. Nine-phase, four-pole, 11kW cage rotor induction motor. A resolver is connected to the motor shaft and used to measure the angular position and hence the speed of the rotor at any instant.
v. Three-phase, four-pole, 11kW induction machine controlled by a Powerflex ®700 drive used as the load drive
vi. Lorenz torque transducer to measure the torque and the speed. The values are displayed on a graphical user interface on the sensor software resident in a computer.

The components are independently tested before the whole system is run for testing. The PWM inverter uses a full H-bridge configuration and is based on IGBTs which are integrated into three-phase intelligent power modules (IPMs). DC link capacitors are used to smooth the DC voltage

supplied through a bridge rectifier. The schematic diagram of the experimental set up for testing the BDCE controlled drive is as shown in Figure 5-1. The workbench schematic diagram shows the equipment used in testing the BDCE controlled nine-phase induction machine drive.

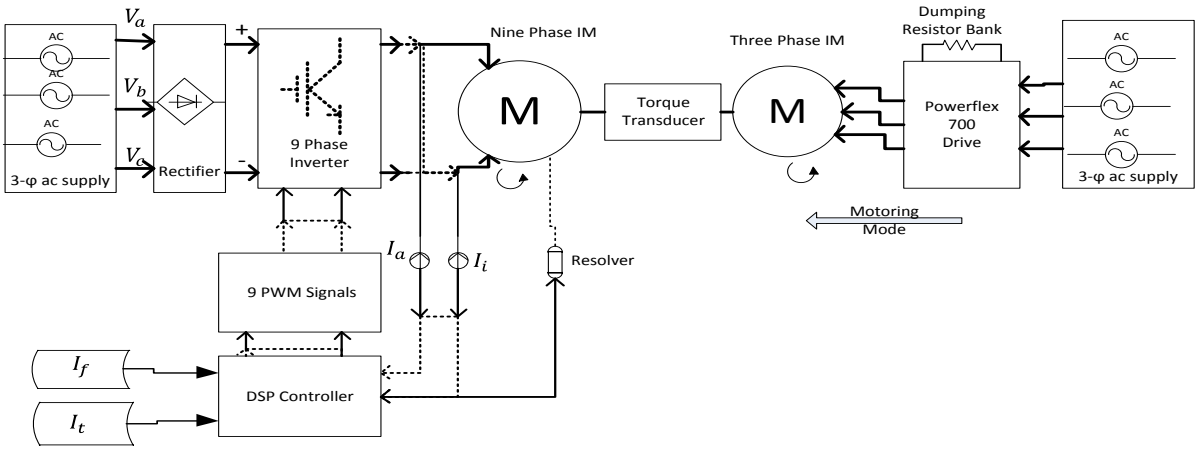

Figure 5-1. Schematic diagram of the test bench used for testing the BDCE controlled drive.

The practical bench set up for testing the drive is shown in Figure 5-2 showing the main components of the test bench. Figure 5-3 shows the connection of the nine-phase BDCE controlled drive to the Powerflex® 700 controlled load drive. When the Powerflex ® 700 drive is in the breaking or in the generator mode, the power generated is dissipated in the break resistor bank.

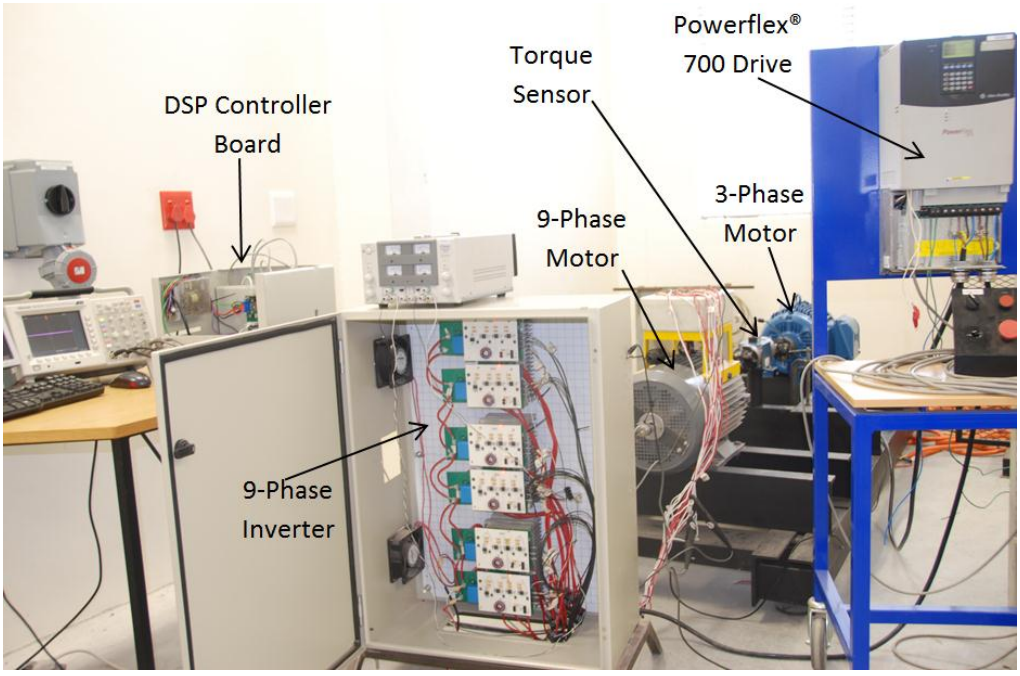

Figure 5-2. The nine-phase induction machine drive system.

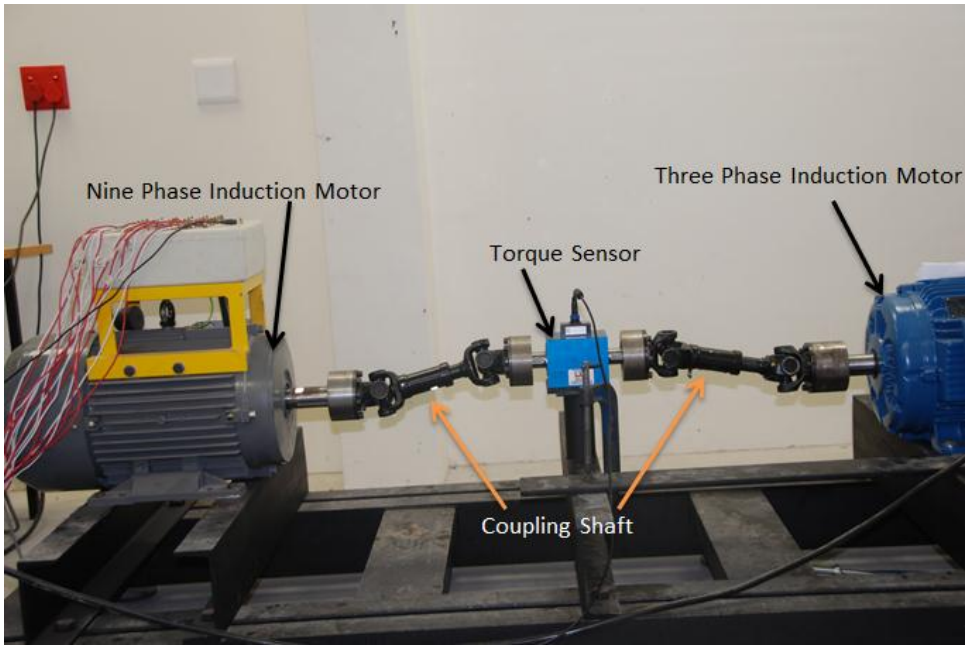

Figure 5-3. Connection of the BDCE controlled drive to the three phase load drive.

5.2 DSP Controller Board Tests

The main components of the controller board are the DSP and the FPGA. The TMS320VC33 DSP is a high performance CMOS 32-bit floating point single chip DSP. It has high speed and can perform up to 60 million operations per second. The DSP is made more efficient by the use of the on-chip DMA for fast memory management. The DMA enables execution of some basic memory access operations without engaging the CPU. The DSP controller board is shown in Figure 5-4. The green boards at the bottom left side are the PWM boards which produce the light for transmitting the PWM signals to the inverter through an optic fibre link.

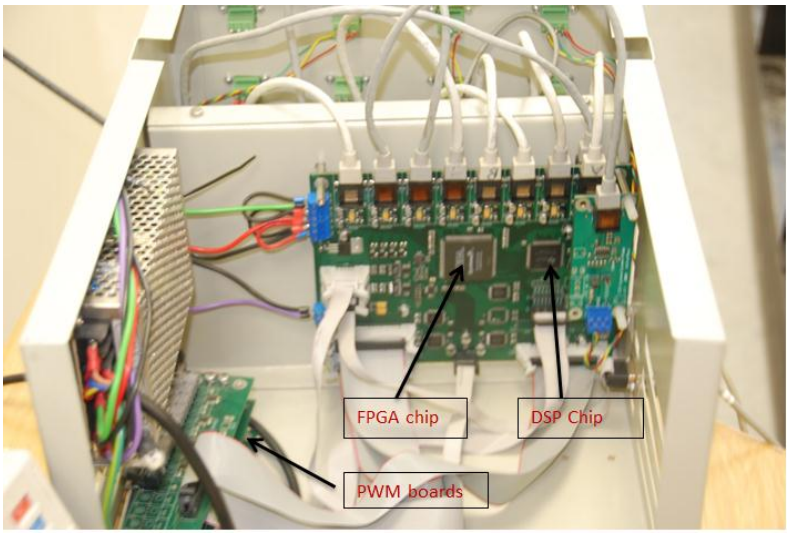

Figure 5-4. DSP based controller board.

The DSP control board uses the EP1C6Q240C8 FPGA to communicate with the peripheral devices like the analogue to digital converters (ADCs), the digital to analogue converters (DACs), the PWM boards and the resolver. The FPGA receives data from the peripheral devices, formats it and pre-processes it for use in the DSP. The implementation of data assignment and switching in the FPGA instead of the DSP simplifies the development of control programs for power electronic applications [66].

The peripheral devices receive data from the control knobs, the voltage and current measuring cards and the resolver. The data is converted to values between 0 and 5 for use in the ADCs and the results of the conversion are used in the FPGA. The basic operation of the controller is based on the DSP event management system which generates interrupts to start and stop the various procedures used in the control program. Figure 5-5 shows the functional diagram of the DSP controller board and its external connections.

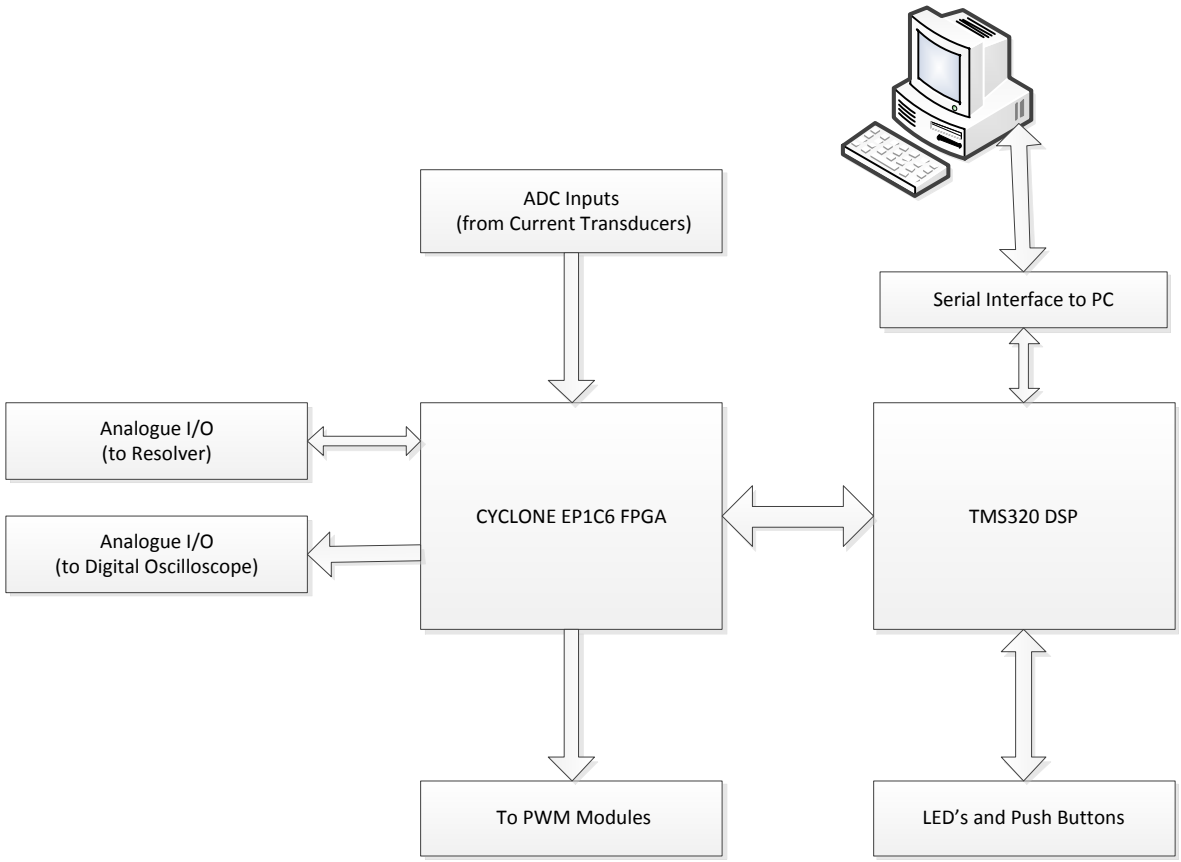

Figure 5-5. Functional diagram of the DSP controller board and peripheral devices.

A sample program is used to test the general functionality of the DSP controller board. The program is written using the C programing language and compiled to produce an executable file that is run in the DSP. The DSP has a high efficiency C language engine for this purpose. The test program uses LEDs to show the functionality of timers and DAC modules. The functionality of ADC modules is

shown by the output of the program when push buttons and control knobs are activated. The tests also confirm the proper communication between the PC and the DSP controller board.

5.3 Testing the PWM Boards and the Inverter

A PWM test program is downloaded to the controller board to test the functionality of the PWM modules. The PWM generator consists of the gate drive software program which defines the PWM dead time and the PWM driving software program which determines switching states of the inverter. As the PWM control program runs, the PWM outputs are observed as the LEDs switch on and off, showing the switching action of the PWM outputs. To verify corresponding PWM outputs and inverter inputs, one set of outputs is activated in software while the rest are deactivated. The program is run and the inverter energised, tested and labelled accordingly. The nine-phase full H-bridge inverter uses eighteen PWM outputs to control the inverter switches. The nine-phase inverter is shown in Figure 5-6 showing the isolated power supply board for the IPM driver circuit and the opto-couplers with voltage level shifters.

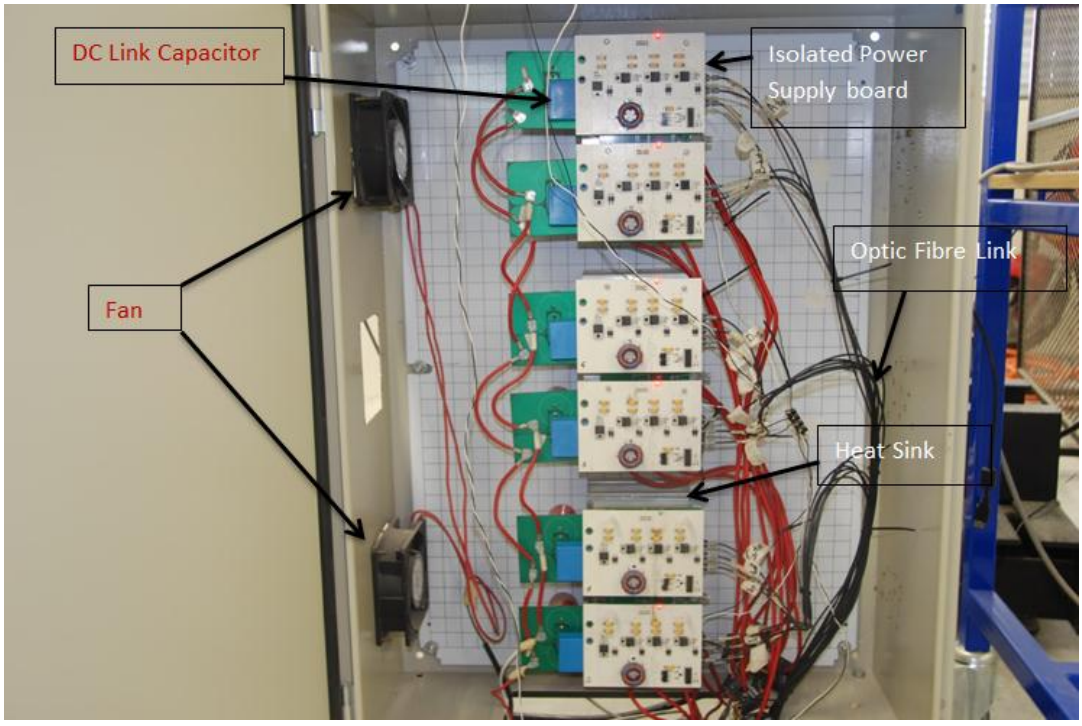

Figure 5-6. Nine-phase PWM voltage source inverter.

The PWM outputs are connected to the inverter through an optic fibre link. The optic receiver circuit converts the optic signals into voltages that drive the IPM modules using HCPL0661 opto-couplers. Figure 5-7 shows the circuit which receives the optic signals from the controller board and the voltage level converters that convert the optic signal to voltages that drive the IPM gate drive circuit. Four isolated +15V power supplies are used to power up the IPM pre-driver circuit as shown in the diagram.

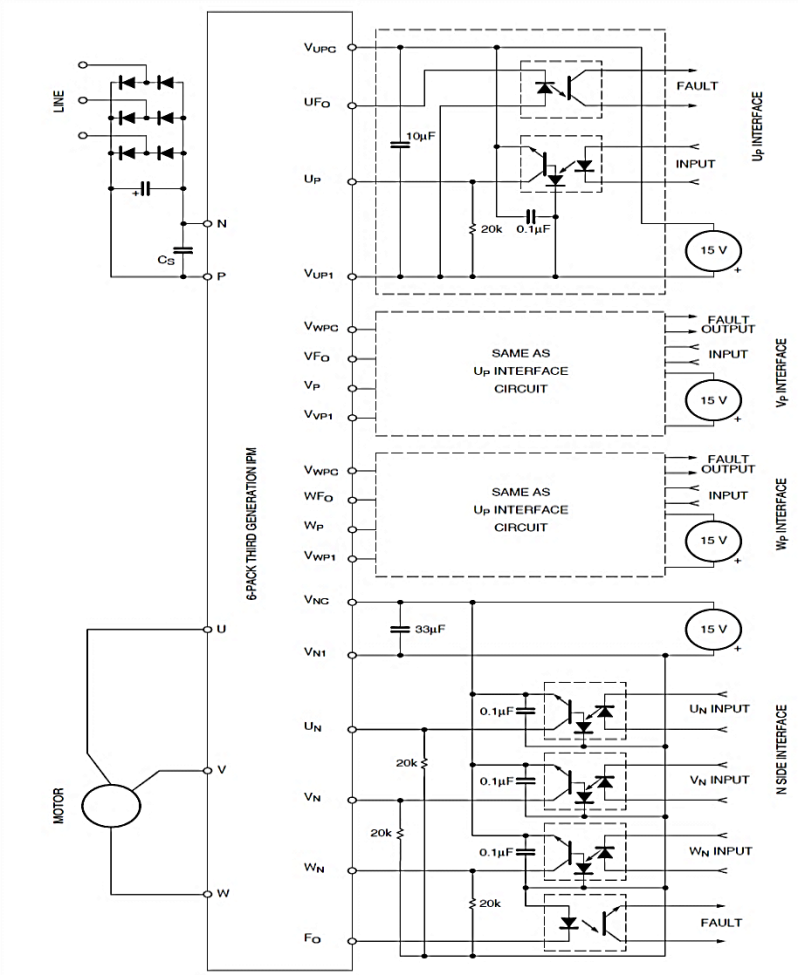

Figure 5-7. Schematic diagram of the inverter board for a three phase IPM module showing the optic link interface, the isolated power supplies, the IPM and the connection to a three phase motor.

The diagram shows connections made to a three phase system. Since a full H-bridge inverter configuration is used in the nine-phase inverter, two outputs are used for each phase and the connection required for a three phase system using a full H-bridge inverter is shown in Figure 5-8. Two IPMs are required to drive a three phase system using the full H-bridge configuration. The nine-phase inverter therefore uses six IPM modules. The H-bridge configuration enables independent control of the stator current per phase and also gives inherent fault tolerance.

A phase is driven by two PWM signals whereby one signal drives the positive voltage and the other signal drives the negative voltage across the machine phase. From Figure 5-8, it can be observed that PWM signal A1 drives the two switches which push current in the clockwise direction (negative) and signal A2 pushes current in the anti-clockwise direction (positive) through phase A.

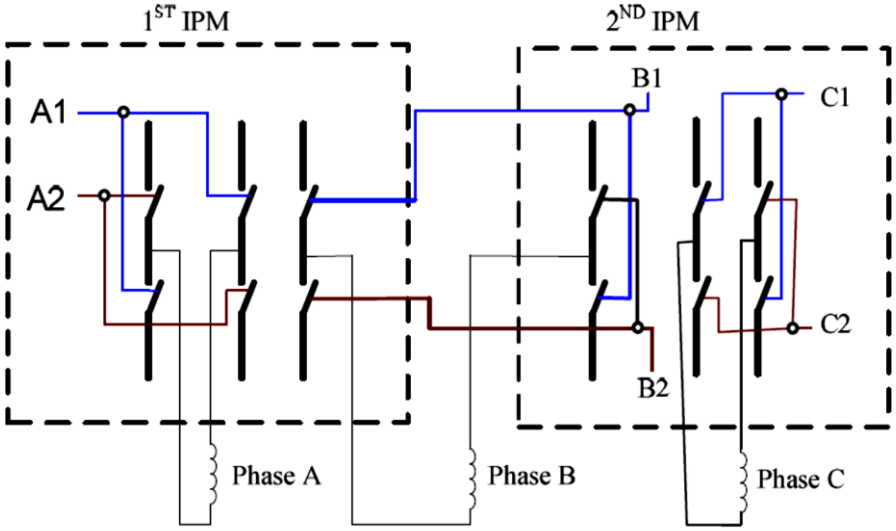

Figure 5-8. Connection diagram of two IPMs for three full bridge inverter blocks.[46]

5.4 Testing of the Current Measuring Cards

The current flowing in the machine phases is measured using the Telcon Hall Effect Current transformer. The current transducer has a 1000:1 current conversion ratio. The current measuring card is designed such that it converts the current from the transducer into a voltage between 0V and 5V for conversion in the ADC. The ADC voltage is converted back to the equivalent current in software and the value is sent to the scope through the DAC module. The experimental set up used to test the current measuring cards is shown in Figure.5-9. The measured currents are used in the hysteresis controller to generate the PWM inverter switching signals.

A current probe is used in parallel with the transducer to make a comparison between the DAC output and the value from the current probe. The scaling factor is adjusted in software until the DAC output is equal to the output of the probe. The variable resistor is used to limit the current flowing in the circuit and to vary the magnitude and observe the changes in the readings from the DSP controller.

5.5 Testing the Voltage Measurement Cards

The test procedure is almost similar to the one used in testing the current measuring cards. In place of an ammeter, a voltmeter is used to measure the voltage across the variable resistor in Figure.5-9. The variable resistor is connected to a voltage measuring card input ports for voltage measurement. The card uses the ADC in the DSP controller and the DAC to enable the displaying of the voltage on the oscilloscope. A variable frequency signal generator is used in place of the fixed frequency AC source. The value of the voltage is set at a constant value (3.9V was used in the test) and the relationship between the measured value from the voltmeter and the measured value from the voltage card at various frequencies is observed.

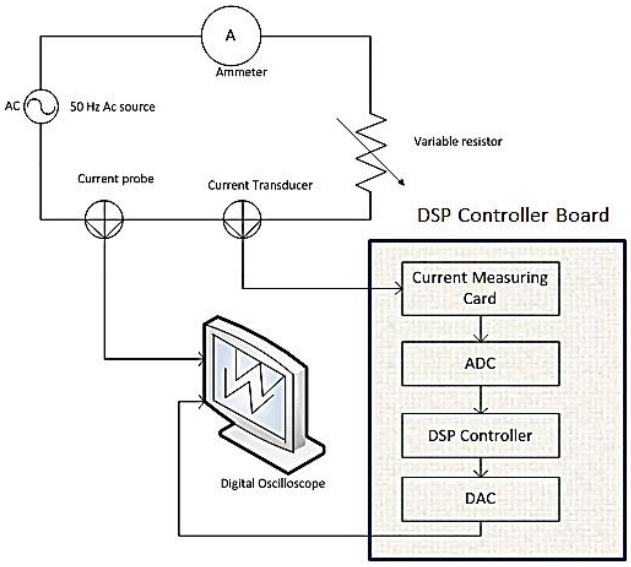

Figure.5-9. Experimental set up for testing the current measuring card.

Table 5-1 shows the variation of the voltage measured by the voltage measuring card with frequency at a fixed source voltage. The values show that the voltage measuring card gives lower values as the frequency of the voltage increases above 500Hz. This can be attributed to the fact that the cards were originally designed to measure DC values therefore they attenuate higher frequencies. After this observation, an alternative delta modulation scheme was designed to test the feasibility of implementing the delta modulated current controller with the trapezoidal reference waveforms without measuring the stator voltages. The results presented in this chapter were obtained using the alternative delta modulated current controller.

Table 5-1. Variation of measured voltage with voltage supply frequency.

Supply Frequency (Hz)	**Supply Peak value (V)**	**Measured Value (V)**	**Measured/Supply ratio**
50	3.9	3.9	1
100	3.9	3.9	1
200	3.9	3.9	1
500	3.9	3.5	0.9
1000	3.9	3.0	0.77
2000	3.9	2.0	0.51
3000	3.9	1.5	0.38
4000	3.9	1.4	0.36
5000	3.9	1.1	0.28

Figure 5-10 shows the variation of measured output voltage with input voltage frequency. The graph shows that the measuring card attenuates the input signal for frequencies above 500Hz. This is an indication that the card was designed to measure dc bus voltages.

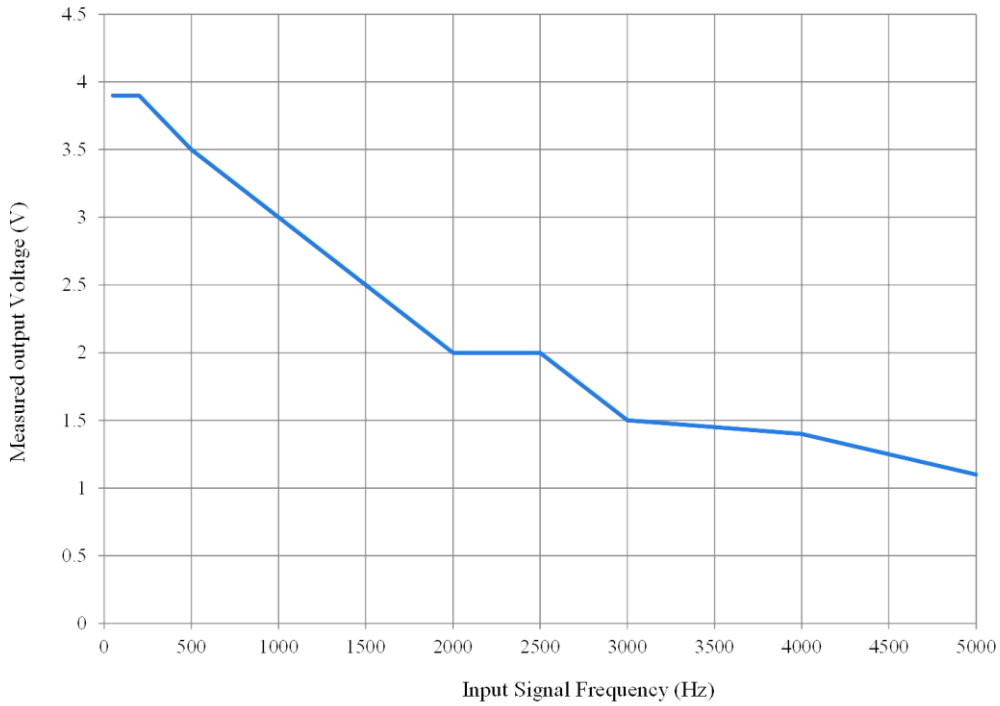

Figure 5-10. Variation of measured output voltage with input voltage frequency using voltage measuring cards. (Input voltage is 3.9V)

5.6 Resolver Testing

The position of the rotor as it rotates is decoded using a resolver attached to the motor shaft. The schematic presentation of the resolver is shown in Figure 5-11. The labelled connections are the connections made to the DSP controller to make angle measurements. The connections and colour of the connectors used in connecting the resolver to the DSP controller are shown in Table 5-2. A 9-pin D serial connector is used to connect the resolver to the DSP board.

The reference winding is supplied with the sinusoidal reference signal generated in the DSP controller board through a rotary transformer. The signal induces voltages in the sine and the cosine windings as the rotor of the resolver rotates at the motor speed. The induced voltage values are measured by the controller and their magnitudes are used to calculate the position of the rotor in angular radians. The expression for the angle is given by:

$$(t) = \arctan\left(\frac{V_{sine}(t)}{V_{\cos(t)}}\right) \qquad (5\text{-}1)$$

where $V_{sine}(t)$ is the magnitude of the voltage induced in the sine winding and $V_{\cos(t)}$ is the magnitude of the voltage induced in the cosine winding. The rotor speed is calculated by determining the rate of change of the angle with time, that is:

$$\omega_r = \frac{d\theta(t)}{dt} \tag{5-2}$$

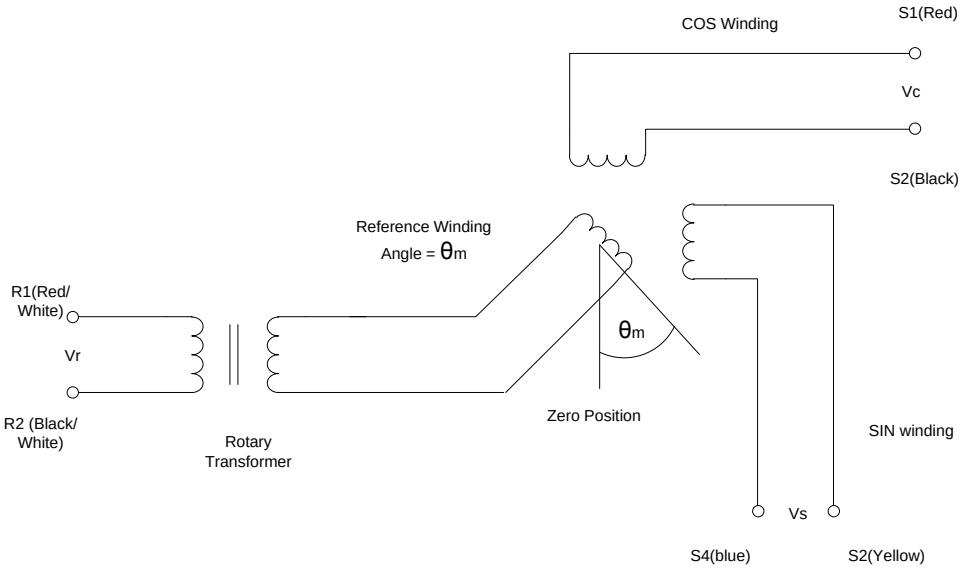

Figure 5-11. The schematic representation of the resolver [66].

Table 5-2. Pin connections between the resolver and the DSP controller board

Colour of wire from Resolver	**Colour of wire to connecting Cable**	**D-Connector pin Number**	**Designation**
Red and White	Green	2	Ref (+)
Red	Red	3	Cos (+)
Yellow	Yellow	4	Sin (+)
Black and White	White	7	Ref (-)
Black	Black	8	Cos (-)
Blue	Blue	9	Sine (-)

The rotor angle and the speed value calculated in software are sent to the digital oscilloscope for display to confirm the operation of the resolver. Figure 5-12 shows the rotor angle waveform displayed on the digital oscilloscope. The angle increases with time showing that the machine is rotating in the right direction thereby confirming that the resolver has been connected correctly. The measurement was done at a rotor speed of 35 rpm and this value can be calculated using the angle waveform to confirm the accuracy of the resolver.

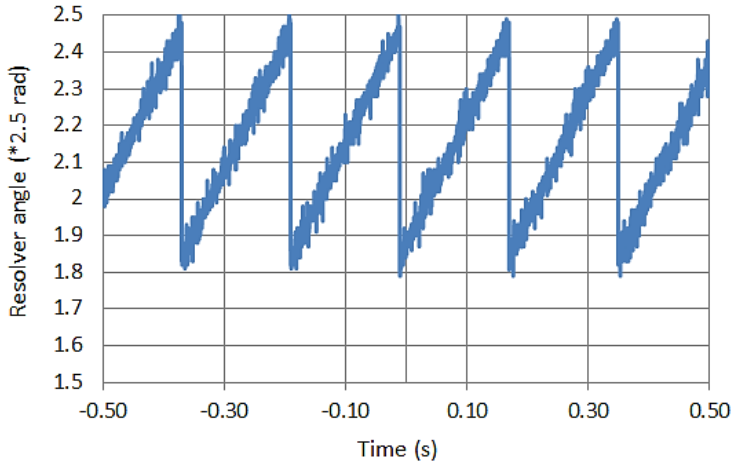

Figure 5-12. Rotor angle waveform produced by the controller.

The rising waveform shows some noise which may be caused by the noise in the ADC and DAC circuits. The resolver uses electromagnetic induction to produce the sine and cosine waveforms and this may also be a possible source of noise. Noise in the oscilloscope cannot be ruled out as this noise is also observed in other measurements.

5.7 Evaluation of the BDCE Controlled Drive

After confirming that all the components of the drive are working properly, the nine-phase drive is coupled to the three-phase drive to test the current controllers. The experimental evaluation of the nine-phase BDCE controlled drive is presented in this section. The stator currents produced by the current controllers are displayed and compared. The torque produced by the drive at different torque current values is measured and the overall efficiency of the drive is also evaluated.

5.7.1 Preliminary Tests Conducted on the Drive

Preliminary test-runs are done on the drive to verify if all the components are operating as expected. The variation of voltage and current with speed is tested to observe if there are any electrical faults in the system. The acceleration, deceleration characteristics are also tested to see the response of the motor to speed command changes. The response of the motor torque to changes in the torque current command is also tested to verify if there is decoupled control of the torque and flux.

5.7.1.1 Variation of dc bus current and voltage with motor speed.

The preliminary tests are important for determining the expected changes in stator current frequency and magnitude with motor speed when using the BDCE control method. The relationships between running speed, DC bus voltage, DC bus current and stator current frequency is tested by taking measurements at different running speeds at no load. This is achieved by varying the magnitude of the supply voltage and observing the changes that occur in the stator current frequency, the DC link

current and the motor speed. Figure 5-13 shows the changes in DC bus voltage and current with motor speed at no load.

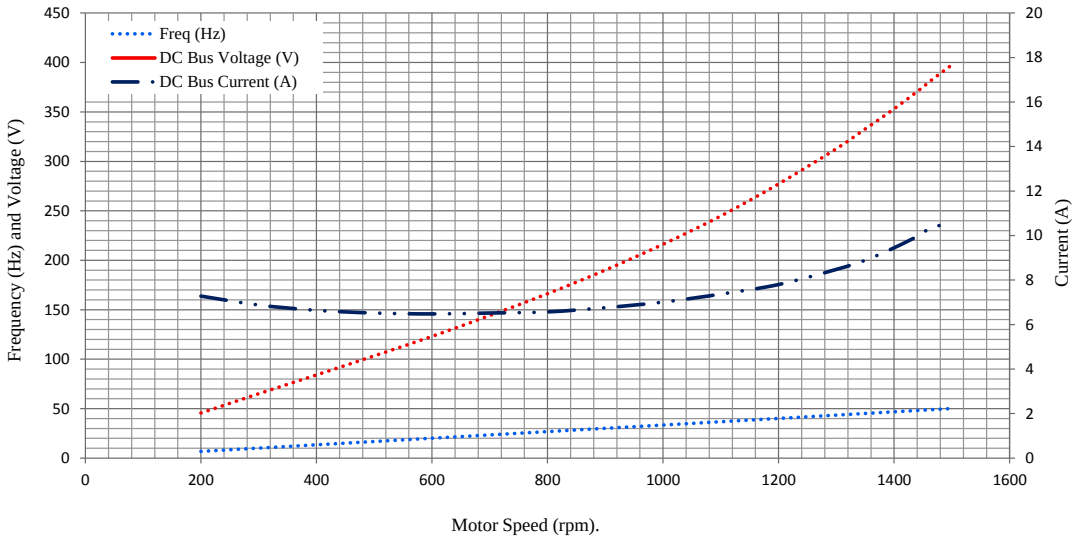

Figure 5-13. Variation of DC bus current and voltage with motor speed under constant v/f control.

There is a linear rise in frequency and voltage with motor speed. The current is higher at 200 rpm, decreases as the speed increases up to 800 rpm and then starts rising again. The initial high current shows that the motor consumes more power at start up to supply the frictional losses at lower speeds and to drive the motor against its inertia. The current increases after the speed of 800 rpm which corresponds to a dc bus voltage of 155V. This increase in current may correspond to the increase in copper losses as voltage increases thereby pushing more current in the phases.

5.7.1.2 Delta modulated current controller tests

The delta modulated current controller is the main design component in this study. The performance of the drive is highly dependent on the quality of the trapezoidal stator current waveform produced when the current controller is used. From simulations, the delta modulated current controller which uses stator voltages as inputs to the integrator gave the best results. However, due to hardware constraints stated in section 5.5, the method could not be implemented. The alternative technique discussed in section 3.3 is implemented. From the analysis done in section 3.7.2, the value of the quantizer output determines the performance of the current controller for a fixed switching frequency and a fixed integrator gain.

The variation of the stator current waveform with the changes in the quantizer output is tested by changing the quantizer output value in software and running the machine under a light load. The stator current waveform is observed for changes in the quantizer output. Figure 5-14 shows the stator current waveform produced using a quantizer output of 6. The waveform produced is smooth but does

not show proper control at the plateau of the field current. This is caused by the fact that the gradient of the carrier is less than that of the reference.

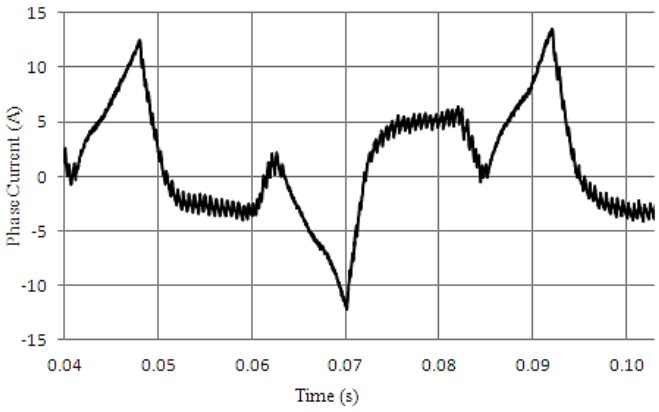

Figure 5-14. Stator current waveform produced using a quantizer output of 6. [I_f = 5.83, I_t = 2].

Figure 5-15 shows the stator current waveform produced using a quantizer output of 12. This value is slightly above the maximum amplitude of the reference which is 11.66 when the phase is acting as a field producing phase. The waveform shows good control of the stator current with a relatively flat plateau. However, a perfect flat plateau could not be attained without overloading the modulator.

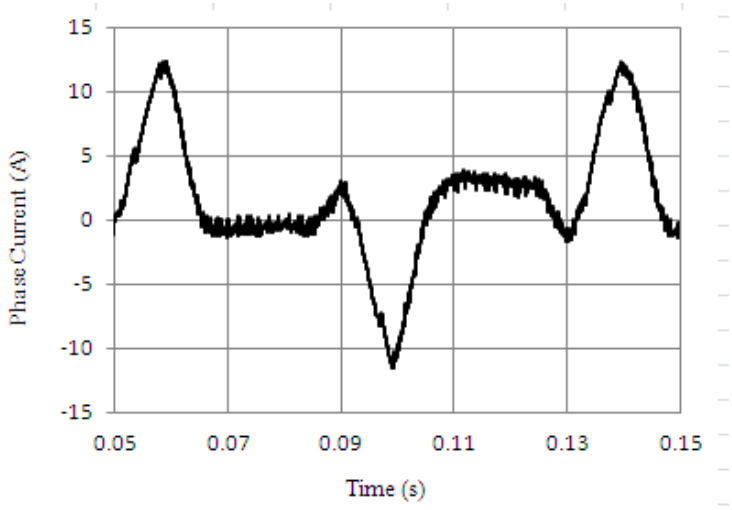

Figure 5-15. Stator current waveform produced using a quantizer output of 12. [I_f = 5.83, I_t = 2].

The waveform in Figure 5-16 shows the effect of overloading the modulator by use of a quantizer output of 18. When the slope of the carrier becomes too steep, the current controller shows granular noise which causes current hysteresis. The optimum value for the controller is found by iterating the quantizer output and observing the changes in the stator current waveform. The current controller gives good results using a quantizer output of 13 and an integrator gain of 15. However from both simulations and practical tests, the alternative delta modulated current controller behaviour is highly dependent on the quantizer output. A large value gives better current control but with granular noise and a low value gives poor current control but with a smooth current waveform.

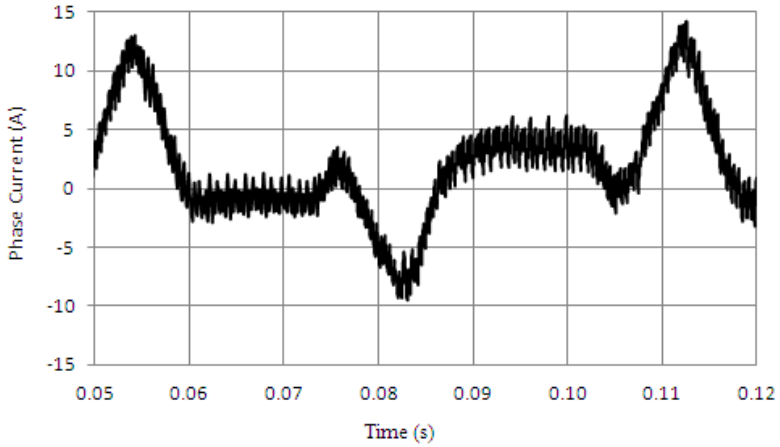

Figure 5-16. Stator current waveform produced using a quantizer output of 18.[I_f = 5.83, I_t = 2].

5.7.1.3 Acceleration and deceleration characteristics at no load

The no load performance of the machine drive is tested to determine the magnitude of the no load torque. The value of the no load torque gives the magnitude of the frictional and windage losses. It also helps to find out if there are any other points of friction that may cause undesired performance. The acceleration and deceleration gives an indication of the inertia of the motor.

The motor is run up to rated speed at no load and then the power supply is switched off. The motor speed decays to zero at a rate determined by the rotational losses and the inertia of the motor. The rate of decay of the speed and the rotational losses are related through the relationship:

$$J\frac{d\omega_r}{dt} = -T_{rot} \tag{5-3}$$

where J is the moment of inertia, ω_r is the rotor speed and T_{rot} is the rotational torque. Figure 5-17 shows the acceleration and deceleration characteristic curve of the nine-phase cage rotor induction motor.

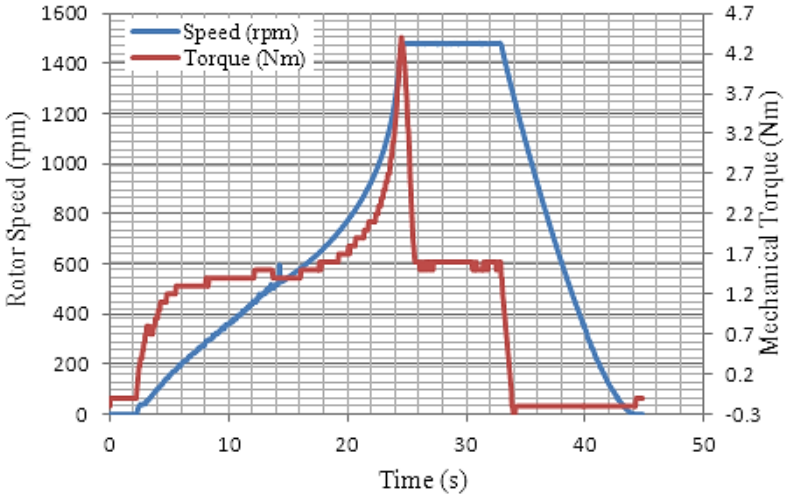

Figure 5-17. The acceleration and deceleration characteristic curve of the nine-phase induction machine.

The moment of inertia can be calculated using the deceleration rate and the deceleration torque using equation (5-3). The speed changes from 1466 rpm to stand still in nine seconds. Therefore the deceleration rate is 17.0577$rads^{-2}$. The rotational torque is -0.28Nm. This implies that the moment of inertia is 0.1102kgm^2. The book value of the moment of inertia of the machine is 0.0724 kgm^2. The calculated value includes the inertia of the three phase induction motor coupled to the nine-phase machine as the load drive.

The motor is also accelerated using the speed command at no load. It is then brought to a standstill using the speed command. The stator current waveform is observed to determine if the frequency of the current waveform changes with speed as was observed in the simulations.

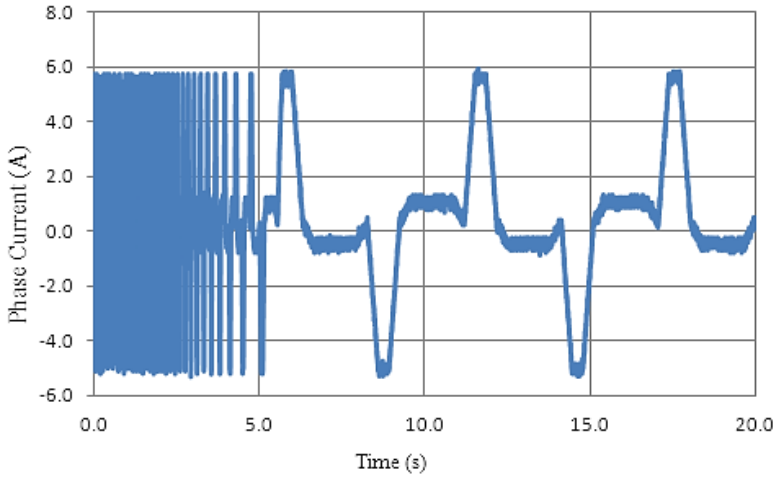

Figure 5-18. Change in stator current frequency with speed.

The frequency of the current waveform decreases with speed when the PI controller is used. Ideally, the torque current should be very small at no load. The torque current is at a value of about 1A to supply the losses and to supply the torque to counter the inertia of the two coupled motors.

5.7.1.4 Testing decoupled control of flux and torque

The main objective of the BDCE control method is to implement decoupled control of torque and flux without using coordinate transformations. The decoupling action is tested by varying the torque current and observing the change in torque. The field current should not to be affected by the change in the torque current to confirm decoupled control. Figure 5-19 shows the change in torque current and the corresponding change in the stator current waveform. It can be seen that only the torque component of the waveform changes while the field component remains constant. This is evidence of decoupled control of the torque current and the field current. Figure 5-20 show the changes in the torque and speed as the torque current changes. When the torque current magnitude is changed, the speed changes for a moment and comes back to the command speed since the load drive is speed regulated. The developed torque changes with the torque current. The ratio of the change in torque to

the change in the torque current is an indication of the torque constant. The value is low because the test was done at 25% of the rated voltage.

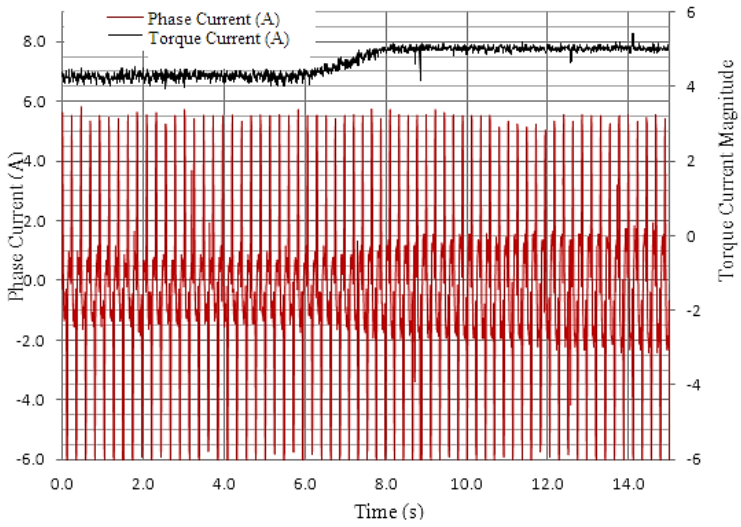

Figure 5-19. Change in torque current and the corresponding phase current

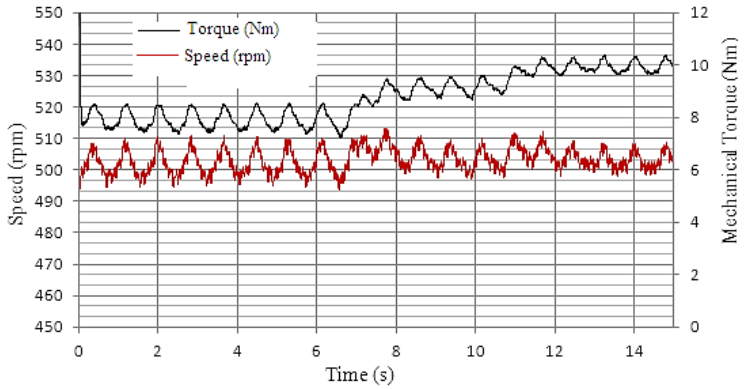

Figure 5-20. Change in developed torque and rotor speed corresponding to change in torque current.

5.7.1.5 Testing the change in developed torque with speed

Figure 5-21 shows the change in torque with rotor speed at 25% rated voltage and rated field current. The torque current is determined by the PI controller. The nine-phase motor speed is set at 500rpm and the three-phase motor speed is varied to determine if it can load the nine phase drive. More torque is developed when there is a bigger difference between the set speed of the nine-phase machine and the set speed of the three-phase machine. Resultantly, the difference between the speeds is used to control the developed torque. The principle behind this operation is that the nine-phase machine tries to run at its set speed while the three-phase machine also tries to run at its set speed. Since the three-phase machine is speed regulated, it develops torque against the nine-phase machine in order to maintain its command speed.

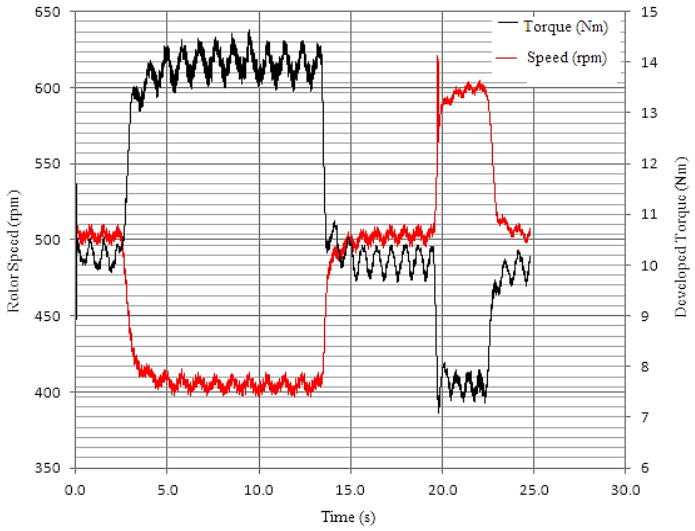

Figure 5-21. Testing the development of torque using three phase induction machine as load drive

5.7.2 Implementation of Current Controlled PWM in the BDCE Controller

The BDCE control algorithm is executed in software using the C programming language for the TMS320VC33 DSP. Some important program snippets are shown in Appendix F. These include the duty cycle calculator, the PWM generator and the numerical integrator implementation algorithm. The inputs to the controller are the speed reference and the flux reference. The reference speed is used in the PI controller to produce the torque current magnitude. The flux reference is used to determine the magnitude of the field current. In this investigation, the flux is set at 0.7T which corresponds to a field current of 5.5A according to the measurements presented in Figure 4-18. These values are used in the reference current generator together with the output of the reference current look up table to determine the polarity and magnitude of the reference current for each phase as shown in Figure 5-22.

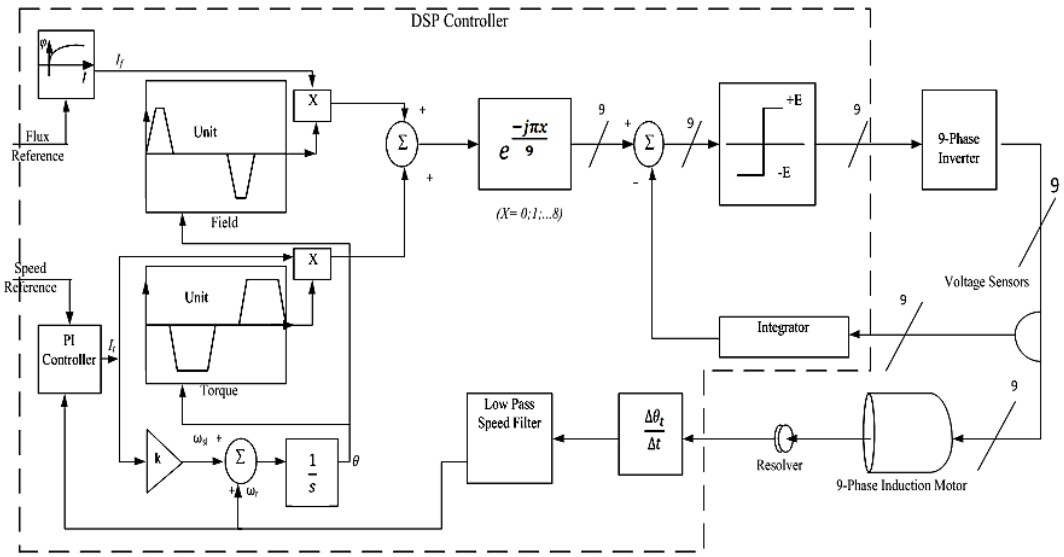

Figure 5-22. Delta modulated controller implementation on BDCE controlled drive.

The generated reference current waveforms are used in the current controllers to generate the PWM switching signals which control the inverter. In the delta modulated controller, the pulse width modulated stator voltage pulses are passed through a low pass filtering integrator to reconstruct the reference current and the reconstructed signal is the carrier signal used in the delta modulator. The carrier and the reference signals are compared to generate an error signal. A PWM stator voltage pulse is generated through the inverter and has the same sign as the error signal. The duty cycle of the PWM signal is determined by the sign of the error signal and is calculated in software. A 0% duty cycle is used for a negative error signal and a 100% duty cycle is used for a positive error signal. Since the inverter switches between positive and negative values, a PWM output with a zero value corresponds to a negative inverter output voltage.

The delta modulated controller algorithm is shown in the flow chart of Figure 5-23. The reference values are set during the initialization. The resolver angle is calculated for use in the reference current generator after which the stator voltage is measured. The measured voltage is low pass filtered through the integrator to generate the carrier signal. The carrier is then compared to the reference current to generate the PWM output pulse corresponding to the sign of the error. When the PWM signal is produced, the process starts again. This algorithm is run for all the nine phases to generate different PWM signals for the H-bridge inverter legs as illustrated in Figure 5-8.

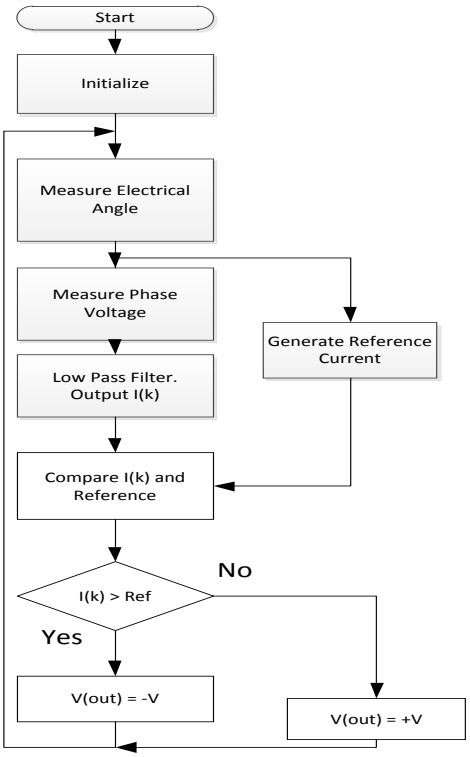

Figure 5-23. Flow chart of the delta modulated current control system algorithm using measured stator phase voltages

In order to observe the switching pulses generated by the current controller, the value of the PWM output pulse is sent to the oscilloscope and the trace is displayed together with the stator current waveform as shown in Figure 5-24. The green trace shows current waveform and the red trace shows the PWM pulses corresponding to the current waveform. The voltage waveform shows the change from single pulse to PWM mode through the use of the delta modulated controller. When the slope is positive, there are more positive pulses than negative pulse as shown during the field phase of the current. The PWM mode exists on the torque phase of the current where the slope is gentle hence the negative pulses and the positive pulses occur at comparable rates and are visible. However, when the sign of the slope does not change, the inverter remains in the single phase mode.

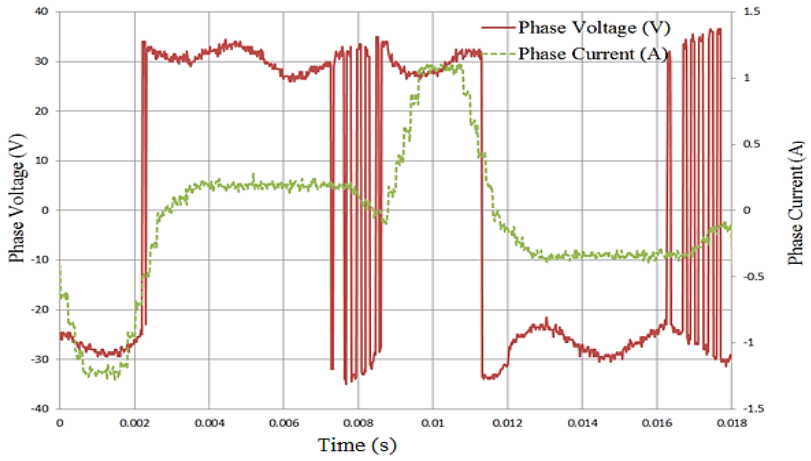

Figure 5-24. PWM switching signals observed while using delta modulated current controller.

The figure shows how the PWM output from the delta modulator smoothly changes from PWM mode to the single pulse mode when the reference signal is persistently constant at some parts of the waveform as noted in [51].

The hysteresis controller program uses the FPGA based hysteresis modulator. The duty cycle in the hysteresis controller is determined by the rate of change of the reference signal with respect to the measured values and hence there is no duty cycle calculation in the controller. The inverter switches change state when the measured value becomes equal to the sum of the reference current and the hysteresis band.

5.7.3 Stator Current Tests

The reference stator current magnitude is set through the control knobs. When the PI speed controller is used, only the field current is set through the knobs while the torque current is determined by the PI controller as explained earlier. Current probes are used to measure the stator currents and display them on the digital oscilloscope.

The hysteresis controller produces the stator current waveform shown in Figure 5-25 when the field current is set at 5.83A and the torque current set at 3A at 500rpm running speed. The effect of

the hysteresis band can be observed in the stator current waveform. Figure 5-26 shows the stator current switching waveform generated by the hysteresis controller. The varying switching frequency is evident in the magnified waveform. The figures are shown at the end of the section for easy comparison with the results obtained using the delta modulation technique.

After testing the stator current waveform produced by the hysteresis controller, the conventional linear delta modulator is implemented by integrating the PWM signals directly in the DSP and using the output as the carrier signal fed back to the forward comparator. A sampling frequency of 10 kHz is used in the sample and hold block. The waveform produced using the conventional linear delta modulator cannot be used to run the machine because it does not exhibit the properties of the trapezoidal waveform required for BDCE control. The conventional linear delta modulated current controller fails to force the stator current to track the reference current and this is in agreement with the analysis done in Section 3.3. Resultantly, the delta modulation program is modified to use stator voltages as inputs to the integrator since this is the configuration used in the simulations done using Simulink. Preliminary tests done show that the available voltage measuring cards fail to measure the voltage signal above 2.5 kHz and hence cannot be used in the control system which uses a 5 kHz switching frequency as shown by the measurement given in Table 5-1

An alternative delta modulation scheme is proposed in which the reference current is first integrated before being compared to the carrier. The carrier is generated by low pass filtering the inverter switching pulse generated in software. The alternative delta modulated controller is implemented to determine if it can produce the desired stator current waveform. Figure 5-27 shows the measured stator current waveform. The waveform shows a smooth curve when the reference signal changes gradient from a high value to zero instantaneously. This is because the integrator acts like a filter and since it uses cumulative addition, its output value cannot change instantaneously and this affects the output stator current waveform.

Figure 5-28 shows the stator current magnified waveform produced by the delta modulation technique. The constant switching frequency can be observed in the waveform. Current spikes are observed during the switching instances and this may be attributed to the high switching frequency of 10 kHz used in the delta modulation technique. The constant switching frequency gives regular and smooth inverter operation.

The hysteresis controller produces a more perfect stator current waveform which accurately tracks the reference current. It exhibits good current control mainly because it uses the measured values and hence the stator dynamics are accounted for in the measured value. The current waveform shown in Figure 5-25 has spikes which may be attributed to noise in the instrumentation electronic circuit. This noise is observed in other measurements taken using the same instrumentation. The spikes occurring

at the switching instances in Figure 5-26 are expected to occur when the IGBT module conduct current.

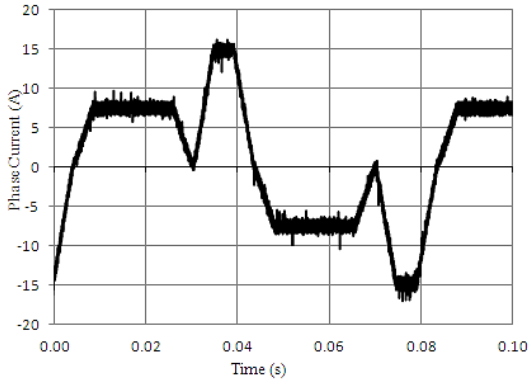

Figure 5-25. Stator current waveform produced by the hysteresis controller at 500 rpm rotor speed. [I_f = 5.83A, I_t =3A]

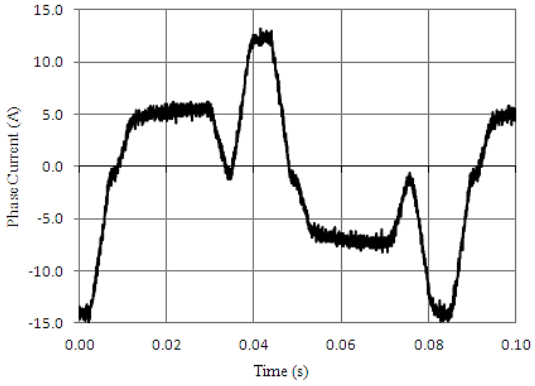

Figure 5-27. Measured stator current waveform produced by the alternative delta modulated current controller at 500 rpm motor speed. [I_f = 5.83A, I_t = 3A]

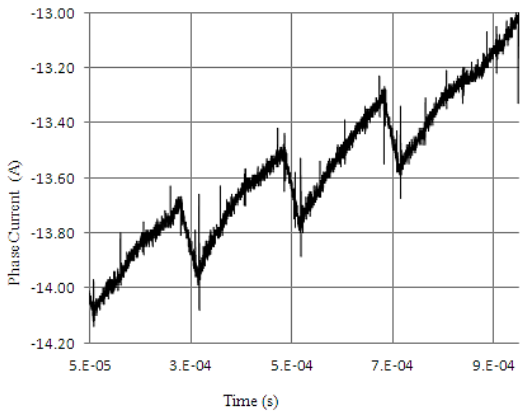

Figure 5-26. Stator current switching waveform produced using the hysteresis controller.

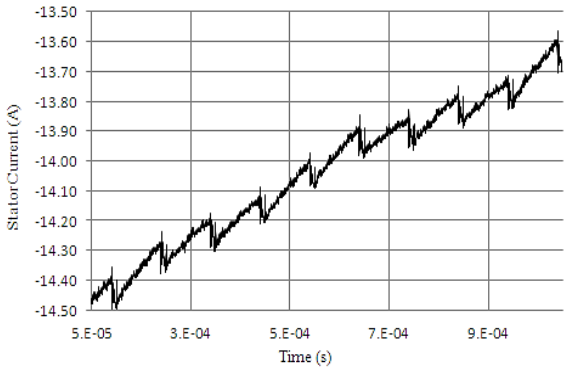

Figure 5-28. Stator current switching waveform produced using the delta modulated controller.

The delta modulated controller produces a stator current waveform which shows some tracking errors at the extreme points of the reference current signal where the slope changes abruptly as shown in Figure 5-27. This is mainly due to the filtering effect of the integrator when a fixed quantizer output is used. The measured stator wave is however more smooth compared to the one produced by the hysteresis controller. The magnified waveform in Figure 5-28 shows considerably higher spikes at the switching instants compared to the hysteresis controller. This is because the delta modulator uses a higher switching frequency than the hysteresis controller. The results would have been better if the stator voltage was used in the feedback loop as suggested in the simulations.

The delta modulated controller output current shows a constant switching frequency which gives smooth inverter operation. The constant switching frequency makes it easy to design filters for the harmonics and current ripples.

5.7.4 Evaluation of Relationship between Developed Torque and Torque Current

The BDCE control is similar to the separately excited dc motor control and hence a linear relationship is expected between the torque current and the developed torque. The relationship is tested by supplying the machine with the rated field current of 5.83A and 25% rated voltage under locked rotor conditions. The same results can also be achieved at a running speed of 800 rpm while using a three phase induction machine as a load. The nine-phase motor speed is fixed at 800 rpm using the Powerflex 700® drive which locks the running speed of the three-phase induction motor at that speed. The maximum torque developed by the machine is determined by the torque developed when the rated torque current is supplied.

Figure 5-29 shows the observed relationship between torque current and developed torque under locked rotor conditions and also at a rotor speed of 800 rpm. The test is done using the hysteresis controller and then using the delta modulated controller. There is a linear relationship between the developed torque and the torque current within practical limits, as expected. The fact that the delta modulated controller also gives a linear relationship shows that it can be used in the BDCE control method.

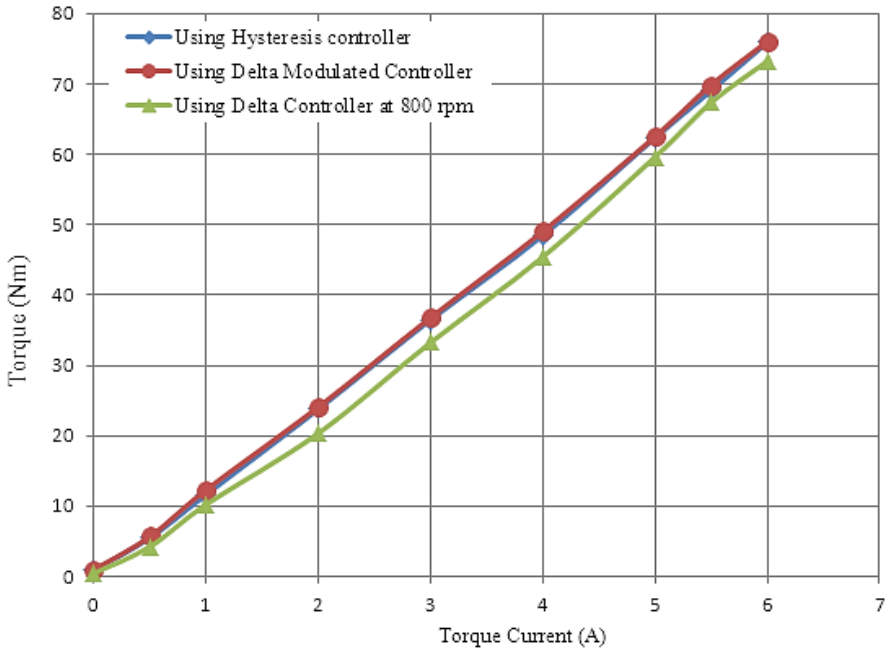

Figure 5-29. Relationship between developed torque and torque current using rated field current (5.83A) under locked rotor conditions using the hysteresis control (blue) and using delta modulation (brown), and at 800 rpm rotor speed using the delta modulated controller (green)

The torque produced by the motor when using the delta modulated current controller at 800 rpm is less than the locked rotor torque. This is attributed to the windage and frictional losses. The torque is also reduced because some torque is required to run the machine against its inertia.

5.7.5 Evaluation of Drive Efficiency

There are various ways of measuring the efficiency of three-phase induction machines as given in [64]. However, there is no standard established yet for the evaluation of the efficiency of multiphase machine drives. The measurement is further complicated by the fact that the system is a coupled motor system which requires the measurement of the losses of the motors separately. As a result, it is challenging to isolate the losses of the system so that the efficiency can be measured accurately.

In this thesis, the relationship between torque, rotor speed and power is used to determine the efficiency of the drive system. The input power is calculated by measuring the DC input voltage and current at every test point. The output power is calculated by multiplying the developed torque and the rotor speed expressed in rad/s.

Figure 5-30 shows the measured efficiency of the nine-phase drive using the direct method described above. The results show a general impression that the hysteresis controller gives better efficiency than the delta modulated controller. This is expected since the delta modulated controller does not give a perfect stator current waveform and the BDCE control is sensitive to the shape of the stator current waveform. The comparison of the two current controllers can be done to give more reliable results if the stator voltages are used in the delta modulated controller as suggested in the simulation results. The inverter efficiency may need to be evaluated separately to determine the actual effect of delta modulation on the inverter.

Above 96% load, the drive reaches its maximum efficiency as observed from the flattening of the efficiency curve. This suggests that the drive should be operated at rated load to have more efficiency.

5.8 Summary

The nine phase BDCE controlled induction machine drive has been experimentally evaluated and the results have been presented. The hysteresis controller produces better tracking of the reference stator current waveform than the alternative delta modulated controller. The delta modulated controller however gives a smoother stator current waveform with constant switching frequency. There exists a linear relationship between the developed torque and the torque current for the nine-phase BDCE controlled cage rotor induction machine drive. The alternative delta modulation scheme proposed produced relatively good stator currents considering that no voltage or current sensors are used and the stator dynamics have not been modelled for the control. The hysteresis controller gives better efficiency than the alternative delta modulated controller when applied to the BDCE controlled drive. The drive has highest efficiency when operated near full load conditions

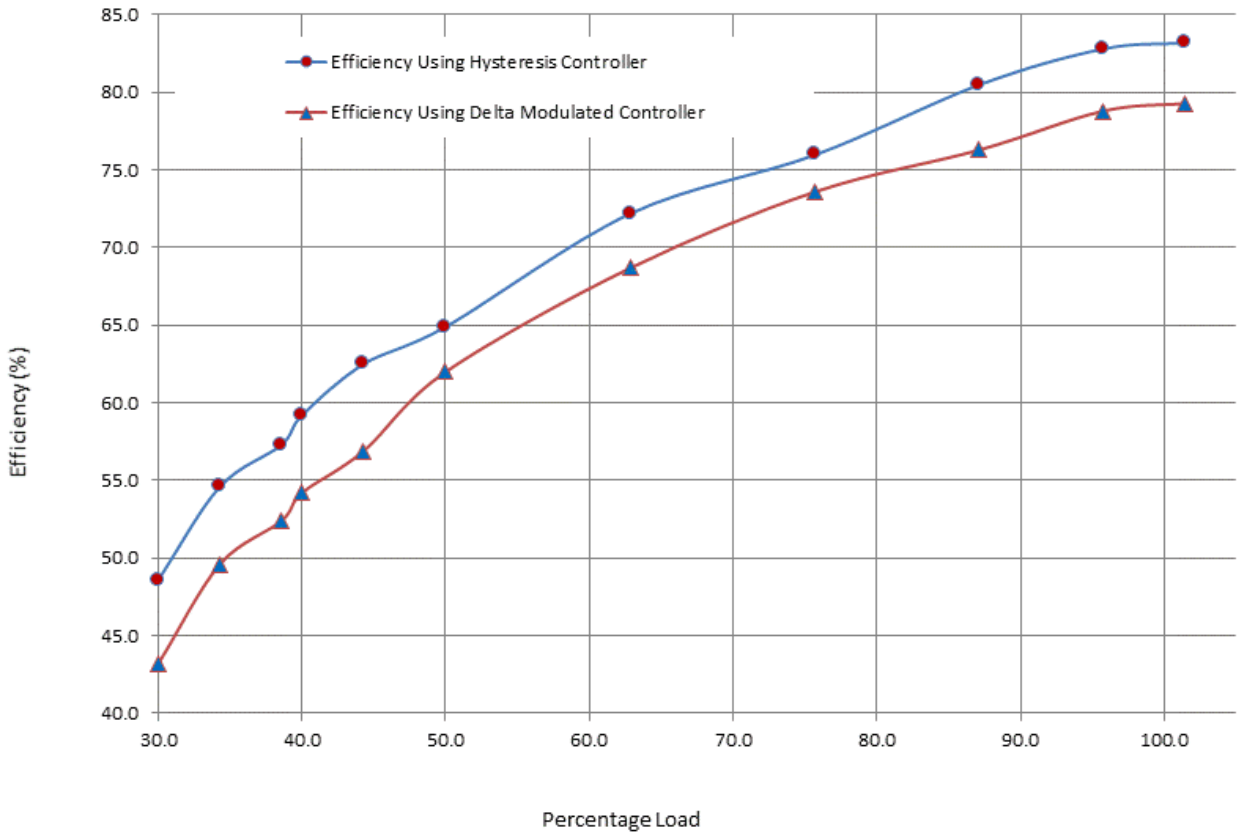

Figure 5-30. Variation of drive efficiency with load.

.

6 Conclusions and Recommendations

The BDCE control method has been investigated to determine the feasibility of using a delta modulated current controller in place of the hysteresis current controller used in the previous studies. The simulation results and the experimental results have been presented and discussed in the previous chapters. The contributions of this study and conclusions drawn are presented in this chapter together with recommendations for possible further study.

6.1 Contributions of the study

The study has contributed the following to the BDCE control method:

i) A method of calculating the leakage inductance of the induction motor and the stator induced voltage using flux linkage values deduced from simulating the nine-phase induction machine using JMAG finite element analysis software has been presented. This method can be used to calculate these parameters for other induction machines.

ii) A model of the nine-phase cage rotor induction machine drive has been developed for simulation using Matlab/Simulink. This model can be used to perform steady state and dynamic tests that need to be done on the nine-phase drive. The model can be modified to suite the requirements for simulating other drives with different number of phases.

iii) A delta modulated current controller which does not use current or voltage measurements has been implemented in software and tested on the drive. The development and implementation of the control method without measuring current or voltage can be a starting point towards sensor-less control of the nine-phase drive.

6.2 Limitations

The initial design strategy was to use the conventional linear delta modulated controller but this was not performed to the end due to the shortfalls of the modulation technique when the reference signal has DC values at some portions of the waveform. The simulated delta modulated control technique which uses the voltage pulses from the inverter could not be implemented to control the drive because the voltage measuring cards available for use failed to measure signals of frequencies above 2 kHz and the use of lower switching frequencies has several disadvantages when using PWM. The alternative delta modulation which was later proposed showed that its performance was highly dependent on the value of the quantizer output as well as the integrator gain as shown by simulations and practical measurements hence might require adaptive control. It also required an accurate voltage estimator to give accurate estimated voltages for use in the delta modulator and the design of an optimised voltage estimator which models the stator dynamics is beyond the scope of the study.

6.3 Conclusions

The results of the study can be used to draw the following conclusions:

i) The conventional delta modulated controller in which the PWM outputs from the two-level quantizer are used to produce the carrier cannot give accurate tracking of the reference signal if the reference signal has a persistently constant value in its waveform as shown from simulation and practical tests.

ii) The delta modulated current controller in which the carrier is generated by low pass filtering the stator voltage can be used in the BDCE control method of the nine-phase drive as shown by the Matlab/Simulink results.

iii) The alternative linear delta modulated controller with an integrator at the input gives better tracking of the reference signal independent of the reference signal frequency as shown by the practical tests as compared to the conventional linear delta modulation.

iv) Practical experimentation results show that the alternative delta modulated current controller can be used on the BDCE controlled drive without physical measurement of the phase currents or voltages.

v) Simulation results suggest that the delta modulated current controller gives better performance of the drive than the hysteresis current controller in terms of torque and current ripples as well as harmonic filtering if the stator voltage is used in the feedback loop although this has not been experimentally verified in this study.

vi) Practical results show that delta modulation gives smooth inverter operation through the use of a constant switching frequency. The scheme works considerably well on the BDCE controlled drive as shown by the torque measurements done under locked rotor conditions. However, the delta modulator showed inferior performance in terms of the shape of the stator current waveform as well as on efficiency.

6.4 Recommendations for further study

The study has not exhaustively compared the delta modulated current controller to the hysteresis controller because of some practical constraints. The following recommendations are made for further study:

i) A medium frequency voltage measuring card can be used to measure the PWM switching voltages and implement the delta modulated controller for proper comparison to the hysteresis controller.

ii) The alternative linear delta modulated controller design optimisation is required to get perfect stator current waveforms and a comparison of the current controllers can be done completely.

iii) Sensor-less control of the drive can be investigated starting with the use of the alternative delta modulated current controller once its design has been optimised for better performance by modelling the stator dynamics and including them in the control program.

References

[1] I. Avitan and V Skormin. "Mathematical Modelling and Computer Simulation of a Separately Excited DC Motor with Independent Armature/Field Control." *IEE Transactions on Industrial Electronics.* Vol.37. No.6. pp. 413-489, 1990.

[2] F. Blaschke. "The Principles of Field Orientation as Applied to the new Trans-vector Closed-loop Control System for Rotating Field Machines." Siemens Review. Vol.34. pp. 217–220, 1972.

[3] D. Casadei, G. Grandi and G. Serra. "Rotor Flux Oriented Torque-control of Induction Machines Based on Stator Flux Vector Control." *Fifth European Conference on Power Electronics and Applications*. Vol. 5. pp. 67- 72, 1993.

[4] C. J. Francis, D. H. Zelayaand K.W.E. Cheng. "Practical Implementation of a Stator Flux Oriented Control Scheme for an Induction Machine." *Fifth International Conference on Power Electronics and Variable-Speed Drives*. pp. 24-59, 1994.

[5] T. Suzuki, A. Chiba, M. A. Rahman and T. Fukao. "An Air-Gap-Flux-Oriented Vector Controller for Stable Operation of Bearingless Induction Motors." *IEEE Transactions on Industry Applications.* Vol. 36. No. 4. pp. 1069-1076, 2000

[6] K. Aissa and K. D. Eddine. "Vector Control Using Iron Loss Model of Induction Motors and Power Loss Elimination." *World Academy of Science, Engineering and Technology, 2009.*

[7] A. Cavagnino, A. Tenconi, G. Rizzoli, M. Mengoni and G. Serra. "Multiphase Induction Machine for Aero-Engine Shaft-Line-Embedded Starter/Generator: Scaled Prototypes Testing." *Proc.International Conference on Electric Machines (ICEM).* pp.2107-2113, 2014

[8] R. Bojoi, M. G. Neacsu and A. Tenconi. "Analysis and Survey of Multi-phase Power Electronic Converter Topologies for More Electric Aircraft Applications." *IEEE International Symposium on Power Electronics, Electrical Drives, Automation and Motion*. pp. 440-445, 2012.

[9] M. Villani, M. Tursini, G. Fabri and L Castellini. "Multi-phase Fault Tolerant Drives for Aircraft Applications." *IEEE Conference on Electrical Systems for Aircraft, Railway and Ship Propulsion*. pp. 1-6, 2010.

[10] F. Terrien, S. Siala and P. Noy. "Multiphase Induction Motor Sensor-less Control for Electric Ship Propulsion."*Proc. IEE Power Electronics, Machines and Drives Conference*. pp. 556-561, 2004.

[11] A. Nanoty and A. R. Chidusama. "Design of Multiphase Induction Motor for Electric Ship Propulsion." *IEEE Symposium on Electric Ship Technologies*. pp. 283-287, 2011.

[12] C. Sun, S. Ai, L. Hu and Y. Chen. "The Development of a 20 MW PWM Inverter for Advanced Fifteen-Phase Propulsion Induction Motors." *Journal of Power Electronics*. Vol. 15. No. 1. pp. 146-159, 2015.

[13] J. M. Apsley, R. Todd, M. Barnes, J. Schuddebeurs and S. Careme. “Experimental Validation of Load Disturbances on a Multiphase Marine Propulsion Drive.” *IET Conference on Power Electronics, Machines and Drives*. pp. 656-660, 2008.

[14] A. Raisemche, M. Boukhnifer, C. Larouciand D. Diallo. “Two Active Fault-Tolerant Control Schemes of Induction-Motor Drive in EV or HEV.” *IEEE Transactions on Vehicular Technology*. Vol. 63, Issue. 1. pp. 19- 29, 2014.

[15] M. Farasat, A. M. Trzynadlowski and M. S. Fadali. “Efficiency Improved Sensor-less Control Scheme for Electric Vehicle Induction Motors.” *IET Electrical Systems in Transportation.* Vol. 4. Issue. 4. pp. 122-131, 2014.

[16] A. Baltatanu amd M. L. Florea. “Multiphase Machines Used in Electric Vehicles.” *IEEE International Conference on Electronics, Computers and Artificial intelligence*. Pp. 1-6, 2013.

[17] F. Bu, H. W. Huang, S. Zhuang and K. Shi. “Control Strategy and Dynamic Performance of Dual Stator-Winding Induction Generator Variable Frequency AC Generating System with Inductive and Capacitive Loads.” *IEEE Transactions on Power Electronics*. Vol. 29. No. 4. pp. 1681-1692, 2014.

[18] K. Nounou, K. Marouani, M. Benbouzid and B. Tabbache. “Six-phase Induction Machine Operating as a Stand Alone Self-excited Induction Generator.” *IEEE International Conference on Green Energy*. pp. 158-163, 2014.

[19] J. M. Apsley, S. Williamson, A. C. Smith and M. Barnes. “Induction motor performance as a function of phase number.” *IEEE Proc. Electr. Power Appl.* Vol. 153. No. 6. pp. 898 – 904, 2006.

[20] K.Rajambal and G.Renukadev. "Modeling and Analysis of Multi-Phase Inverter Fed Induction Motor Drive with Different Phase Numbers." *WSEAS Transactions on systems and Control*. Vol 8. No. 3. pp. 73-80, 2013.

[21] E. E. Ward and H. Harer. “Preliminary investigation of an inverter-fed 5-phase induction motor.” *Proc. IEE,* Vol. 116. No. 6: pp. 980–984, 1969.

[22] D. Ghanbari, N. R. Abjadi and A. Ghanbari. “Direct Torque and Flux Control of Five-Phase Induction Motor using Fuzzy Logic.” *International Journal of Innovative Research in Electrical, Electronics, Instrumentation and Control Engineering*. Vol.2. No. 12. pp. 2196-2202, 2014.

[23] H. Guzman, M. J. Duran, F. Barrero, B. Bogado and S. Toral. “Speed Control of Five-Phase Induction Motors with Integrated Open-Phase Fault Operation Using Model-Based Predictive Current Control Techniques.” *IEEE Transactions on Industrial Electronics*. Vol. 61. No. 9. pp 4474-4484, 2014.

[24] L. Schreier, J. Bendl, M. Chomat. “Comparison of Five-Phase Induction Machine Operation with Various Stator-Winding Arrangements.” *Proc. 39th Annual Conference of IEEE Industrial Electronics*. pp. 2685 – 2690, 2013.

[25] F. Patkar and M. Jones. "Performance of an Asymmetrical Six-phase Induction Machine in Single-and Two-Neutral Point Configurations." *48th International Universities' Power Engineering Conference (UPEC), Dublin*. pp. 1-6, 2013

[26] M. A. Abbas, R. Christen and T. M. Jahns. "Six-Phase Voltage Source Inverter Driven Induction Motor." *IEEE Transactions on Industry Applications*, Vol. IA-20, No. 5. pp 1251-1259, 1984.

[27] R. O. C Lyra and T. A Lipo. "Torque Density Improvement in a Six-Phase Induction Motor with Third Harmonic Current Injection*." IEEE Transactions on Industry Applications*. Vol.38. pp. 1351-1360, 2002.

[28] P. Nagaraj, V. Kannan and M. Santhi. "Modified Multiphase Induction Motor with High Starting Torque." *International Journal of Innovative Research in Science Engineering and Technology*. Vol. 3. No. 3. pp. 519-522, 2014.

[29] N. Akkari, A. Chaghi and R. Abdessemed. "Speed Control of Doubly Star Induction Motor using Direct Torque (DTC) Based on Model Reference Adaptive Control (MRAC)." *International Journal of Hybrid Information Technology*. Vol. 2. No. 2. pp. 19-28, 2014.

[30] Y. Ai, M. J. Kamper and A. D. Le Roux."Novel Direct Flux and Direct Torque Control of Six-Phase Induction Machine with Nearly Square Air-Gap Flux Density." .*IEEE Transactions on Industry Applications*. Vol. 43. No. 6: pp.1534-1543, 2007.

[31] A. Iqbal, S. Moinuddi, M. R. Khan and I. Ashraf. "Indirect Rotor Flux oriented Control of a Seven-Phase Induction Motor Drive." *IEEE Conference on Industrial Technology*. pp. 440-445, 2006.

[32] D. Casadei, M. Mengoni, G. Serra, A. Tami and L. Zarri. "Seven-Phase Induction Motor Drive Based on Stator Flux vector Control." *International Symposium on Power Electronics, Electrical Drives*, Automation and Motion. pp.113-119, 2008

[33] N. Gule and M.J. Kamper. "Multi-Phase cage Rotor Induction Machine Drive with Direct implementation of Brush DC Operation." *IEEE Transactions on Industry Applications*. Vol. 43. No. 6: pp. 2014-2021, 2012

[34] N. Gule and M. Kamper. "Optimal ratio of field to torque phases in multi-phase induction machines using special phase current waveforms." *International Conference on Electrical Machines*. pp. 1-5, 2008.

[35] M.Sowmiya, G.Renukadevi and K. Rajambal. "IFOC of a Nine Phase Induction Motor Drive." *International Journal of Engineering Science and Innovative Technology (IJESIT)* Volume 2, Issue 3. pp.72-78, 2013

[36] A. Abdelkhalik, M. Masoud and W. Barry. "Eleven-Phase Induction Machine: Steady State Analysis and Performance Evaluation with Harmonic Injection." *IET Electric Power Applications.* Vol.4. No.8. pp. 670-685, 2010.

[37] A. M. Ashoush, S. M. Gadoue, A. S. Khalik and M. Z. Mostafa. "Performance Analysis of an Eleven-Phase Induction Machine under Fault Conditions." *Proc.2013 Fourth International Conference on Power Engineering, Energy and Electric Drives.* pp. 479-484, 2013.

[38] J. Jatskevich and M. Maksimcev. "Modelling of a Fifteen Phase Induction Motor Drive for Electric Ship propulsion System." *Proc. Of the 10th WSEAS International Conference on Computers.* pp. 899-904, 2006.

[39] L. Weichao, H. An, G. Shinguang and S. Chi. "Rapid Prototyping of a Fifteen-Phase Induction Motor Drive Based on dSPACE." *International Conference on Electric Machines and Systems.* pp. 1604-1607, 2008.

[40] E. A. Klingshirn. "High Phase Order Induction Motors- Part 1- Description and Theoretical Considerations." *IEEE Transactions on Power Apparatus and Systems, Vol.PSA-102. No. 1. pp 47-53, 1983.*

[41] G.K. Singh. "Multi-phase induction machine drive research—a survey." *Electric Power Systems Research*. Vol. 61. pp. 139–147, 2002.

[42] L. Parsa. "On advantages of multi-phase machines." *Proc. 31st Annual Conference of IEEE Industrial Electronics*, pp. 1574–1579, 2005.

[43] *E*. Levi, R. Bojoi, F. Profumo, H. A. Toliyat, S. Williamson. "Multiphase induction motor drives–a technology status review." *IET Electric Power Applications,* Vol. 1. No. 4: pp. 489–16, 2007.

[44] E. Levi. "Multiphase Electric Machines for Variable-Speed Applications." *IEEE Transactions on Industrial Electronics*. Vol. 55. No. 5. pp. 1893-1909, 2008

[45] J. Huang, M. Kang, Y Jia-qiang, H. Jiang and D. Liu. "Multiphase Machine Theory and its Applications." *Proc. of International Conference on Electrical Machines and Systems.* pp.1-7, 2008

[46] N. Gule, "Analysis and Evaluation of Brush-DC Equivalent Controlled Multiphase Cage Induction machine Drives." *Ph.D. dissertation, Dept. Electrical and Electronic. Eng., Univ. Stellenbosch, South Africa*, 2011.

[47] P.D. Ziogas. "The Delta Modulation Technique in Static PWM Inverters." *IEEE Transactions on Industry Applications,* Vol. 1A-17. No. 2. pp. 199-204, 1981.

[48] V. S. Reddy and B. C. Babu. "Hysteresis Controller and Delta Modulation- Two Viable schemes for Current Controlled Voltage Source Inverter." *IEEE International Conference on Technical Postgratuates (IEEE TECHPOS),* 2009.

[49] A. I. Maswood and S. Anjum. "Delta Modulation with PI Controller – A comparative Study." *Journal of Electromagnetic Analysis and Applications*. Vol. 3. pp 145-151, 2009.

[50] R. K. Srivastava, M. A. Rahman, J. E. Quaicoe and M.A. Choudhury. "Software Control of Delta Modulated Inverters." *Proceedings of Annual Conference of Industrial Electronics Society.* Vol. 3. pp. 836-841, 1988.

[51] E. E. El-Kholy, A. Ahmed, and A. Alwadie. "Vector Control Based Delta Modulation Inverter of Induction Motor Drives." *IEEE Electric Machines & Drives Conference (IEMDC)* Vol.1. pp. 413- 418, 2007.

[52] Y. M. Chen, Y. C. Chen and H. C. Wu. "Improved Delta modulated control for PWM Inverters." *IEEE Conference on Industrial Technology (ICIT)*, pp. 1-6, 2008

[53] Agarwal and V. Agarwal. "Design of an FPGA Based Controller for Delta Modulated Single-Phase Matrix Converters." *Journal of Power Electronics*. Vol. 12, No. 6. pp.974-981, 2012

[54] S. Callegari and F. Bizzarri. "Should ΔΣ modulators used in AC motor drives be adapted to the mechanical load of the motor?" *Proc. IEEE International Conference on Electronics, Circuits and Systems (ICECS)*. pp. 849 - 852, 2012

[55] B. Jacob M.R. Baiju "Simple multilevel inverter-based induction motor drive scheme using sigma delta converter with space-vector quantiser." *IET Power Electronics.* Vol. 5, No. 8. pp. 1483–1490, 2012

[56] D. N. Trip, C. Gordan, M. I. Gordan, A. Schiop and R. Reiz. "Time Frequency Analysis of the Delta Modulation and PWM Control for the asynchronous Motors." *IEEE International Conference on "Computer as a Tool (EUROCON*), pp. 1586-158, 2005.

[57] J. Nieznanski. "Performance characterization of vector sigma-delta modulation." *Proceedings of IEEE Annual Conference of the Industrial Electronics Society*. Vol. 1. pp. 531- 536, 1998

[58] K. Taniguchi and H. Irie. "Trapezoidal Modulating Signal for Three-Phase PWM Inverter." *IEEE Transactions on Industrial Electronics*. Vol.33. No.2. pp. 193-200, 1986.

[59] T. A. Lipo, H.A. Toliyat and J.C. White. "Analysis of a concentrated winding Induction machine for Adjustable Speed Drive Applications Part 1 (Motor Analysis)." *IEEE transactions on Energy Conversion.* Vol. 6. No. 4. pp. 679-683, 1991.

[60] A. Agrawal and V. Agarwal. "Delta Modulated Cyclo-Inverter." *Proceedings of the IEEE 30th International Telecommunications Energy Conference*. pp. 1-6, 2008

[61] V. Tipsuwanporn, C. Sodaban, and P. Thepsatorn. "Adaptive Switching Frequency in Delta Modulation Inverter for Single Phase Induction Motor Drives." *Proc. IEEE International Conference on Industrial Technology*, ICIT. pp. 599-603, 2005.

[62] S. Sae-Sue, V. Kinnares, C. Tangsiriworakul and S. Potivejkul. "Comparative Performance Evaluation of Fixed and Adaptive Hysteresis Band Delta Modulation Techniques for UPS." *Proc. IEEE 1999 International Conference on Power Electronics and Drive Systems*, PEDS. Vol. 2. pp. 956-960, 1999.

[63] S. Sae-Sue, V. Kinnares, K. Sirichanpong and K. Kleebbua. "Design and analysis of delta modulated PWM inverter with regulated output voltage for 1-φ induction motor drives." *Proc. IEEE 1999 International Conference on Power Systems Technology*, Vol. 1. pp. 317-320, 2000.

[64] IEEE Power Engineering Society. "IEEE Standard Test Procedure for Polyphase Induction Motors and Generators." *IEEE Std 112. pp. 54. 2004.*

[65] H. D. Swardt. "The Locked Rotor Test Explained." *Marthinusenn & Coults. Johannesburg. 2007*

[66] S. U Electric Machines Lab *TMS320VC33 DPS Based Motor Control System User's Guide*

[67] A. A. Jimoh, P. J. Venter and E. K. Appiah. "Modelling and Analysis of Squirrel Cage Induction Motor with Leading Reactive Power Injection, Induction Motors - Modelling and Control." *R. E.Araújo (Ed.), 2012. ISBN: 978-953-51-0843-6, InTech, DOI: 10.5772/50011. Available from: http://www.intechopen.com/books/induction-motors-modelling-and-control/modelling-and-analysis-of-squirrel-cage-induction-motor-with-leading-reactive-power-injection.*

[68] S. Srilad, S. Tunyasrirut and T Suksri. "Implementation of a Scalar Controlled Induction Motor Drive." *SICE-ICASE International Joint Conference*. pp. 3605- 3610, 2006.

[69] O.I. Okoro. "Dynamic and Thermal Modelling of Induction Machine with Non-linear Effects." *PhD Thesis. Kassel University Press, GmbH, Kassel.* pp. 11-13, 2002.

Appendix A Control of Induction Machines

The control theory of electrical machines is mainly focused on three phase systems which run from the three phase supplies. To fully analyze the multiphase control systems, it is important to present the underlying three phase control techniques and develop the multiphase techniques from there.

A.1 Vector control

Vector control is the control strategy used where accuracy and dynamic performance are critical variables. The machine model used in vector control is valid for both steady state and transient conditions. Both the magnitude and phase alignment of the vector variables are controlled using space vector theory. The overall control is performed by decoupling of the stator current into a direct and a quadrature component so that the analysis becomes similar to that of a separately excited DC motor.

Vector control is based on coordinate transformation of the stator and or rotor variables for the execution of the control algorithms. Figure A-1. The figure shows the stages in the control algorithm where the vector control transformations are performed.

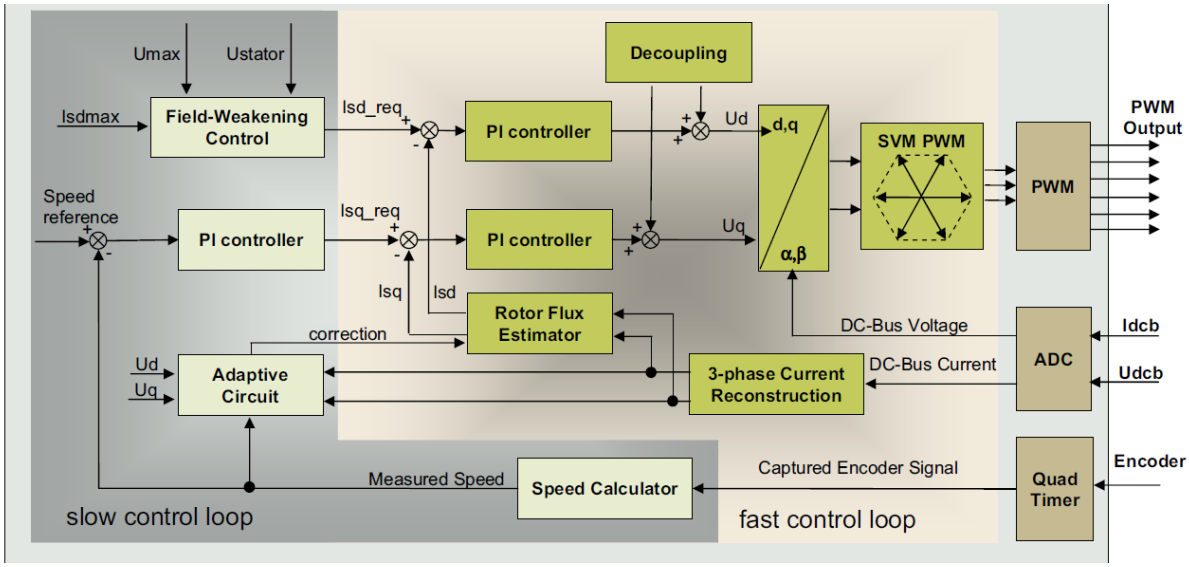

Figure A-1. Vector control algorithm overview.

Vector control is implemented in a three phase system by first transforming the three phase quantities into a two phase, stationary (α,β) frame using the Clark transformation. The Clarke transformation in general is represented by:

$$T_{\alpha\beta 0} = \frac{2}{3}\begin{bmatrix} 1 & -\frac{1}{2} & -\frac{1}{2} \\ 0 & \frac{\sqrt{3}}{2} & -\frac{\sqrt{3}}{2} \\ \frac{1}{2} & \frac{1}{2} & \frac{1}{2} \end{bmatrix} \tag{A-1}$$

To convert the three phase quantities I_a, I_b and I_c to the two stationary orthogonal quantities I_α and I_β, the following relationships are used:

$$I_\alpha = \frac{2}{3} * I_a - \frac{1}{3}(I_b - I_c) \tag{A-2}$$

$$I_\beta = \frac{2}{\sqrt{3}} * (I_b - I_c) \tag{A-3}$$

After performing the transformation, the rotor flux vector is calculated and the currents in the stationary (α,β) frame are transformed into the rotating (d,q) reference frame using the Park transformation to enable the separate control of the torque (I_q) and the flux (I_d) components. The Park transformation in general is given by:

$$T_{dq0} = \frac{2}{3}\begin{bmatrix} cos\theta & cos(\theta - \frac{2\pi}{3}) & cos(\theta + \frac{2\pi}{3}) \\ sin\theta & sin(\theta - \frac{2\pi}{3}) & sin(\theta + \frac{2\pi}{3}) \\ \frac{1}{2} & \frac{1}{2} & \frac{1}{2} \end{bmatrix} \tag{A-4}$$

The conversion from the stationary frame to the rotating frame is achieved using the following relationships:

$$I_d = I_\alpha cos\theta + I_\beta sin\theta \tag{A-5}$$

$$I_q = I_\beta cos\theta - I_\alpha sin\theta \tag{A-6}$$

Where θ is the rotating angle.

The stator voltage space vector is calculated after the transformation and is transformed back into the stationary frame using the inverse Park transformation:

$${T_{dq0}}^{-1} = \begin{bmatrix} 1 & 0 & 1 \\ -\frac{1}{2} & \frac{\sqrt{3}}{2} & 1 \\ -\frac{1}{2} & -\frac{\sqrt{3}}{2} & 1 \end{bmatrix} \tag{A-7}$$

The inverse Park transformation is performed using the relationships:

$$I_\alpha = I_d cos\theta - I_q sin\theta \tag{A-8}$$

$$I_\beta = I_q cos\theta + I_d sin\theta \tag{A-9}$$

A.2 Scalar Control

Scalar control defines a simple electric motor control method using non-vector control schemes. The control method deals with steady state performance and only the magnitude of the controlled quantities is adjusted and hence the term scalar control. The simplified steady state equivalent circuit of the induction motor is used in analysing scalar control and is shown in FigureA-2.

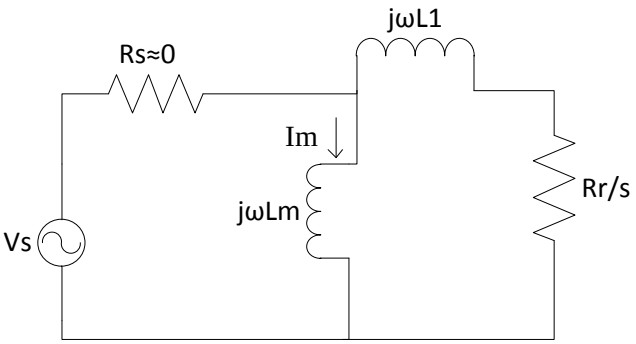

FigureA-2. Simplified steady state equivalent circuit of an induction motor.

Under steady state conditions, the stator resistance R_s can be approximated to zero and the magnetising current for producing the flux can be approximated by:

$$I_m = \frac{V_s}{j\omega L_m} \qquad \text{(A-10).}$$

When the machine is operating in the linear magnetic region, L_m is constant and the magnetic flux is approximated by:

$$\lambda = I_m * L_m = \frac{V_s}{\omega} \cong \frac{V_s}{2*\pi*f} \qquad \Rightarrow \lambda \propto \frac{V_s}{f} \qquad \text{(A-11)}$$

The equation shows that the ratio of the supply voltage to the supply frequency should always be constant to maintain constant flux and this is achieved through the use of constant volts per hertz (V/Hz) control. In constant V/Hz control, the speed of the motor is controlled by adjusting the frequency and magnitude of the supply voltage such that the air gap flux is always maintained at the desired value for the induction machine to operate properly under steady state conditions.

Figure A-3 shows the schematic diagram of the scalar controlled induction machine in which a feedback loop is used to measure the motor speed.

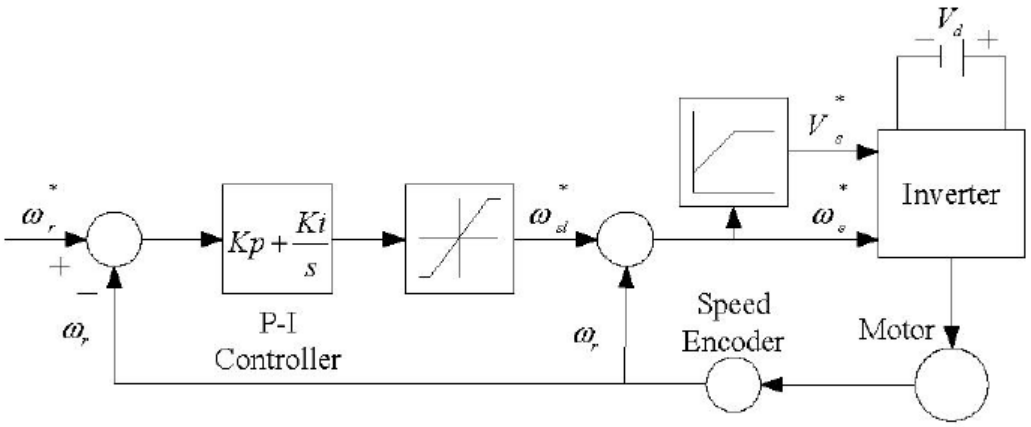

Figure A-3. Schematic of scalar controlled induction motor[68].

Appendix B Current Control methods for PWM Inverters

Current controllers are used because they give quick response and accurate control and they force the load current to follow the current command for higher drive performance

B.1 Hysteresis Controller

The hysteresis controller is characterised by the use of a hysteresis band within which a measured quantity is allowed to oscillate. The controller uses the measured stator currents and the reference current to determine the switching instants of the PWM inverter. The hysteresis controller block is shown in Figure B-1 where a reference current I_{ref} is compared to the measured stator currentI_x to determine the magnitude of the error signal e_x. The magnitude of the error signal is bound by the defined hysteresis band and the switching logic is always such that the error does not exceed the hysteresis band value. Figure B-2 shows the waveforms produced from the hysteresis controller. The difference between the upper band and the lower band is the width of the hysteresis band. A smaller hysteresis band produces a higher switching frequency. The switching instant occurs when the measured signal becomes equal to either the upper of the lower band.

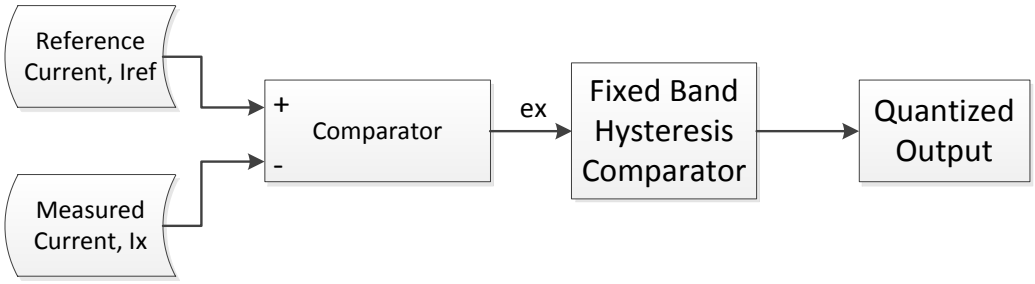

Figure B-1. Hysteresis current controller block.

The accuracy of this method is highly dependent on the accuracy of the current measuring devices as well as the shape of the reference signal. It also exhibits a varying switching frequency which depends on the value of the hysteresis band and the slope of the reference signal. The number of hysteresis controller blocks used is the equal to the number of machine phases since each machine phase current is measured separately.

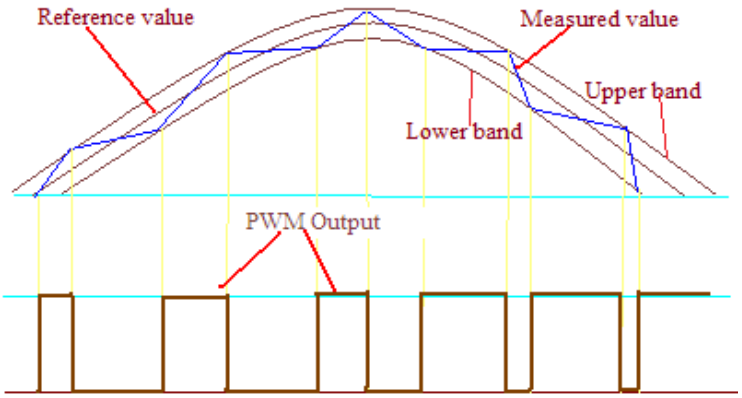

Figure B-2. Hysteresis controller waveforms.

B.2 PI current Controller

PI controllers are used where small steady state errors and adjustable response times need to be achieved by adjusting the controller gains. Figure B-3 shows the simple PI controller block.

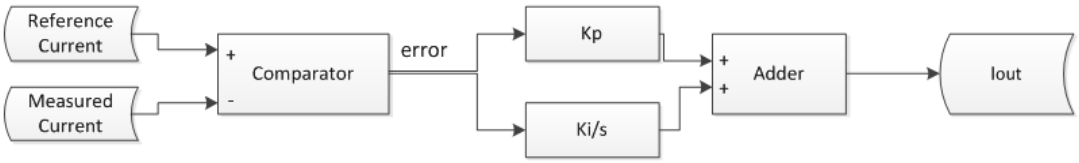

Figure B-3. Conventional PI controller block

The PI controller is used to determine the magnitude of the current required by the machine depending on the difference between the measured value and the reference. In other applications, the PI controller uses the speed error to determine the magnitude of the required current. The proportional controller reduces the response time of the system but also amplifies the error. The integral controller reduces the steady state error but also tends to make the system slower. The design of the PI controller therefore aims to strike a balance between the effect of the two controllers

The comparator compares the set value to the measured value and produces an error signal. The error value is passed through a PI control block which produces the desired current magnitude. If the error is e(t), then the output of the PI controller is given by:

$$I_{out} = K_p * e(t) + K_i \int e(t)dt. \qquad \text{(B-1).}$$

Appendix C Inductance Calculation

The detailed winding functions for a nine phase BDCE controlled induction machine are presented. The winding functions are used to calculate the inductance of an induction machine by considering the angular spacing of the windings in the design.

C.1 Calculation of Self Inductance using Winding Functions.

Phases are distributed in three groups spaced by 120 degrees. In each group, the phases have a spacing of 20 degrees.

For Phase A :$N_{as}(\theta) = N_{s1}Sin(\theta) + N_{s3}\,Sin(3\theta)$ (a)

For Phase B :$N_{bs}(\theta) = N_{s1}Sin(\theta - \frac{\pi}{9}) + N_{s3}\,Sin3\left(\theta - \frac{\pi}{9}\right)$ (b)

For Phase C :$N_{cs}(\theta) = N_{s1}Sin(\theta - \frac{2\pi}{9}) + N_{s3}\,Sin3\left(\theta - \frac{2\pi}{9}\right)$ (c)

For Phase D :$N_{ds}(\theta) = N_{s1}Sin(\theta - \frac{2\pi}{3}) + N_{s3}\,Sin3\left(\theta - \frac{2\pi}{3}\right)$ (d)

For Phase E :$N_{es}(\theta) = N_{s1}Sin(\theta - \frac{7\pi}{9}) + N_{s3}\,Sin3\left(\theta - \frac{7\pi}{9}\right)$ (e)

For Phase F :$N_{fs}(\theta) = N_{s1}Sin(\theta - \frac{8\pi}{9}) + N_{s3}\,Sin3\left(\theta - \frac{8\pi}{9}\right)$ (f)

For Phase G :$N_{gs}(\theta) = N_{s1}Sin(\theta - \frac{4\pi}{3}) + N_{s3}\,Sin3\left(\theta - \frac{4\pi}{3}\right)$ (g)

For Phase H :$N_{hs}(\theta) = N_{s1}Sin(\theta - \frac{13\pi}{9}) + N_{s3}\,Sin3\left(\theta - \frac{13\pi}{9}\right)$ (h)

For Phase I :$N_{is}(\theta) = N_{s1}Sin(\theta - \frac{14\pi}{9}) + N_{s3}\,Sin3\left(\theta - \frac{14\pi}{9}\right)$ (i)

N_{s1} andN_{s3} are the equivalent stator turns per phase per pole.

Table C-1. Value of Inductances Calculated using Winding Function.

Parameter	L_a	L_{ab}	L_{ac}	L_{ad}	L_{ae}	L_{af}	L_{ag}	L_{ah}	L_{ai}
Value (H)	2.45	1.76	0.326	0.612	-0.326	-1.76	0.612	0.40	-0.40

N_{s1} and N_{s3} are the equivalent stator turns per phase per pole.

Due to identity of coils and symmetry of winding,

$L_a = L_b = L_c = L_d = L_e = L_f = L_g = L_h = L_i$

$L_{ab} = L_{bc} = L_{cd} = L_{de} = L_{ef} = L_{fg} = L_{gh} = L_{hi}$

$$L_{ac} = L_{bd} = L_{ce} = L_{df} = L_{eg} = L_{fh} = L_{gi}$$

$$L_{ad} = L_{be} = L_{cf} = L_{dg} = L_{eh} = L_{gi}$$

$$L_{ae} = L_{bf} = L_{cg} = L_{dh} = L_{ei}$$

$$L_{af} = L_{bg} = L_{ch} = L_{di}$$

$$L_{ag} = L_{bh} = L_{ci}$$

$$L_{ah} = L_{bi}$$

C.2 Calculation of Inductance using Characteristic curves

Inductance can be calculated by using the motor characteristic graphs and extracting required values to make calculations as demonstrated in [69].

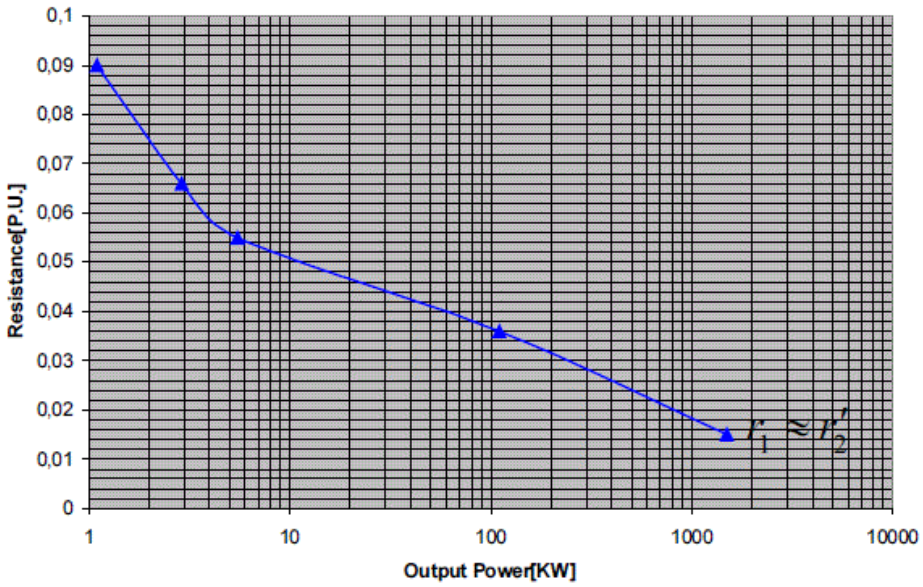

Figure C-1. Graph of per unit resistance of 4 pole induction motors.

The machine being considered is a nine-phase, four-pole, 11kW induction motor. From the graphs, the stator resistance is estimated to be 0.052 per unit (p.u) and the leakage inductive reactance is estimated to be 0.15 p.u and the magnetising reactance is 2.53 p.u. Assuming 0.82 power factor[69], a 400V phase voltage and 5.83A field current,

Base Impedance: $Z_b = 400/11.66 = 34.31\Omega.$

Base Resistance: $R_b = 34.31 \times 0.82 = 28.13\Omega$

Base Reactance: $X_b = 34.31 \times 0.57 = 19.56\Omega.$

For the machine: $R = 28.13 \times 0.052 = 1.46\Omega$

$$X = 19.56 \times 0.15 = 2.93\Omega.$$

Since the operating frequency is 50Hz for the stator current, then: $L = \frac{X}{2*\pi*50} = 0.00934\ H.$

The value above is for the field phase. Using the same method for the torque phase, L=0.0099H.

Table C-2. Inductances and Resistances measured on the machine.

Phase	A	B	C	D	E	F	G	H	I	Avg
R (Ω)	0.7	0.7	0.7	0.7	0.7	0.7	0.7	0.7	0.7	0.7
L(mH)	7.386	8.228	7.452	7.455	7.469	7.504	7.445	7.335	7.340	7.513

Table C-3. Inductance values obtained using the different methods.

Method	**Winding Function**	**Using Flux**	**Using Graphs**	**Practical measurement**
Torque Inductance L_t (mH)	2450	9.13	9.90	7.513
Field Inductance L_f (mH)	2450	6.50	9.34	7.513

Appendix D JMAG FEA Simulations for Inductance Calculation

The nine phase induction motor being modelled has 28 rotor slots and 36 stator slots and half of the machine model is used in the geometry because of symmetry.

D.1 Geometric Machine Model

The geometric construction of the machine stator and rotor is modelled to scale as shown in Figure D-1. For purposes of simulation, the material for each machine component is selected in order to give accurate simulation results. M470-50A steel is used as the rotor and stator core material in the model presented, copper is used as the stator coil material and aluminium as the rotor bar material.

.

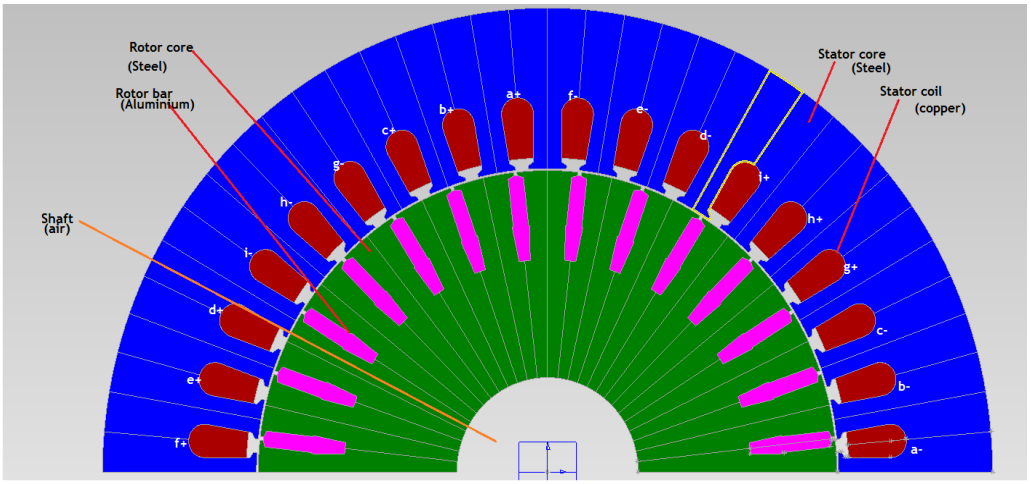

Figure D-1. Geometry of the motor model developed using JMAG for finite element analysis.

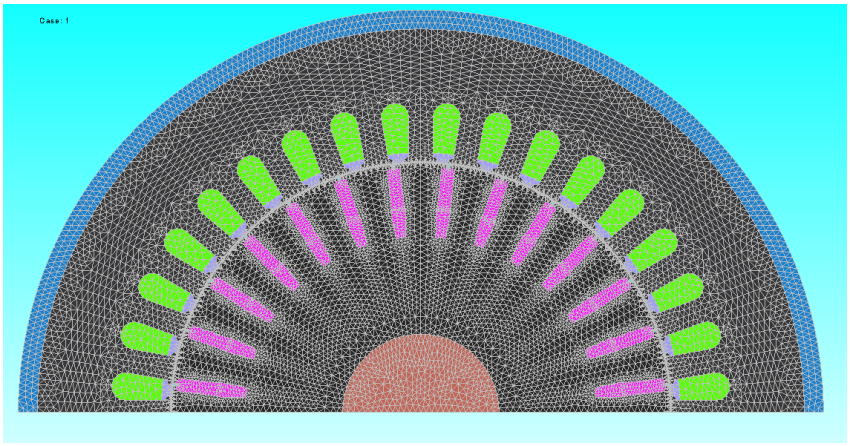

Figure D-2. Meshed motor model showing the rotor and the stator.

D.2 Magnetic Flux Linkage Simulation.

The magnetic flux pattern produced in the machine after supplying the field current to the stator is shown in Figure D-3 at an arbitrary rotor position since the flux pattern changes with the position of the rotor. Figure D-4 shows the flux linkage pattern of phase A. Phase A is used in the calculations and other phase parameters are deduced by introducing the phase shift with respect to phase A.

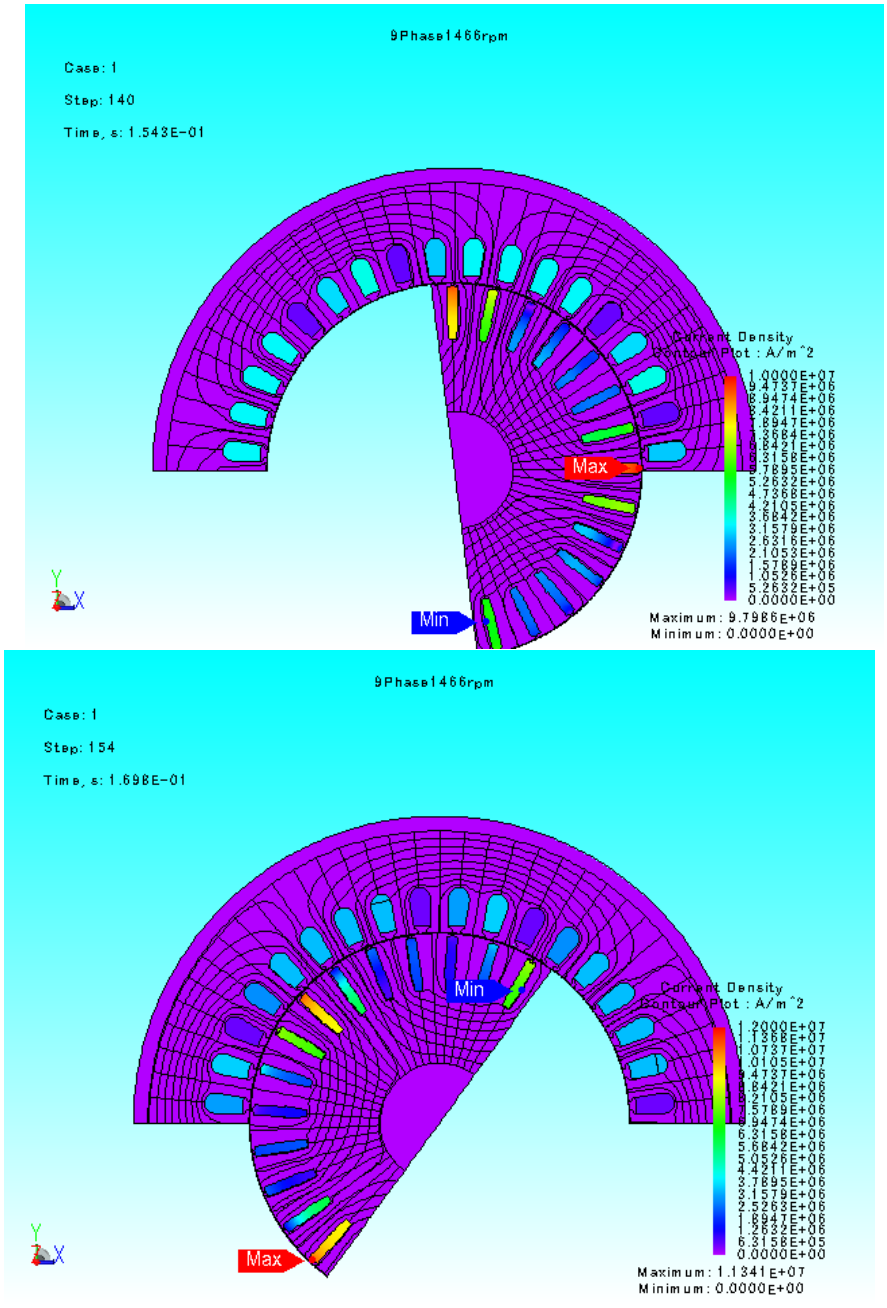

Figure D-3. Motor model showing the magnetic flux pattern at two different time instances as the motor rotates.

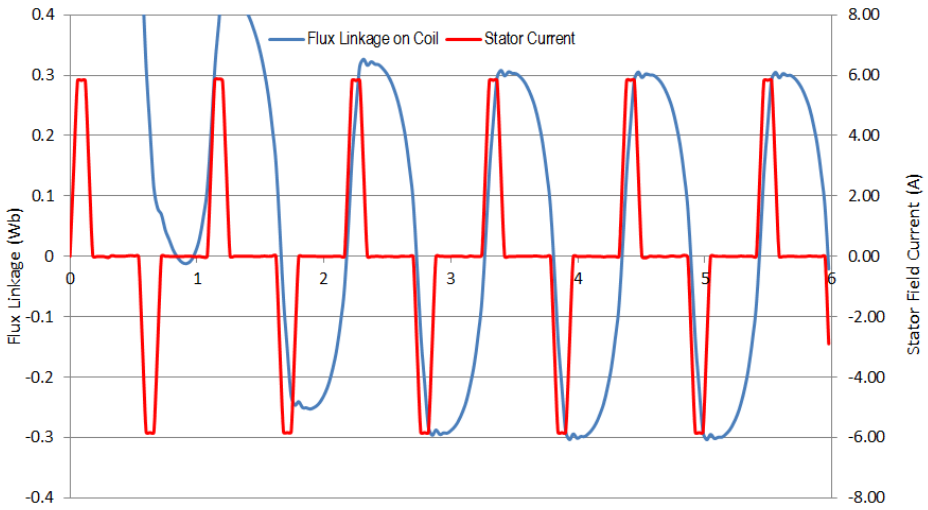

Figure D-4. Flux linkage to phase 'A' stator coil under locked rotor conditions: field current (red), flux linkage (blue).

D.3 Calculation of Inductance using Flux Linkages

Since the flux linkage varies with current, the inductance is calculated using the forward difference equation:

$$L_a = \frac{\lambda_a(i_a + \Delta_i) - \lambda_a(i_a)}{\Delta_i}, \qquad \text{(D-1)}$$

where, λ_a is the instantaneous flux linkage, i_a is the instantaneous phase current and Δ_i is a small change in the current which causes a small change in flux linkage without affecting the balanced mmf condition.

The effective stator inductance changes when the phase is acting as a torque and when the phase is acting as a field phase. Table D-1 shows the calculated inductances.

Table D-1: Calculated Inductances using flux linkage.

Parameter	L_a	L_{ab}	L_{ac}	L_{ad}	L_{ae}	L_{af}	L_{ag}	L_{ah}	L_{ai}
Value	2.45	1.76	0.326	0.612	-0.326	-1.76	0.612	0.40	-0.40

D.4 Mutual induced voltage constant calculation

The mutual induction voltage constant is calculated using the induced voltage on phase A due to the other eight phase currents. The voltage induced in phase A is the overall induced voltage which takes care of all the mutual inductances. The plot of the mutual induced voltage is shown in Figure D-5

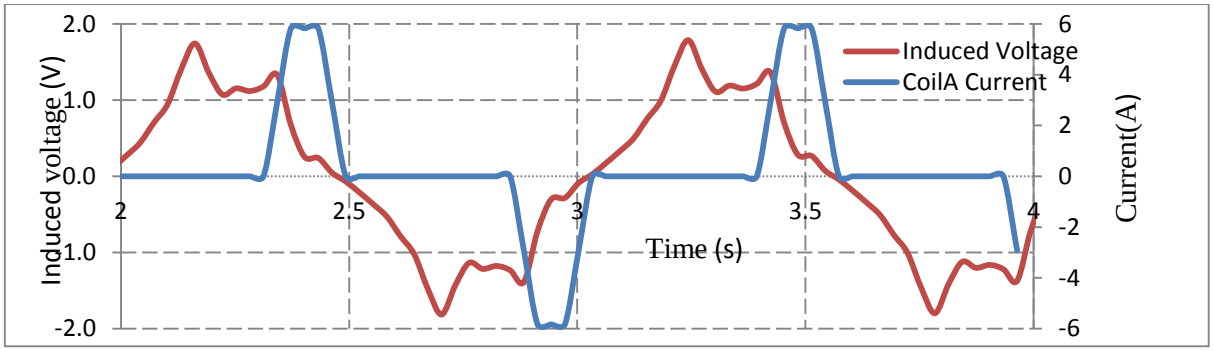

Figure D-5. Induced voltage and current against time.

In [30], the induced voltage constant is calculated using the change in current with angular position using the equation

$$e_{mj} = \sum_{j=a}^{j=i} L_{mji} \frac{di}{d\theta} . \frac{d\theta}{dt} = k * \omega_s \;\; ; [j \neq i], \tag{D-2}$$

k is the voltage constant and ω_s is the synchronous speed of the motor in rad/s. The induced voltage constant also varied with whether the phase acted as a torque or field phase. The calculated field phase value $k_f = 0.241$ and the torque phase value $k_t = 0.068$.

Therefore if the synchronous speed is known, the induced voltage can be calculated for any other speed using the constant k and the speed.

The equations and calculated values obtained are used in the next chapter to develop and simulate the nine phase induction machine drive using Simulink.

Appendix E Development of Torque Equation for Brush-DC Motor with Compensating Windings.

When a DC motor rotates, the magnetic field produced by the field current induces a back electromotive force (emf) in the armature. The back emf is given by:

$$E_b = K_a \emptyset \omega_m \quad (E\text{-}1),$$

where K_a is the terminal armature constant, $\emptyset$ is the flux linkage to the armature and ω_m is the mechanical speed. The product of the back emf and the armature current is the power developed in the rotor. The power developed by the machine P_{dev} is given by:

$$P_{dev} = K_a \emptyset \omega_m I_a \quad (E\text{-}2)$$

where I_a is the armature conductor current. The torque developed at a speed ω_m is given by:

$$T = \frac{P_{dev}}{\omega_m} = K_a \emptyset I_a \quad (E\text{-}3)$$

When the armature constant is evaluated and the flux expressed in terms of the magnetic flux density, then the developed torque is given in [46] as:

$$T = M_{rg} r_g l B I_a \quad (E\text{-}4)$$

where M_{rg} is the number of active armature conductors, r_g is the rotor radius, B is the air gap magnetic flux density. The air gap magnetic flux density is given by:

$$B = \frac{\mu_0 N_f I_f}{g} \quad (E\text{-}5)$$

where μ_0 is the permeability of free space, N_f is the number of field turns and I_f is the field current. Substituting for (G-5) in (G-4) gives:

$$T = \frac{M_{rg} r_g \mu_0 l N_f}{g} I_f I_a \quad (E\text{-}6)$$

If I_f is fixed, then torque is controlled by controlling I_a and a linear relationship between developed torque and armature current is realised. This analysis is based on the assumption that there is perfect commutation and that the magnetic flux density is constant

Appendix F C program snippets

Some important C program snippets used in the design of the controller are shown in this appendix

F.1 Trapezium Integration Block Code

```
Ia_out += GAIN*Ts/0.00318*2 * (Ia_prev + Ia);      //Integrate Ia using trapezium method
Ia_prev = Ia;                                      //Store current value for later use
```

F.2 Determining Duty Cycle for use in PWM Generator

```
if (Ia_out>Ia_ref + ADC_V_BAND) Dt_a = -1.0;  //Carrier greater than reference, negative output
if (Ia_out<Ia_ref + ADC_V_BAND) Dt_a = 1.0;//Carrier less than reference, positive output
```

F.3 Assigning Switching Times to PWM Generator

```
timer_on = _fpga_timer_translate_time(2*PWM4s - 2*Ia_ref_duty); //Timer On
timer_off = _fpga_timer_translate_time(2*PWM4s + 2*Ia_ref_duty);//Timer off
_fpga_pwm_set_ticks(&fpga_pwm[0], timer_on, timer_off);   //PWM set
```